Chem Soc Rev

REVIEW ARTICLE

View Article Online
View Journal | View Issue

Cite this: *Chem. Soc. Rev.*, 2024, **53**, 7590

Fluorescent probes for targeting the Golgi apparatus: design strategies and applications

Silin Xu,†[a] Kai-Cheng Yan,†[c] Zhi-Hong Xu,*[ab] Yuan Wang*[d] and Tony D. James*[ce]

The Golgi apparatus is an essential organelle constructed by the stacking of flattened vesicles, that is widely distributed in eukaryotic cells and is dynamically regulated during cell cycles. It is a central station which is responsible for collecting, processing, sorting, transporting, and secreting some important proteins/enzymes from the endoplasmic reticulum to intra- and extra-cellular destinations. Golgi-specific fluorescent probes provide powerful non-invasive tools for the real-time and *in situ* visualization of the temporal and spatial fluctuations of bioactive species. Over recent years, more and more Golgi-targeting probes have been developed, which are essential for the evaluation of diseases including cancer. However, when compared with systems that target other important organelles (*e.g.* lysosomes and mitochondria), Golgi-targeting strategies are still in their infancy, therefore it is important to develop more Golgi-targeting probes. This review systematically summarizes the currently reported Golgi-specific fluorescent probes, and highlights the design strategies, mechanisms, and biological uses of these probes, we have structured the review based on the different targeting groups. In addition, we highlight the future challenges and opportunities in the development of Golgi-specific imaging agents and therapeutic systems.

Received 31st January 2024

DOI: 10.1039/d3cs00171g

rsc.li/chem-soc-rev

[a] *Key Laboratory of Chemo/Biosensing and Detection, Xuchang University, 461000, P. R. China. E-mail: xuzhihong1980@xcu.edu.cn; Fax: +86 374 4369257; Tel: +86 374 4369297*
[b] *College of Chemical and Materials Engineering, Xuchang University, Xuchang, 461000, P. R. China*
[c] *Department of Chemistry, University of Bath, Bath, BA2 7AY, UK. E-mail: t.d.james@bath.ac.uk*
[d] *College of Chemistry and Chemical Engineering, Henan Key Laboratory of Coal Green Conversion, Henan Polytechnic University, Jiaozuo 454000, P. R. China. E-mail: wangyuan08@hpu.edu.cn*
[e] *School of Chemistry and Chemical Engineering, Henan Normal University, Xinxiang 453007, P. R. China*
† These authors are equally contributed to this work.

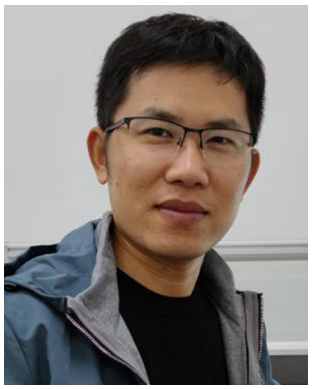

Silin Xu

Si-Lin Xu received his PhD degree in 2020 from Jiangxi Normal University, China. Now he is a lecturer at Xuchang University (Xuchang, China). His current research interests include development of novel synthetic methodologies for peptide and the design and synthesis of small molecule with structural diversity for chemical biology research.

Kai-Cheng Yan

Kai-Cheng Yan received his bachelor's degree in Industrial Engineering (2017) and Master's degree in Pharmaceutical Engineering from ECUST at the School of Chemistry and Molecular Engineering (2020). He is currently pursuing his PhD degree in Chemistry, at the University of Bath, UK, where his projects are related to chemical biology for pathogenic microorganism theranostics.

1. Introduction

Prokaryote organisms are different from eukaryotic cells in that they do not contain subcellular organelles, such as lysosomes/endosomes, mitochondria, lipid droplets (LDs), plasma membranes, nucleus, Golgi apparatus and endoplasmic reticulum (ER).[1] These organelles exhibit distinctive properties and performs unique and/or essential biological functions in various cellular processes.[2]

The Golgi apparatus which is widely distributed in eukaryotic cells and is dynamically regulated during cell cycles, exhibits a slightly acidic environment (6.0–6.7) and expresses several specific enzymes or proteins such as cyclooxygenases and furin. The organelle is formed by the stacking of flattened vesicles and plays an important role in a variety of metabolic pathways and cell signaling mechanisms. Where one of the primary biological functions is collecting, processing, sorting, transporting and secreting important proteins/enzymes from the endoplasmic reticulum to intra- and extra-cellular destinations. The Golgi apparatus is not only involved in protein processing and transport, but also in many physiological processes such as ion exchange, oxidative stress and apoptosis, which helps maintain normal physiological function and cell survival.[3–8]

Redox homeostasis, the organelle microenviroment, metal ion homeostasis, and enzyme activity are intimately associated with the correct function of the Golgi. It has been established that Golgi-related functions are closely related to many important biological species (ions, reactive oxygen species, reactive nitrogen species, reactive sulfur species, enzymes *etc.*) and microenvironmental parameters (pH, viscosity, polarity *etc.*) present in the Golgi, and the deficiency or excess of such bioactive species can cause morphological changes and dysfunction of the Golgi apparatus, which is directly linked to a range of human disorders including cancer, neuronal, kidney, eye, and liver diseases.[9,10] Therefore, the accurate *in situ* monitoring of bioactive species in the Golgi will provide a comprehensive appreciation of the biological functions and pathological processes linked with the Golgi apparatus, which can help facilitate the diagnosis of Golgi related diseases and monitor therapeutic agents during the treatment of diseases.[11–15]

Organelle-specific fluorescent probes provide powerful non-invasive tools for the real-time and *in situ* visualization of the temporal and spatial fluctuations of bioactive species in cells and *in vivo* with high selectivity and high sensitivity.[16–35] However, compared with systems for other key organelles (*e.g.* lysosomes and mitochondria), Golgi-targeting strategies which are vital to monitor cellular health are still in their infancy.

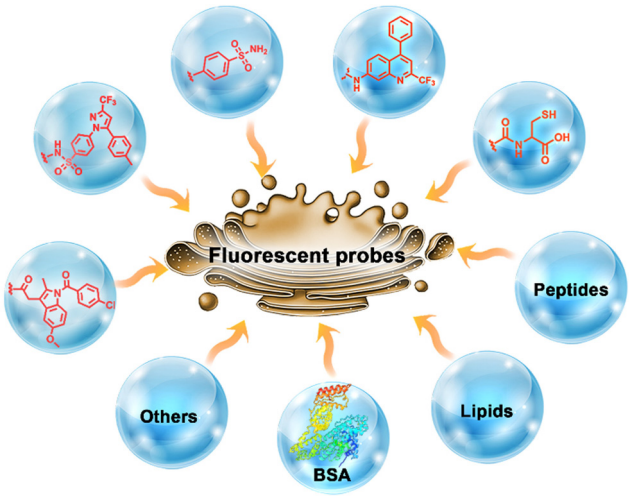

Scheme 1 Common Golgi-targeting groups.

With this review, we have summarized Golgi-specific fluorescent probes, which can respond to specific bioactive molecules, and highlighted the design strategies, mechanisms, and biological applications. We also provide insights and provide guidance for the future development of this area of research. It worth to mentioning that some Golgi-targeting markers that simply stain the Golgi were excluded from this review. We expect that this review will steer the development of probes targeting the Golgi and facilitate the evaluation of related biomedical areas.

2. Golgi targeting probes design

Visualization of the Golgi apparatus is of great significance for real-time monitoring of the functions of the Golgi apparatus. Over a hundred years ago, Camillo Golgi invented the silver staining method for the Golgi apparatus and instigated research into Golgi structure-function correlations.[36] In the

From left to right: Tony D. James, Zhi-Hong Xu and Yuan Wang

Tony D. James is a Professor at the University of Bath and Fellow of the Royal Society of Chemistry. He received his PhD from the University of Victoria (1991). He has an h-index of 90 and has been listed by Clarivate as a Highly Cited Researcher since 2022. Zhi-Hong Xu: received his PhD degree in 2008 from Lanzhou University, China. He is professor at the College of Chemical and Materials Engineering in Xuchang University. His current research interests include development of chemosensors and nanosensors for biological and environmental relevance. Yuan Wang: received his PhD degree in 2008 from Lanzhou University (Lanzhou, China). Now he is professor at Henan Polytechnic University (Jiaozuo, China). His main scientific interests are the design and synthesis of small molecule with structural diversity for chemical biology research.

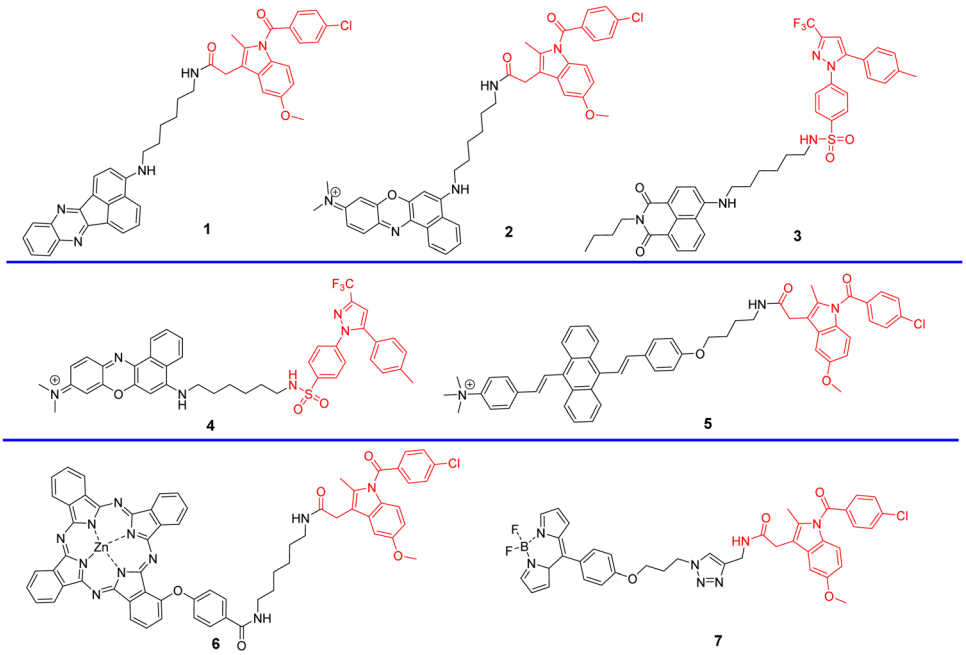

Scheme 2 Golgi-targeting probes containing cyclooxygenase-2 (COX-2) inhibitors as the functional motif. The Golgi-targeting units are highlighted in red.

mid-20th century, Felix observed the basic shape of the Golgi apparatus using an electron microscopy. While in 1985, Lipsky *et al.* observed the Golgi apparatus for the first time in living cells using ceramide derivative staining.[37] In the late 20th century and early 21st century, the discovery of fluorescent proteins (green fluorescent protein, yellow fluorescent protein, and so on) and Furin cleavage technology provided biological methods for Golgi imaging.[38,39] However, these classical methods can only achieve intracellular Golgi imaging, but are unsuitable for the real-time detection of biomolecules in the Golgi apparatus. Significantly, the recent development of fluorescence imaging technologies has provided many probes for Golgi imaging and the monitoring of the concentration of bioactive molecules in the Golgi apparatus.[40]

Although Golgi apparatus targeting fluorescent probes have previously been developed, the targeting mechanism needs clarifying. When developing Golgi-specific fluorescent probes, the main obstacle is the lack of precise Golgi-targeting groups, as such determining appropriate systems that can improve localization efficiency of a targeting group is essential for the development of Golgi-targeting fluorescent probes.

Generally speaking, in order to obtain good Golgi-targeting efficiency, the Golgi localization groups should tightly and selectively bind to specific enzymes present in the Golgi apparatus, or match well with the weakly acidic environment of the Golgi or form non-convalent or covalent bonds with biomacromolecules present in the Golgi, or linked with Golgi-targeting peptides. In this review, we illustrate some representative targeting groups for the development of Golgi-specific fluorescent probes. For example, cyclooxygenase-2 (COX-2) inhibitors such as indomethacin and celecocoxib can bind tightly and selectively to the side pocket of COX-2 in the Golgi apparatus,

Table 1 Golgi-targeting fluorescent probes with cyclooxygenase-2 (COX-2) inhibitors as functional motif

Probe	$\lambda_{ex}/\lambda_{em}$ (nm)	Detection range	LOD	Pearson's correlation coefficient	Application	Ref.
1	OP 457/547 TP 800/—	0.12–0.72 μg mL^{-1}	0.11 μg mL^{-1}	0.97	Differentiate cancer cells from normal cells; imaging of Golgi apparatus during cancer cell apoptosis	55
2	630/670	—	—	0.96, 0.97, 0.93	Differentiate cancer cells from normal cells; *In vivo* tumor optical imaging	56
3	OP 488/— TP 870/—	—	—	0.96	Differentiate cancer cells from normal cells; Tissue slice and tumor mouse imaging	57
4	630/700	—	—	0.94	Differentiate cancer cells from normal cells; Tissue slice and tumor mouse imaging	58
5	420/574	0.14–0.8 μg mL^{-1}	0.24 μg mL^{-1}	—	Differentiate cancer cells from normal cells; tumor-bearing mice imaging	59
6	674/687	—	—	0.92	Photosensitizer for tumor cells	60
7	488/515	1.8–950 cP	—	0.923, 0.930	Fluorescence lifetime imaging in live cells and zebrafish	61

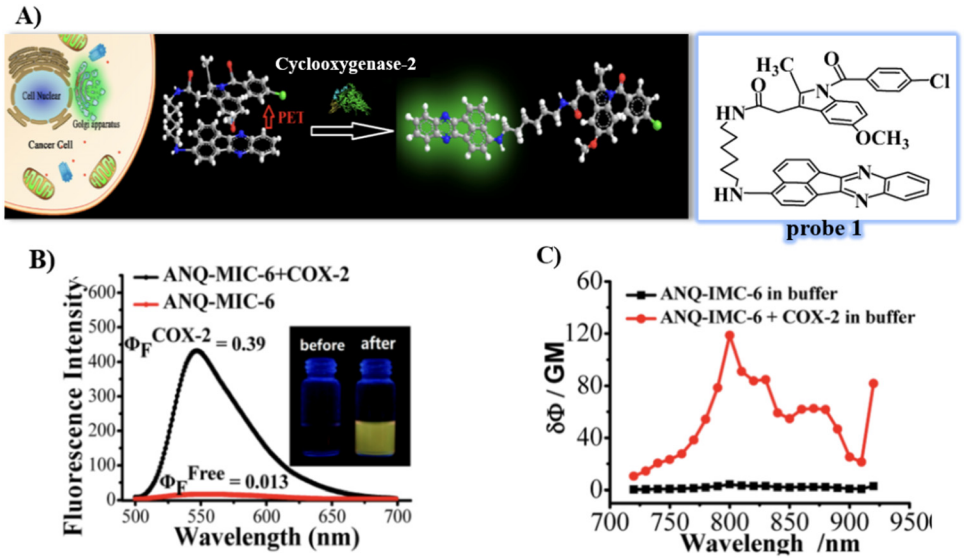

Fig. 1 (A) Detection mechanisms of probe **1** for COX-2. (B) Fluorescence emission spectra of probe **1** with and without addition of COX-2. (C) Two-photon spectra of probe **1** in the absence and presence of COX-2. Reproduced with permission from ref. 55. Copyright 2013, American Chemical Society.

and phenylsulfonamide also can bind to specific regions of COX-2, and 2-trifluoromethyl-7-aminoquinoline with a pyridyl moiety matches well with the slightly acidic microenvironment of the Golgi, while cysteine or cysteine-enriched BSA can form disulphide bonds by binding with thiol groups present in the Golgi. As such these are common targeting groups for evaluating the Golgi apparatus using non-covalent or covalent interactions with biomacromolecules present in the Golgi. Herein, we have classified the reported fluorescent probes based on their Golgi-targeting functional motif (Scheme 1).

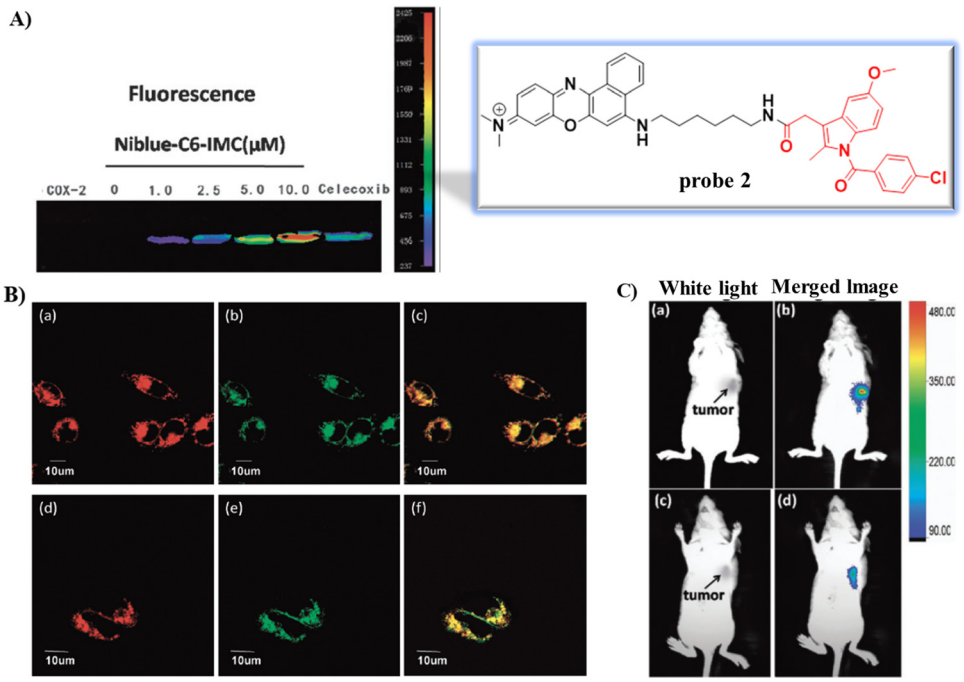

Fig. 2 (A) Fluorescence images of COX-2 with various concentration of probe **2** and in the presence of Celecoxib. (B) Fluorescence images of MCF-7 (a)–(c) and HeLa cells (d)–(f) stained with probe **2**. (a) and (d) **2**; (b) and (e) NBD C6-ceramide; (c) overlay of (a) and (b); (f) overlay of (d) and (e). (C) *In vivo* tumor optical imaging. (a) and (c) White light images of nude mice with tumor (b) treated with **2**; (d) pre-dosed with Celecoxib. Reproduced with permission from ref. 56. Copyright 2015, The Royal Society of Chemistry.

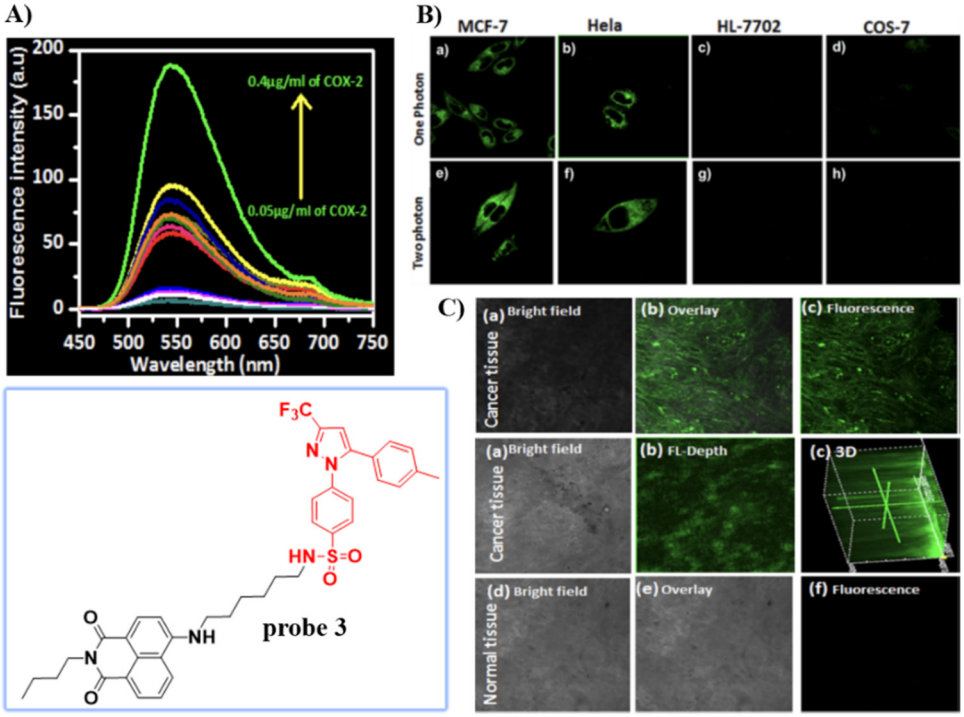

Fig. 3 (A) Fluorescence spectra of **3** upon the addition of COX-2. (B) One (a)–(d) and two photon (e)–(h) fluorescence images of cancer cells MCF-7 cells (a) and (e), HeLa cells (b) and (f) and normal cells HL-7702 cells (c) and (g), COS-7 cells (d) and (h) stained with **3**. (C) Fluorescence imaging of cancerous and normal tissue. Reproduced with permission from ref. 57. Copyright 2018, American Chemical Society.

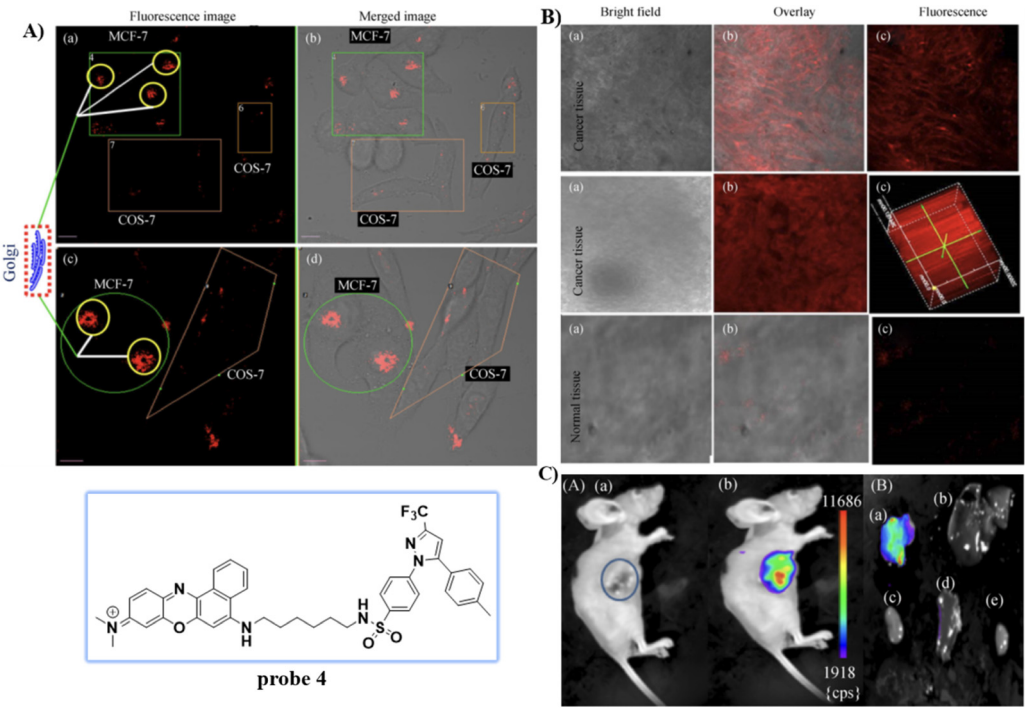

Fig. 4 (A) Normal cells (COS-7) and cancer cells (MCF-7) co-cultured and stained with **4**. (a) and (c) Overlay fluorescence imaging of co-cultured cancer and normal cells (b) and (d). (B) Fluorescence imaging of cancerous and normal tissue stained with **4**. (C) Fluorescence imaging of tumor mouse and organs. Reproduced with permission from ref. 58. Copyright 2020, Springer.

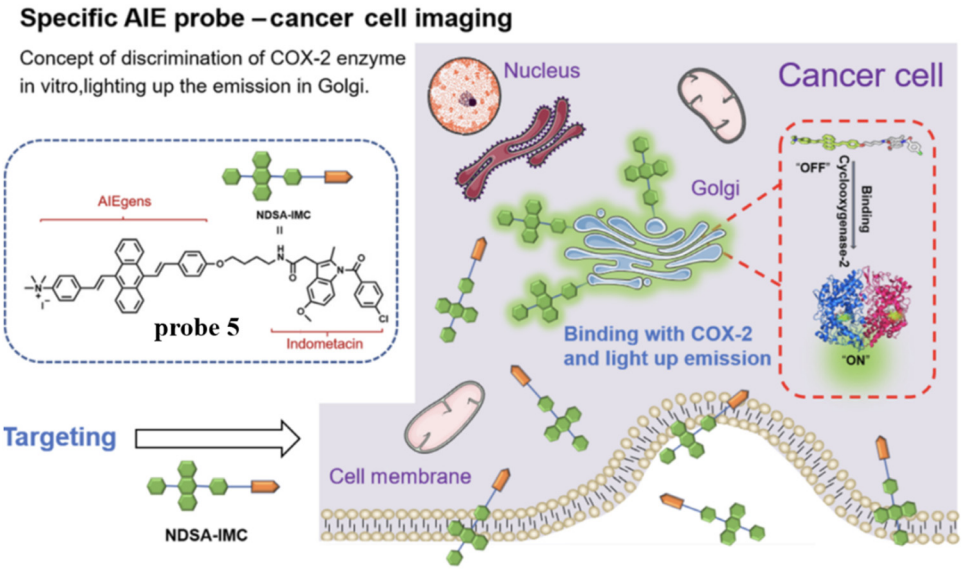

Fig. 5 Discrimination of COX-2 enzyme using probe **5**. Reproduced with permission from ref. 59. Copyright 2021, Chinese Chemical Society.

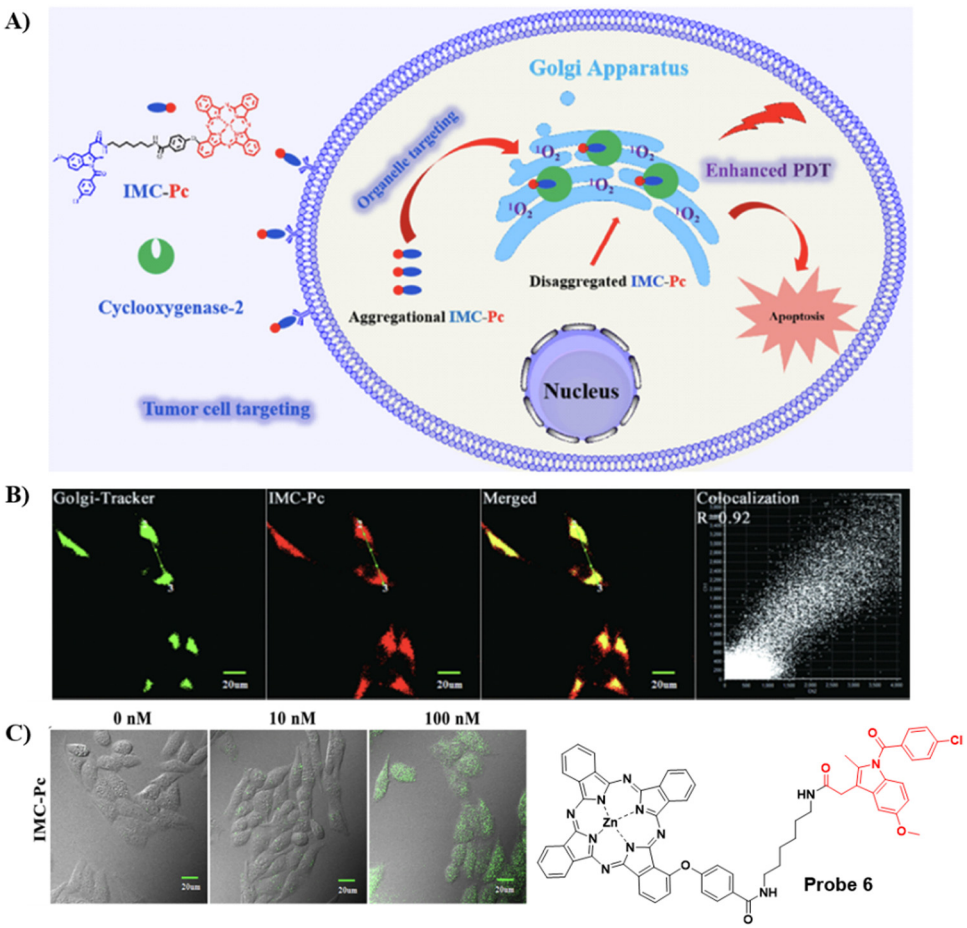

Fig. 6 (A) Illustration of **6** for highly-efficient anticancer therapy. (B) Co-localization fluorescence cell imaging of **6** with Golgi Tracker Green. (C) Fluorescence images of intracellular ROS production by **6** in HepG2 cells. Reproduced with permission from ref. 60. Copyright 2022, Elsevier.

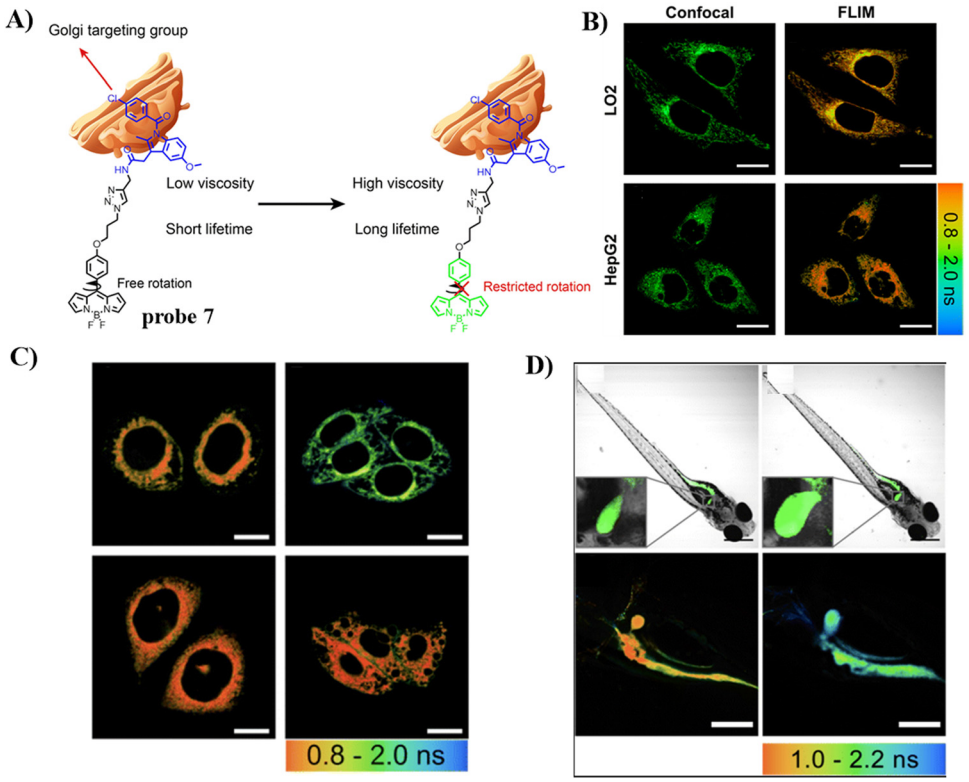

Fig. 7 (A) Structure and response mechanism of probe **7**. (B) Fluorescence and FLIM imaging of LO2 and HepG2 cells with probe **7**. (C) FLIM imaging in an alcohol-induced liver injury LO2 cell model of the Golgi with probe **7**. (D) Fluorescence and FLIM imaging of zebrafish with the stimulation of ethanol. Reproduced with permission from ref. 61. Copyright 2022, The Royal Society of Chemistry.

3. Classification of Golgi-targeting probes based on the functional motif

3.1 Probes containing cyclooxygenase-2 (COX-2) inhibitors

Cyclooxygenases (COXs) control the synthesis of prostaglandins and are pivotal in tumor development and progression.[41] The evolution of the Golgi apparatus and tumorigenesis, is associated with cyclooxygenase COX-2, which is an inducible enzyme accumulating in the Golgi apparatus. COX-2 is an attractive target for molecular imaging because it is upregulated in most cancer cells but less expressed in normal cells.[42–49] COX-2 has been detected in premalignant lesions of the esophagus and colon, and its levels appear to increase during tumor progression, which indicates the importance of COX-2 in tumor progression.[50,51] In addition, it has been confirmed that COX-2 inhibitors such as indomethacin (IMC) and Celecoxib (CXB) conjugates bind tightly and selectively to the side pocket of COX-2.[42,52–54] Thus, IMC and CXB can be used as targeting groups for COX-2 and used for imaging the Golgi apparatus. Scheme 2 and Table 1 highlight Golgi-targeting probes using cyclooxygenase-2 (COX-2) inhibitors as the functional motif and their uses. Non-Golgi-targeting research using COX-2 inhibitors will not be covered in this section.

In 2013, the group of Peng developed a COX-2 turn-on fluorescent probe **1** (Scheme 2) for the Golgi apparatus of cancerous cells based on photoinduced electron transfer (PeT), which integrated a COX-2 inhibitor indomethacin (IMC) with the fluorophore acenaphtho[1,2-*b*]-quinoxaline (ANQ) using a hexanediamine linker.[55] The free probe **1** exists in a folded conformation owing to the weak π-stacking interactions between ANQ and IMC, PeT from IMC to ANQ quenched the fluorescence of the probe (Fig. 1A). However, the fluorescence was activated (Fig. 1B) by attenuating the PeT process upon binding with COX-2, where probe **1** was forced to adopt an unfolded form. In addition, probe **1** exhibited significant two-photon properties (Fig. 1C) and was used for 3D depth imaging of living cancer tissues, probe **1** targeted the Golgi apparatus of cancer cells and was successfully used to monitor real-time changes of the Golgi apparatus during cancer cell apoptosis.

In 2015, using the same strategy, and taking advantage of Near-infrared (NIR) fluorophores that exhibit minimum photodamage, minimal interference and deep tissue penetration, the group of Fan developed a Golgi-localized NIR fluorescent probe **2** (Scheme 2) for COX-2 (Fig. 2A) by replacing ANQ with Nile Blue, which was used to detect cancer cells.[56] Probe **2** localized in the Golgi apparatus (Fig. 2B) and was used to image deep tissue tumors in a mouse model (Fig. 2C).

Celecoxib (CXB) is an effective inhibitor of COX-2, which has been used for non-steroidal treatment of inflammation. In 2018 and 2020, the group of Peng developed two Golgi-targeting fluorescent probes **3** and **4** (Scheme 2) for COX-2, using CXB as

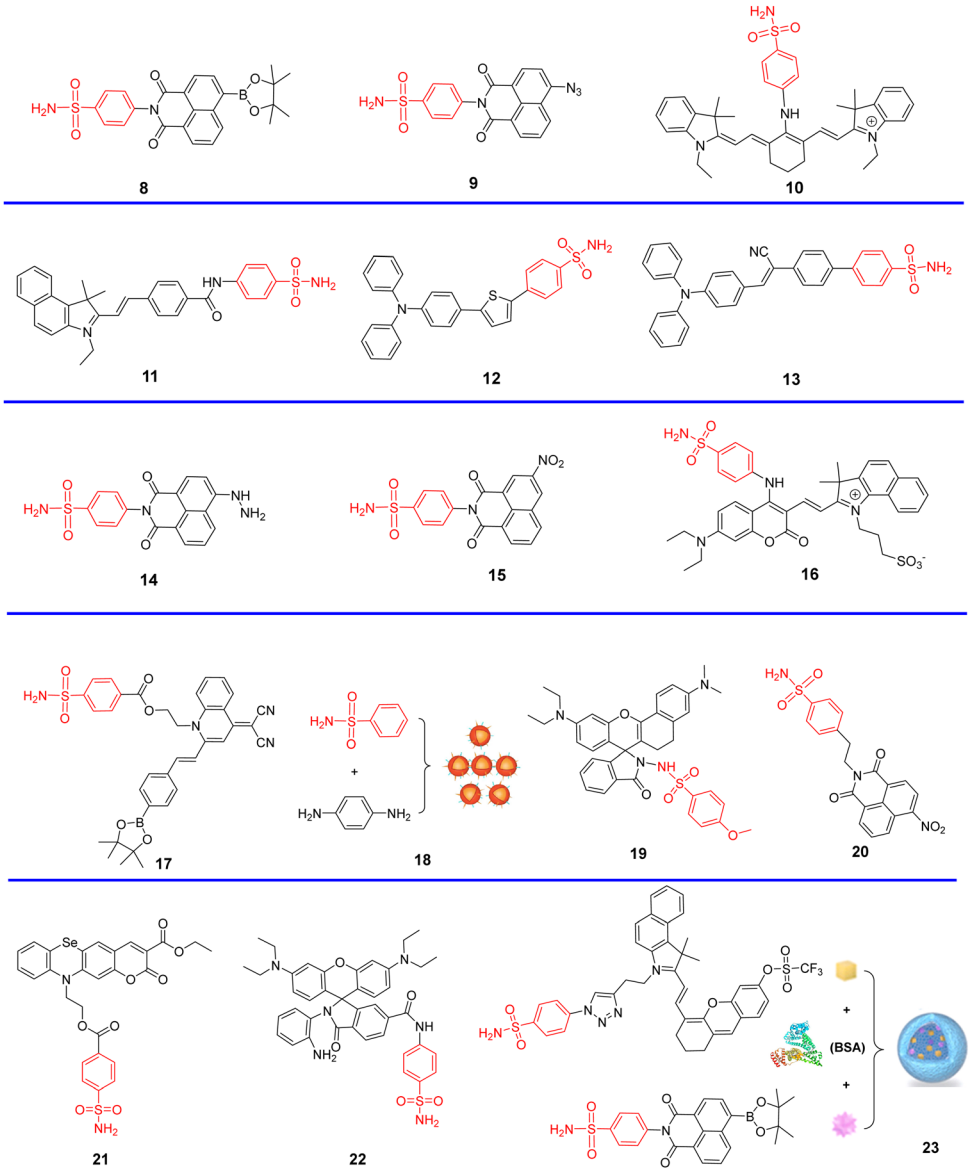

Scheme 3 Golgi-targeting probes using phenylsulfonamide as the functional motif. Red moiety represents the Golgi-targeting unit.

Table 2 Golgi-targeting fluorescent probes with phenylsulfonamide as functional motif

Probe	Analyte	$\lambda_{ex}/\lambda_{em}$ (nm)	Detection range	LOD	Pearson's correlation coefficient	Application	Ref.
8	H_2O_2	405/470, 560	0–350 μM	0.20 μM	0.94	TP imaging in living cells and the kidney tissues of mice with hypertension	63
9	H_2S	440/550	0–30 μM	0.10 μM	0.92	Imaging in living cells and zebrafish; the production of H_2S under Golgi stress	64
10	pH	675/750, 810	pH 5.9–7.7	—	0.9	Fluorescent images in cell; PAI *in vivo*; TMEM165 deficiencies influence the pH homeostasis	65
11	Polarity	675/405, 442	—	—	0.94	TP ratiometric imaging in cells; TP fluorescence imaging of kidney tissues	66
12, 13	—	—	—	—	0.91, 0.92	Golgi apparatus localization	67
14	FA	440/546	0–100 μM	0.35 μM	0.806	In food; imaging in live cells	68
15	CORM-3	430/520	0.5–80 μM	0.35 μM	0.93	Imaging in live cells and zebrafish	69
16	$ONOO^-$	675/477, 650	—	13 nM	0.9	Imaging in live cells and DILI	70
17	$ONOO^-$	420/600	8–40 μM	250 nM	0.9191	Imaging in live cells	71
18	—	366/612	—	—	0.92	*In vivo*/*vitro* imaging	72
19	pH	580/664	—	—	0.88	Imaging in live cells	73
20	NTR	440/534	0.1–5.0 μg mL^{-1}	0.623 μM	0.84	Imaging in live cells and in tumor tissue sections	74
21	ClO^-	488/550	0–300 μM	27 nM	0.98	Imaging in live cells	75
22	NO	560/589	0–20 μM	45 nM	0.95	Imaging in live cells	76
23	$O_2^{\bullet-}$, H_2O_2	633/740	0–35 μM	62 nM	0.827, 0.839	Imaging in live cells and mice	77

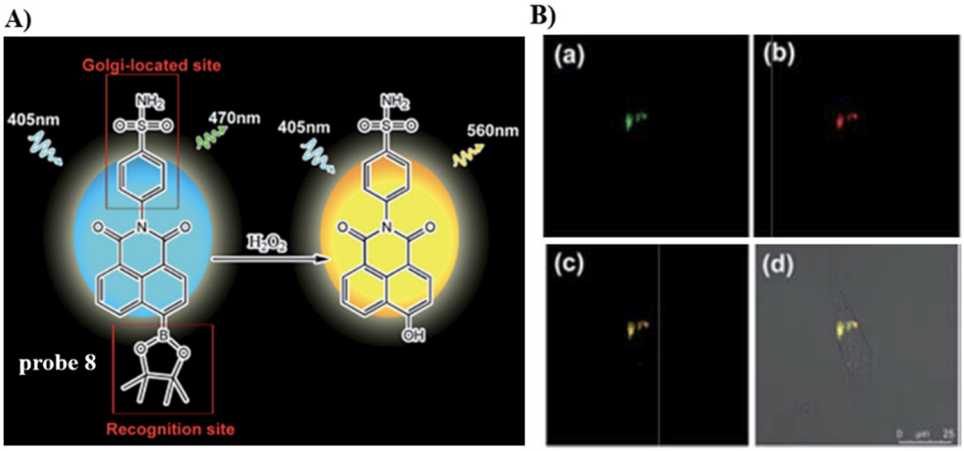

Fig. 8 (A) Probe **8** response mechanism. (B) Co-localization cell fluorescence imaging of **8** and Golgi Tracker Red. Reproduced with permission from ref. 63. Copyright 2019, The Royal Society of Chemistry.

a Golgi targeting group, which was then conjugated with naphthalamide and Nile Blue respectively *via* a flexible six-carbon linker.[57,58] Probe **3** displays intense one- and two-photon fluorescence emission in cancer cells that express elevated levels of COX-2, and can be used for the fluorescence imaging of tumors (Fig. 3). Probe **4** exhibits strong NIR fluorescence in tumor cells/tissues with enhanced expression of COX-2, and can distinguish cancer cells from healthy cells, exhibits Golgi apparatus localization, and was used for the fluorescence visualization of tumors in mice and tissue slices (Fig. 4).

To overcome the aggregation-caused quenching found with traditional organic dyes including Nile blue, naphthalamide, and so on, in 2021, the group of Tian developed a "turn-on" aggregation-induced emission (AIE) based COX-2 fluorescent probe **5** (Scheme 2), using 9,10-distyrylanthracene as fluorophore and IMC as the targeting group. As such probe **5** could visualize sites that over express COX-2 in the Golgi apparatus of cancer cells, due to the restriction of intramolecular motion of the AIE-active probe **5** when bound to COX-2, enabling the discrimination of cancerous from normal cells and could be used to image tumor-bearing mice (Fig. 5).[59]

Concerned by the poor tumor targeting and aggregation of photosensitizers, limited radius of activity and lifetime of reactive oxygen species that results in the limited therapeutic efficiency of photosensitizers in photodynamic therapy (PDT). The Chen group developed an ultra-efficient photosensitizer **6** by conjugating a COX-2 binding IMC with a zinc phthalocyanines (ZnPc) photosensitizing agent in order to improve therapeutic efficacy, the indomethacin moiety enhances the action of ZnPc by selectively targeting COX-2 expressing tumor cells, and targeting the Golgi apparatus. As such photosensitizer **6** is an encouraging candidate for improved therapeutic efficacy (Fig. 6).[60]

To detect and diagnose the early stages of alcoholic liver injury, the Xiao group designed a Golgi-targeting fluorescent probe **7** for monitoring Golgi viscosity, which consists of a BODIPY fluorophore and a Golgi-targeting IMC moiety.[61] Variations in viscosity of the Golgi during alcohol-induced liver injury were then evaluated quantitatively using fluorescence lifetime imaging in zebrafish and live cells, providing information on the link between viscosity of the Golgi and alcohol-induced liver injury (Fig. 7).

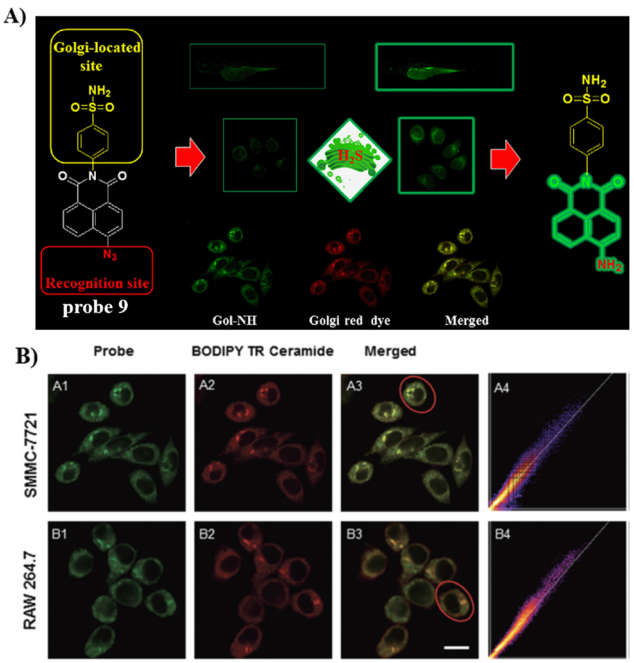

Fig. 9 (A) Probe **9** response mechanism. (B) Co-localization cell imaging of **9** and BODIPY TR ceramide. Reproduced with permission from ref. 64. Copyright 2020, The Royal Society of Chemistry.

3.2 Probes containing a phenylsulfonamide group

Given that COX-2 is upregulated in the Golgi apparatus of most cancer cells, fluorescent derivatives of COX-2 inhibitors represent an appropriate approach for Golgi-targeted imaging and monitoring. Research has shown that Golgi enzyme COX-2 inhibitor SC-558, derives selectivity from the phenylsulfonamide group which binds to specific regions of COX-2.[62]

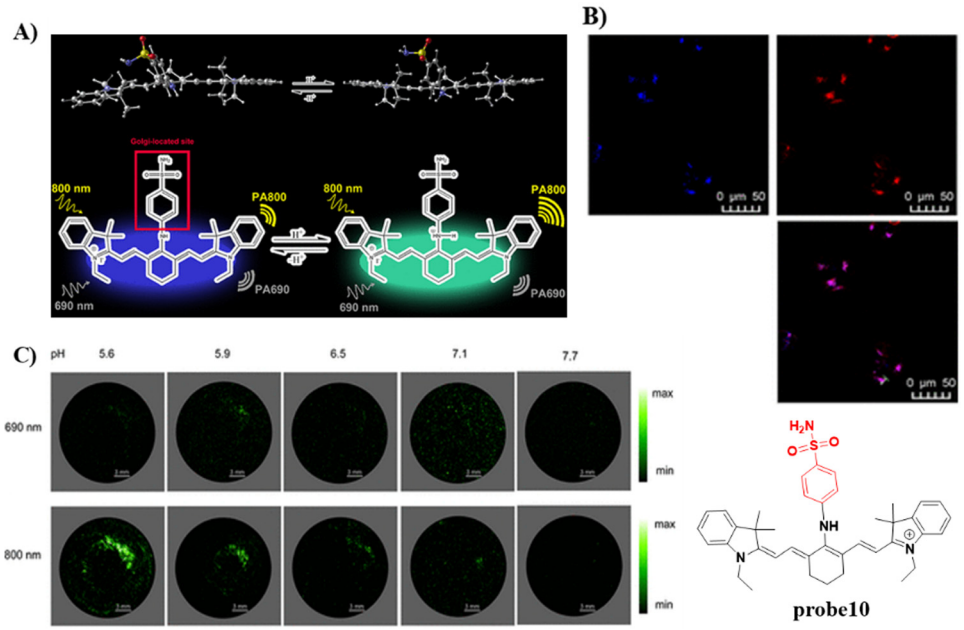

Fig. 10 (A) Probe **10** response mechanism. (B) Co-localization cell fluorescence imaging of **10** and Golgi Tracker Red. (C) pH monitoring by *in vitro* PA imaging. Reproduced with permission from ref. 65. Copyright 2020, American Chemical Society.

therefore, the phenylsulfonamide unit is a promising Golgi targeting group for the Golgi apparatus.[22,63] Scheme 3 and Table 2 highlight Golgi-targeting probes using phenylsulfonamide as the targeting group.

At this point it should be noted that *p*-toluenesulfonamide is an ER targeting group which can localize within the ER through binding to sulfonylurea receptors in the ER, while a Golgi-targeting group is phenylsulfonamide, which can target Golgi

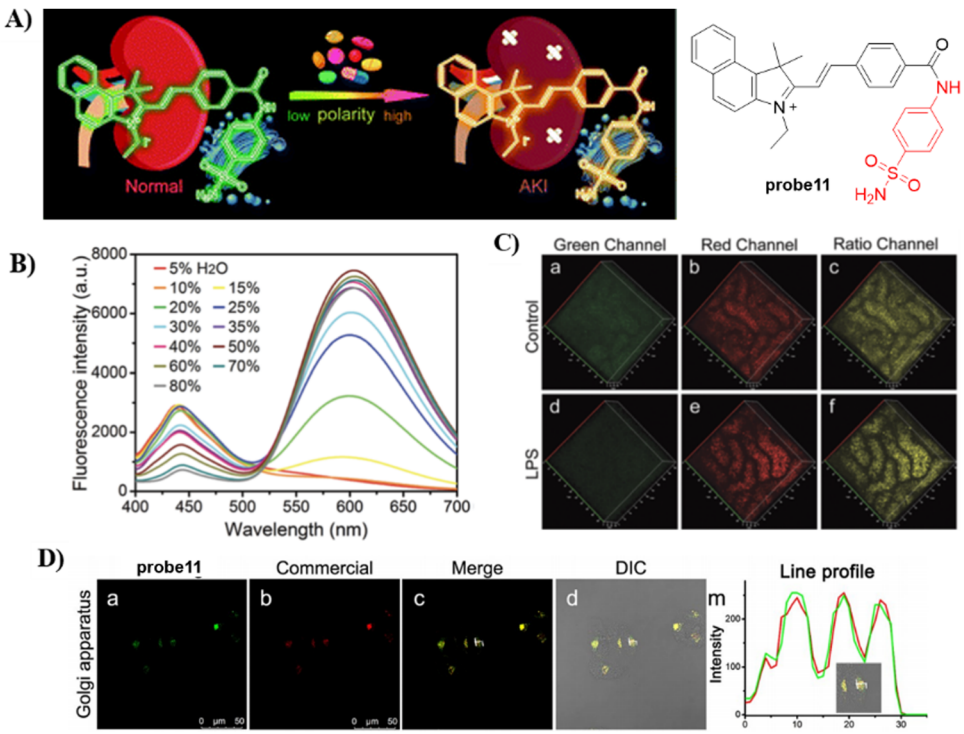

Fig. 11 (A) Probe **11** fluorescence and photoacoustic based dual-mode response mechanism. (B) Ratiometric fluorescence spectra of **11** towards polarity. (C) Two-photon fluorescence imaging in control mice and lipopolysaccharide (LPS) induced AKI mice of kidney tissues. (D) Co-localization cell imaging of **11** and Golgi Tracker Red. Reproduced with permission from ref. 66. Copyright 2021, The Royal Society of Chemistry.

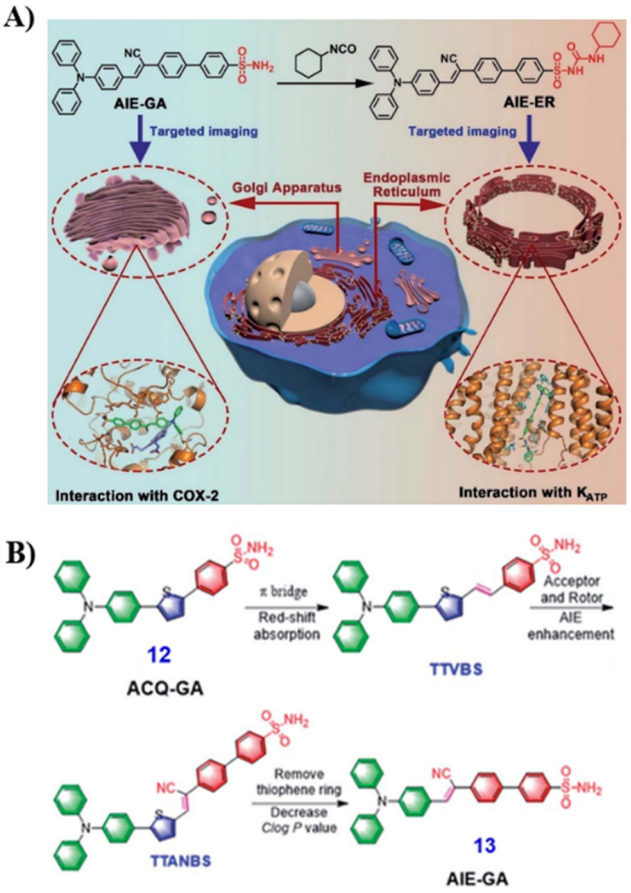

Fig. 12 (A) Schematic illustration of GA and ER targeting by AIEgens. (B) Rational design of GA probes. Reproduced with permission from ref. 67. Copyright 2021, The Royal Society of Chemistry.

apparatus through binding to COX-2 in the Golgi. While the *p*-toluenesulfonamide and phenylsulfonamide have very similar structures, they localize specifically in the ER and Golgi organelles respectively.

Using the Golgi-targeting phenylsulfonamide group, the Tang group developed a two-photon (TP) fluorescent probe **8**, for evaluating oxidative stress in the Golgi apparatus during hypertension,[63] where a phenylsulfonamide acts as the Golgi-targeting group and the boronic acid ester acts as a H_2O_2-recognition group. Probe **8** was used to ratiometrically image the generation of H_2O_2 *in situ* and revealed an increase of H_2O_2 levels in the Golgi of kidney tissues from mice with hypertension (Fig. 8). These outcomes indicate that phenylsulfonamide is an effective Golgi-targeting group. In addition, phenylsulfonamide is readily available, and can be chemically modified. Therefore, this targeting group can provide an ideal strategy for developing Golgi-targeting probes.

Using the same Golgi-targeting group with a naphthalimide fluorophore as structural skeleton, the Zhu group developed a Golgi-targeting H_2S fluorescent probe **9**, for the visualization of endogenous and exogenous H_2S in zebrafish and living cells (Fig. 9).[64] The Golgi-targeting probe exhibited good sensitivity and biocompatibility and was used to monitor the production of H_2S in the Golgi under stress.

In 2020, the Tang group developed a dual mode ratiometric photoacoustic (PA) and fluorescent imaging probe **10** (Fig. 10) for measuring the pH of Golgi in real-time with high sensitivity and excellent selectivity.[65] The phenylsulfonamide moiety was selected as an effective Golgi-targeting anchor, and tricarbocyanine was selected as the fluorophore and PA reporter given that the tricarbocyanine fluorescence emission was in the NIR region[78–83] and the tricarbocyanine unit also generates PA signals.[84–89] The probe exhibited strong fluorescence emission at 810 nm under an acidic pH, and the emission of the probe shifts to 750 nm under basic conditions. As such acid–base changes of the system, resulted in the ratiometric fluorescence values (F750/F810) of the probe increasing by more than 100-fold. While at 800 nm the photoacoustic response of the probe was reduced with increasing pH, whilst at 690 nm the PA intensity was hardly affected. Significantly, the pH of the Golgi increases dramatically during monensin induced oxidative stress. Additional experiments indicated that transmembrane protein 165 (TMEM165) deficiency affected the proton equilibrium and resulted in Golgi acidification. This research not only provides confirmation that TMEM165 regulates pH homeostasis of the Golgi but also provided a potential Golgi pH indicator for various biological processes.

In 2021, by anchoring a Golgi-targeting moiety phenylsulfonamide onto a hemicyanine, the Tang group developed a TP ratiometric fluorescent probe **11** for Golgi polarity.[66] Probe **11** was not only used for monitoring the changes of Golgi polarity in the kidneys of mice with acute kidney injury (AKI), but was used to image the variability of Golgi polarity during different physiological and biochemical processes (Fig. 11). This research confirms that Golgi polarity and AKI are correlated, and provides a potential high-throughput tool for AKI detection during drug development.

The development of efficient and cost-effective endoplasmic reticulum (ER) and Golgi apparatus (GA) specific probes based on the AIE platform is of particular importance since it could provide a route to explore the interplay of organelles in living systems, but the development of such systems remains challenging. In 2021, the Tang group developed an AIE based fluorescence platform for GA and ER probes (**12** to **13**), which was achieved by changing the phenylsulfonamide to a glibenclamide unit attached to the fluorophore (Fig. 12A).[67] For the design of organelle targeting probes, the phenylsulfonamide moiety was used to achieve GA-targeting and the glibenclamide unit binds to the ATP-sensitive potassium channel (KATP)[55,62] to provide ER-targeting, and the triphenylamine (TPA) unit was used as rotor an electron donor (D). For Golgi localized probes, double bonds and cyano groups can be introduced to extend π-conjugation and enhance the D–A interaction, leading to transformation from ACQ-to-AIE (**12** to **13**) (Fig. 12B). Cellular imaging experiments indicated that these AIE-based probes which were simple to prepare exhibited good photostability, specificity, biocompatibility and high brightness when compared with commercially available probes.

In 2021, the Kim group prepared a fluorescent probe **14** for formaldehyde (FA) which contains hydrazine as the FA reaction

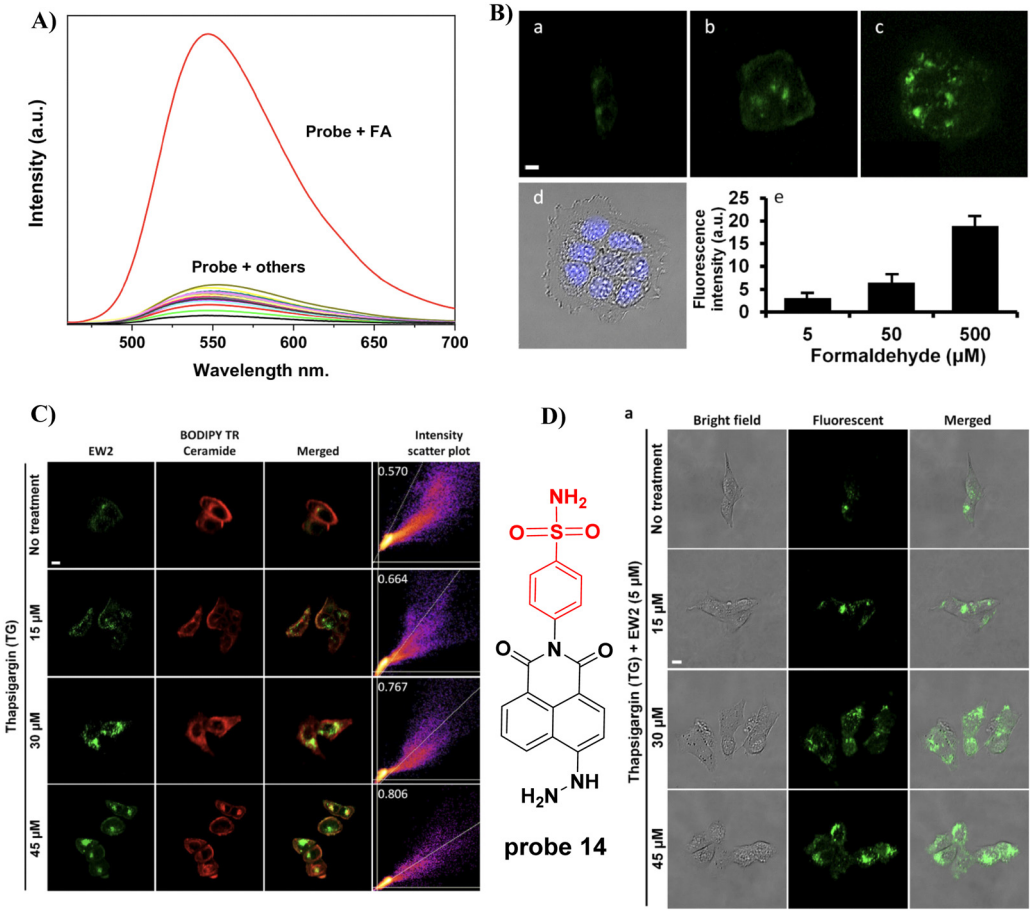

Fig. 13 (A) Fluorescence selectivity of probe **14**. (B) The fluorescence imaging of FA in live MCF7 cells. (C) Co-localization of **14** and BODIPY TR ceramide tracker. (D) Imaging endogenous FA in Cells. Reproduced with permission from ref. 68. Copyright 2021, MDPI (Basel, Switzerland).

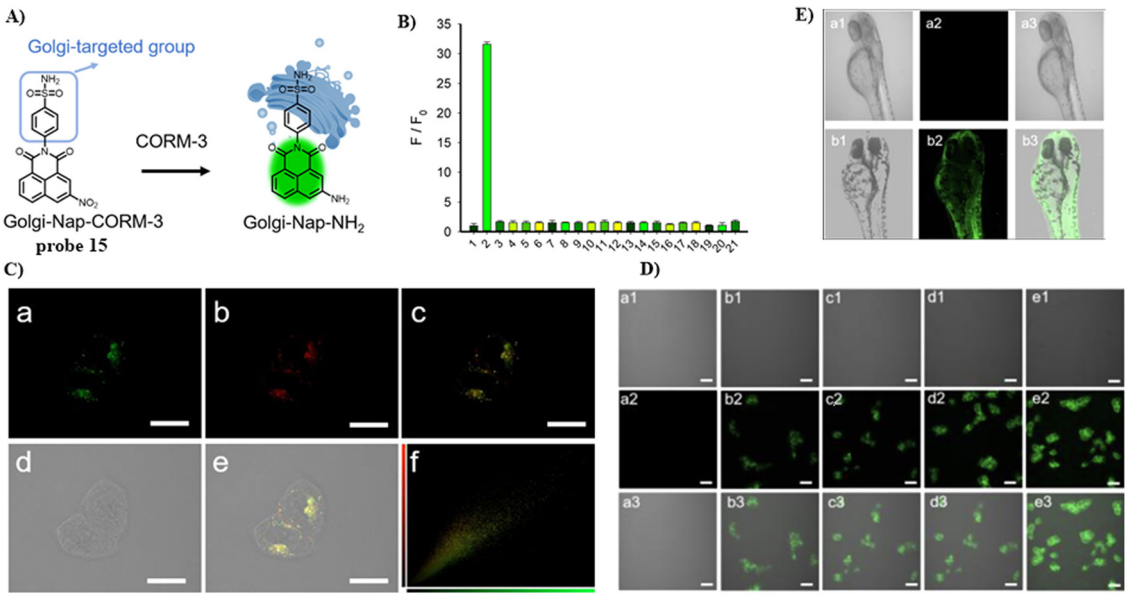

Fig. 14 (A) Probe **15** response mechanism. (B) Probe **15** fluorescence selectivity. (C) Co-localization of **15** and Golgi Tracker Red. (C) Confocal fluorescence images of HeLa cells. (E) Confocal fluorescence images of zebrafish. Reproduced with permission from ref. 69. Copyright 2022, American Chemical Society.

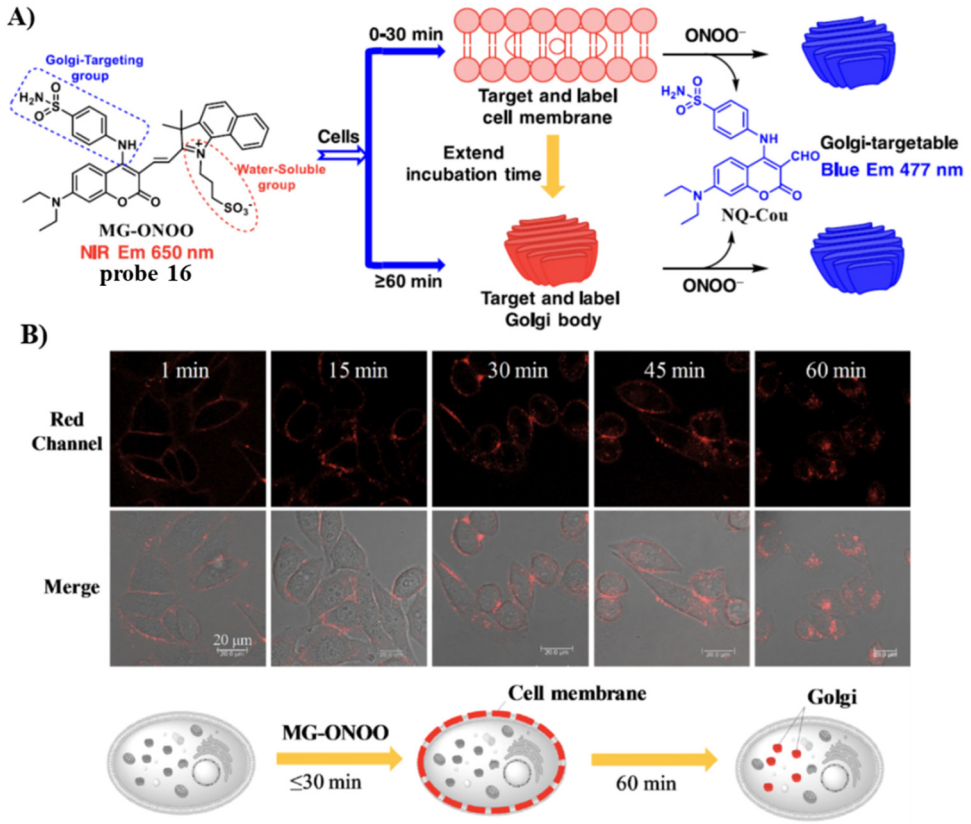

Fig. 15 (A) Membrane and Golgi-targeting fluorescent probe **16** for the ratiometric detection of $ONOO^-$. (B) HeLa cell imaging with **16** at varying times. Reproduced with permission from ref. 70. Copyright 2022, Elsevier.

site, integrated with a naphthalimide fluorophore and Golgi-targeting phenylsulfonamide moiety. Probe **14** exhibits a turn-on response due to the formation of a hydrazone and suppression of PeT and was suitable for the imaging of breast cancer cells (Fig. 13).[68]

In 2022, the He group developed a Golgi-targeting fluorescent probe **15** for the detection of CO-releasing molecule-3 (CORM-3), with a naphthalimide fluorophore, and Golgi-targeting phenyl sulfonamide group, in addition a CORM-3-responsive nitro group was incorporated into the probe (Fig. 14).[69] Probe **15** was used to monitor changes of CORM-3 in zebrafish, HepG2 and HeLa cells.

In 2022, the Feng group developed a Golgi-targeting fluorescent probe **16** for $ONOO^-$, generated by linking a Golgi-targeting sulfanilamide group with a conjugated hemicyanine and coumarin.[70] Probe **16** exhibited good sensitivity and selectivity rapid response for $ONOO^-$ and distinct ratiometric fluorescence changes and exhibited low cytotoxicity. Significantly, probe **16** can target the cell membrane and then the Golgi apparatus, making it suitable for detecting $ONOO^-$ in the Golgi and also cell membranes, the probe could be used to observe fluctuations of $ONOO^-$ during oxidative stress of the Golgi and in drug-induced liver injury (DILI) (Fig. 15).

Using a quinolinemalononitrile based fluorophore, benzenesulfonamide targeting group, and a pinacol boronate ester as the recognition site the Ye group developed a AIE Golgi-

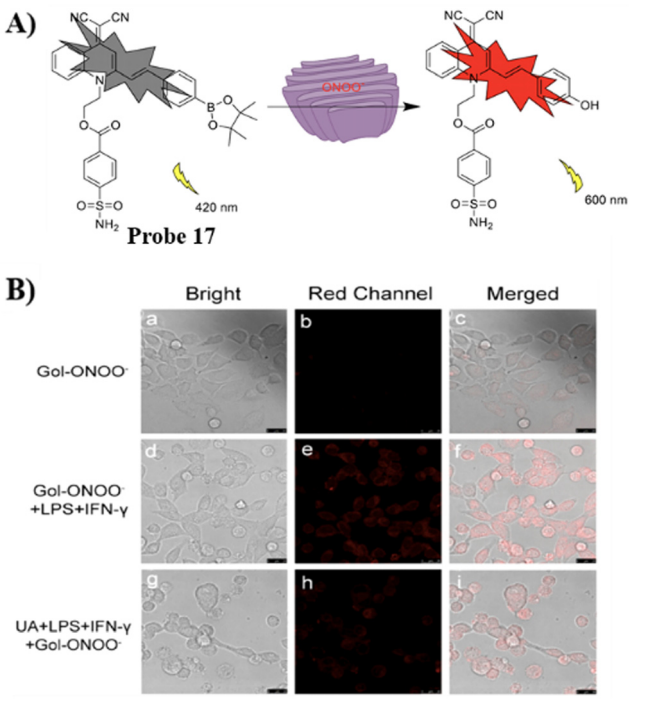

Fig. 16 (A) Possible reaction mechanism of **17** for detecting $ONOO^-$. (B) Fluorescence imaging of probe **17** for endogenous $ONOO^-$. Reproduced with permission from ref. 71. Copyright 2022, Elsevier.

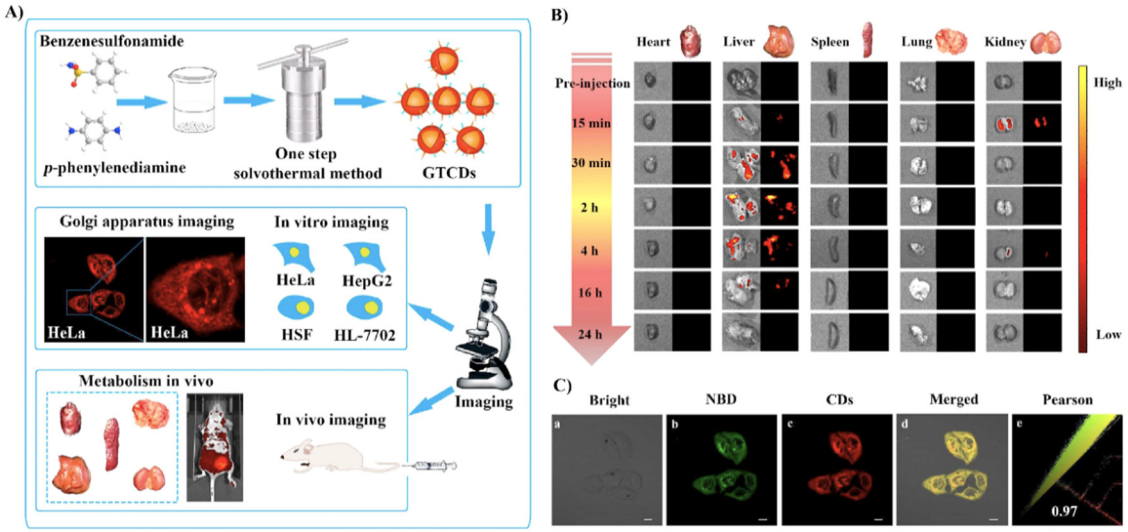

Fig. 17 (A) Synthesis and biological characterization of **18**. (B) Optical and *ex vivo* fluorescence imaging of BALB/c mice organs at different treatment times with **18**. (C) Co-localization cell imaging of **18** and NBD. Reproduced with permission from ref. 72. Copyright 2022, Elsevier.

targeting probe **17** to detect $ONOO^-$ in cells.[71] Probe **17** exhibits a rapid response, good selectivity, large Stoke's shift and low detection limit. As such, the probe was used to detect endogenous and exogenous $ONOO^-$ in HeLa cells, and for monitoring the levels of $ONOO^-$ in the Golgi apparatus during monensin-induced oxidative stress (Fig. 16).

Using hydrogen bonding between the COX-2 and benzenesulfonamide groups, the Yang group developed Golgi-targeting orange-emitting carbon dots (**18**) to image and monitor the Golgi apparatus. The carbon dots were prepared from *p*-phenylenediamine and benzenesulfonamide using one-step solvothermal methods. Probe **18** exhibits low toxicity and was suitable for imaging over 200 min (Fig. 17).[72]

In 2022, using a NIR rhodamine derivative as the fluorophore and *p*-methoxylbenzsulfamide as the targeting group, the Wang group developed a Golgi-targeting fluorescent probe **19** to detect changes in pH.[73] The probe exhibits pH-dependent sensing behavior from pH 7.4–3.0 at 664 nm with a remarkable fluorescence "off–on" responses and a p*K*a value of 3.62. The probe selectively diffused into Golgi and was successfully used for visualizing and real-time tracking of Golgi pH variations in living cells (Fig. 18).

Using naphthalimide as the fluorescent core and a nitro group as the response group, attached to a Golgi targeting sulfonamide group, the Lin group developed a Golgi-targeting fluorescent probe **20** (Gol-NTR) for detecting nitroreductase (NTR).[74]

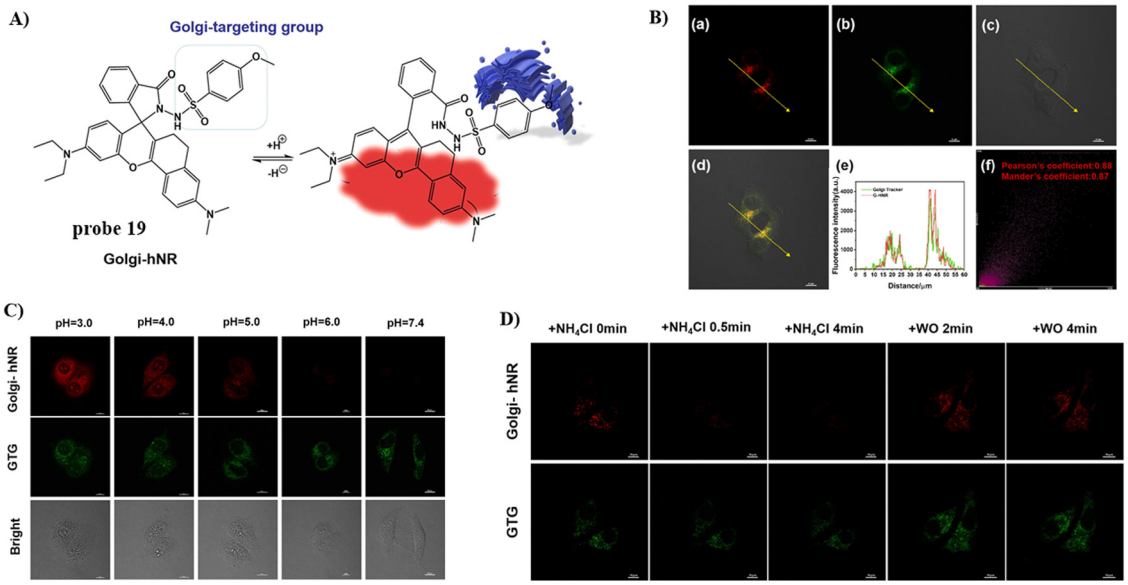

Fig. 18 (A) Possible reaction mechanism of **19** for pH. (B) Co-localization cell imaging of **19** and Golgi Tracker Green. (C) Fluorescence imaging using probe **19** for pH. (D) Visual monitoring of the pH changes upon different stimulations in the Golgi apparatus. Reproduced with permission from ref. 73. Copyright 2022, Elsevier.

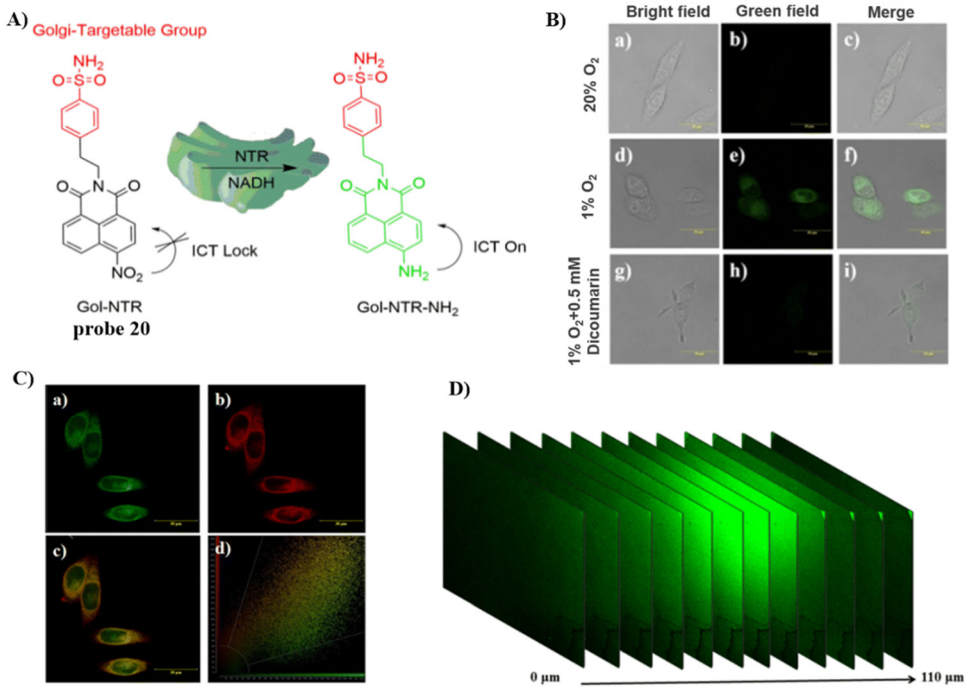

Fig. 19 (A) Structure and possible mechanism of **20** for monitoring NTR. (B) Fluorescence imaging of NTR using probe **20** in HeLa cells. (C) Co-localization cell imaging of **20** and Golgi Tracker Red. (D) Two-photon fluorescence imaging of NTR in live tumor tissue sections. Reproduced with permission from ref. 74. Copyright 2022, The Royal Society of Chemistry.

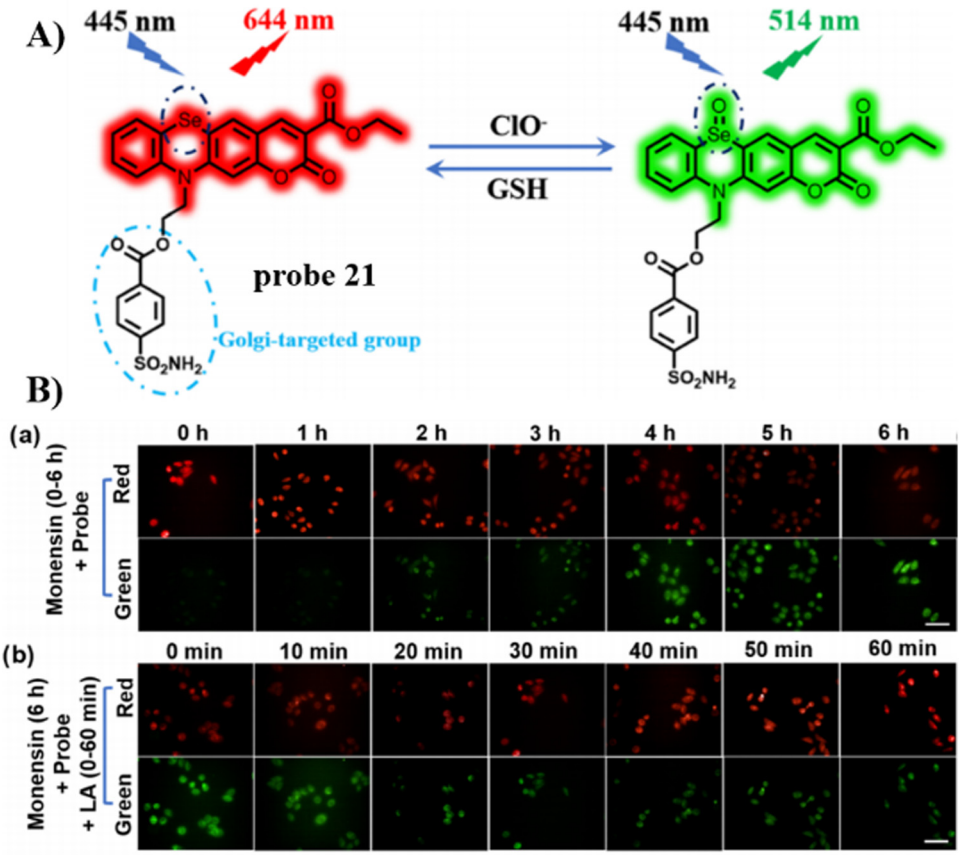

Fig. 20 (A) Possible reaction mechanism of **21** for sensing ClO^-/GSH redox pair. (B) Fluorescence images of HeLa cells undergoing different treatments. Reproduced with permission from ref. 75. Copyright 2023, American Chemical Society.

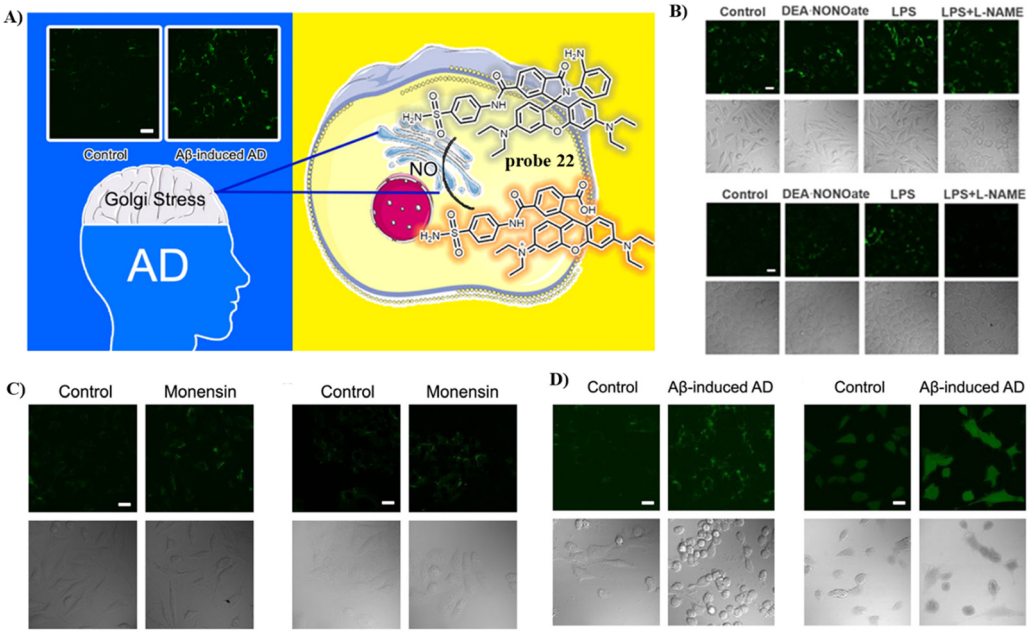

Fig. 21 (A) Structure and possible reaction mechanism of **22** for monitoring NO. (B) Confocal fluorescence images exogenous NO of SH-SY5Y (upper) cells and HepG2 (down) cells. (C) Confocal fluorescence images of SH-SY5Y (left) cells and HepG2 (right) cells during Golgi stress. (D) Confocal fluorescence images of SH-SH5Y cells with Golgi-NO (left) and DAF-DA (right) in the cellular AD model. Reproduced with permission from ref. 76. Copyright 2022, American Chemical Society.

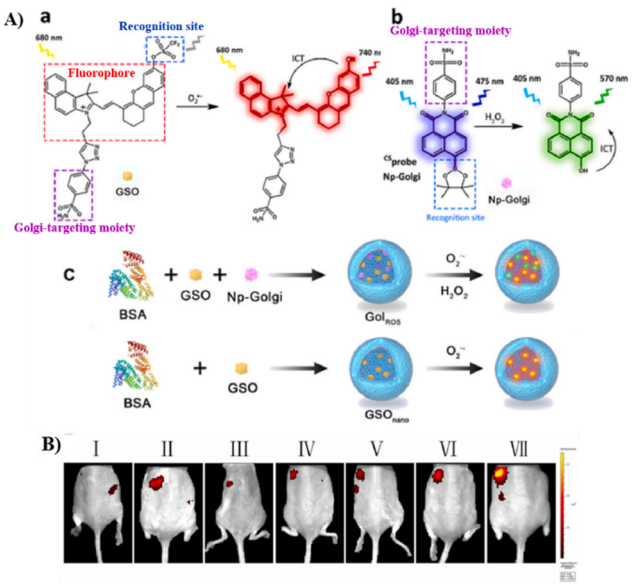

Fig. 22 (A) (a) Hemicyanine probe GSO and response mechanism towards $O_2^{\bullet-}$. (b) The structure of Np-Golgi (probe **8**) and the response towards H_2O_2. (c) **23** and GSO_{nano} preparation and response mechanism. (B) Fluorescence imaging of control mice (I), therapeutic group mice (II: hydrochlorothiazide, III: hydrochlorothiazide + tiron, IV: tiron, V: reserpine + tiron, VI: reserpine) and hypertension mice (VII). Reproduced with permission from ref. 77. Copyright 2022, Elsevier.

The probe exhibits high biocompatibility, good photostability, high sensitivity and selectivity for NTR recognition, and was used to detect NTR in the Golgi apparatus. Consequently, the Golgi apparatus state could be monitored under different oxygen levels *via* the detection of NTR (Fig. 19).

In 2023, the Song group developed a dual-functional, reversible, and ratiometric fluorescent probe **21** with coumarin fluorophore, benzenesulfonamide for Golgi-targeting, and selenium (Se) as the recognition site.[75] Probe **21** could evaluate dynamic changes of Golgi oxidative stress by monitoring dynamic changes in the ClO^-/GSH-mediated redox state in HeLa cells with rapid response, high selectivity, high sensitivity and low detection limit. More importantly, the probe facilitates the monitoring of the progression acute lung injury through the imaging of the dynamic redox state (Fig. 20).

The Ma group incorporated a 4-sulfamoylphenylamide group as a Golgi-targeting moiety with 6-carboxyrhodamine B containing an *o*-diaminobenzene NO recognition moiety to generate the Golgi-targeting fluorescent probe **22** for imaging and monitoring NO in the Golgi apparatus.[76] Probe **22** exhibits accurate Golgi-targeting and high selectivity towards NO, and thus was used to monitor increases of NO in the Golgi apparatus of an AD model, providing an appropriate means for studying the function of NO in the Golgi apparatus during disease progression (Fig. 21).

Phenylsulfonamide-modified and bovine serum albumin (BSA) encapsulated probes have been shown to exhibit excellent Golgi-targeting ability. Recently, the Tang group developed a Golgi-targeting NIR fluorescent probe GSO for the *in situ* detection of $O_2^{\bullet-}$ in the Golgi which was constructed using phenylsulfonamide as the Golgi-targeting group, a hemi-cyanine as the NIR fluorophore, and a trifluoromethanesulfonate group as the recognition site for $O_2^{\bullet-}$. The fluorescent probe **23** (Gol_{Ros})

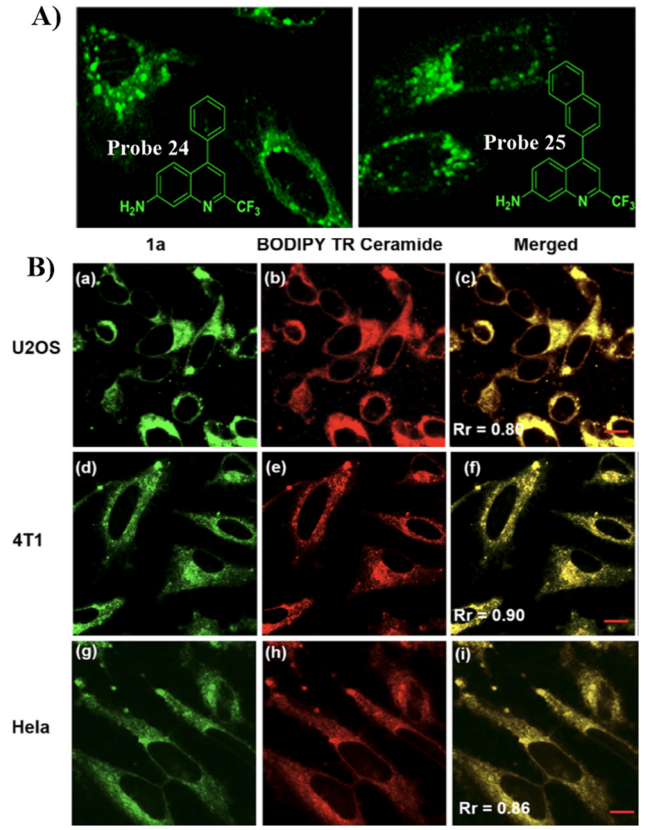

Fig. 23 (A) Schematic illustration of GA targeting quinoline fluorophore. (B) Co-localization cell imaging of **24** and BODIPY TR ceramide. Reproduced with permission from ref. 91. Copyright 2019, American Chemical Society.

was then prepared by encapsulating GSO and Np-Golgi (probe **8**) with BSA (1 : 2).[77] The probe was successfully used for the simultaneous multicolored detection of both Golgi H_2O_2 and $O_2^{\bullet-}$ in cells and in hypertensive mice, for the evaluation of various antihypertensive drugs, and for the identification of post-transcriptional modification sites on dihydrofolate reductase (DHFR) induced by the ROS. Moreover, the system is suitable for exploring the eNOS-associated oxidative stress signaling pathway in inflammation-induced hypertension (Fig. 22).

3.3 Probes with 2-trifluoromethyl-7-aminoquinoline group

Quinoline derivatives have been extensively used for the assembly of fluorescent probes owing to the excellent fluorescent properties. However, applications in probing organelles have been rarely explored. Quinoline primarily fluoresces in the near ultraviolet region, and its absorption and emission signals can be migrated to longer wavelengths by structural adjustment. Moreover, for quinoline derivatives the pyridyl moiety perfectly matches the slightly acidic (6.0–6.7) environment in the Golgi apparatus, making it excellent for Golgi-targeting.[90] In 2019, the Chen group developed a dual-functional 2-trifluoromethyl-7-aminoquinoline fluorophore, which exhibits strong intramolecular charge-transfer fluorescence with large Stokes shifts due to the presence of amino group and trifluoromethyl group. The 2-trifluoromethyl-7-aminoquinoline group is not only Golgi-targeting but also contains an amine group that can be used to construct a wide range of fluorescent probes **24**/**25** (Fig. 23).[91] Both Scheme 4 and Table 3 highlight Golgi-targeting probes using 2-trifluoromethyl-7-aminoquinoline as a functional motif and their applications.

In 2020, the Zhu group developed a Golgi-targeting and Cys-specific probe **26** where a dithioester was selected as the receptor for Cys, and a quinoline derivative was selected as the fluorophore as well as the targeting group for the Golgi apparatus (Fig. 24).[92] In addition to exhibiting sensitivity to

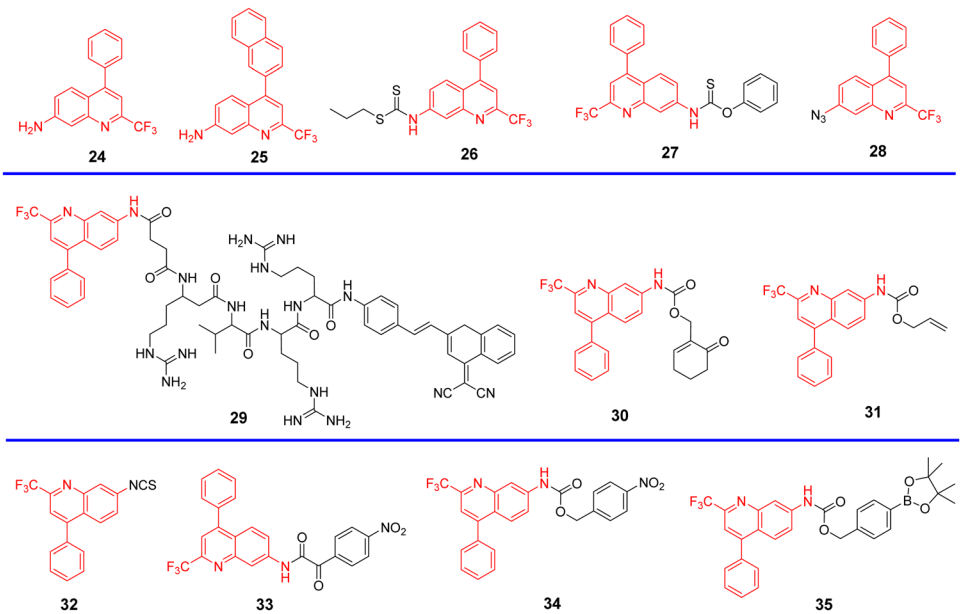

Scheme 4 Golgi-targeting probes with 2-trifluoromethyl-7-aminoquinoline. Red indicates the Golgi-targeting unit.

Table 3 Golgi-targeting fluorescent probes with 2-trifluoromethyl-7-aminoquinoline as functional motif

Probe	Analyte	$\lambda_{ex}/\lambda_{em}$ (nm)	Detection range	LOD	Pearson's correlation coefficient	Application	Ref.
24, 25	—	389 nm/507 nm 392 nm/513 nm	—	—	0.90	Golgi apparatus localization	91
26	Cys	390 nm/515 nm	0–10 μM	105 nM	0.92	Imaging in live cells and zebrafish	92
27	Cys	390 nm/518 nm	0–40 μM	51 nM	0.91	Imaging in live cells and zebrafish	93
28	H_2S	375 nm/515 nm	0–30 μM	0.11 μM	0.94	Imaging in live cells and zebrafish	94
29	Furin	350, 470 nm/420, 640 nm	0–500 U mL^{-1}	0.265 U mL^{-1}	0.84, 0.80	Imaging in live cells	95
30	GSH	320 nm/425, 510 nm	0–75 μM	0.388 U mL^{-1}	0.92, 0.85, 0.92	Imaging in live cells	96
31	CO	360 nm/425, 520 nm	0–10 μM	0.49 μM	0.81	Imaging in live cells and zebrafish	97
32	Cys	405 nm/520 nm	0–40 μM	41 nM	0.913, 0.906, 0.924	Imaging in live cells and zebrafish	98
33	$ONOO^-$	405 nm/490 nm	0–30 μM	115 nM	0.81	Imaging in live cells and mice	99
34	—	405 nm/450 nm	—	57 nM	0.99	Monitoring and assessing treatment response of sepsis-induced ALI	100
35	H_2O_2	760 nm/820 nm	0–40 μM	54.8 ng mL^{-1}	0.98	Imaging in live cells and zebrafish	101

native Cys in zebrafish and cells, the monitoring of Cys levels during Golgi stress was achieved.

By substituting the dithioester with thionobenzoate, the Zhu group explored a Golgi targeting Cys-specific probe **27** for detecting the generation of Cys in response to Golgi stress. Thionobenzoate was used as the recognition group, with the 4-CF_3-7-aminoquinoline dye chosen as the fluorophore and Golgi targeting unit (Fig. 25).[93] Probe **27** exhibited good sensitivity to both exogenous and endogenous Cys during biological imaging.

Similarly, by using the quinoline moiety as the Golgi-targeting group/fluorophore and, and azido unit as a H_2S recognition site, the group of Zhu developed a Golgi-targeting H_2S probe **28**, which responds sensitively to H_2S in the Golgi apparatus of both zebrafish and cells. *In situ* visualization of H_2S under Golgi stress was achieved using a specific-Golgi stressor (Fig. 26).[94]

In 2021, the Liang group integrated the principles of intramolecular charge transfer (ICT) and fluorescence resonance energy transfer (FRET). A quinoline dye was chosen as a Golgi-targeting fluorophore and donor, while a dicyanomethylene-4H-pyran (DCM) was chosen as the acceptor fluorophore. The quinoline and DCM were linked using a Arg-Val-Arg-Arg (RVRR)

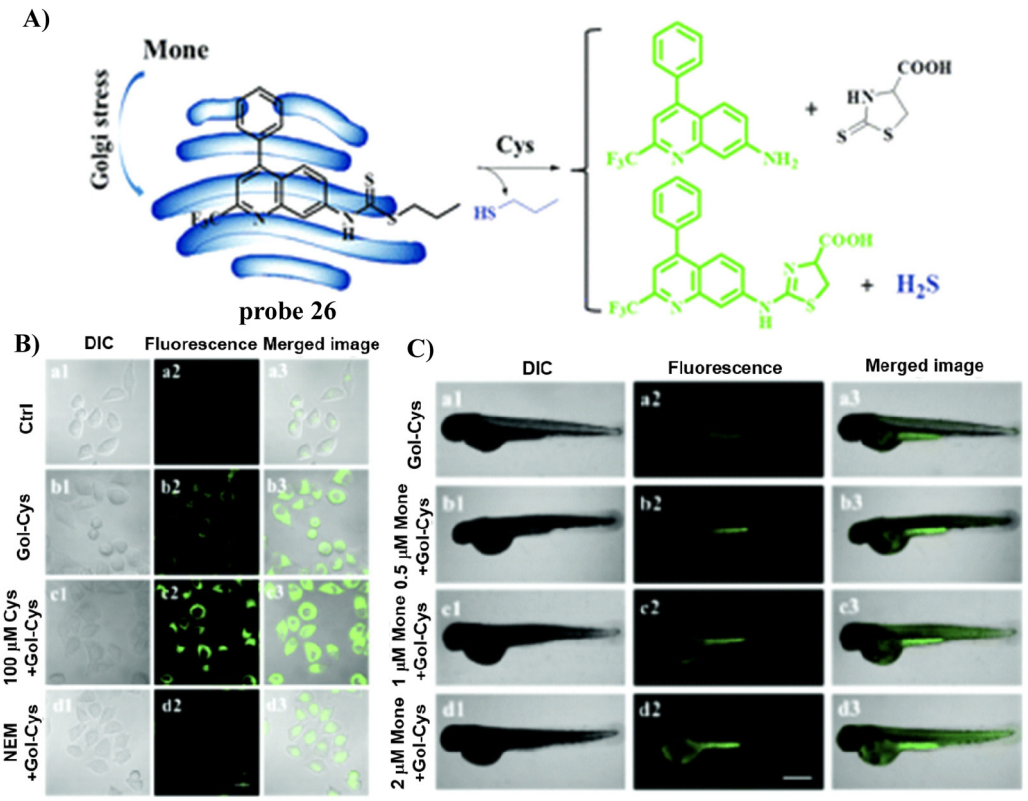

Fig. 24 (A) Probe **26** response mechanism for Cys. (B) Fluorescence images of HeLa cells. (C) Confocal microscopic images of Cys changes during Golgi stress in zebrafish. Reproduced with permission from ref. 92. Copyright 2020, The Royal Society of Chemistry.

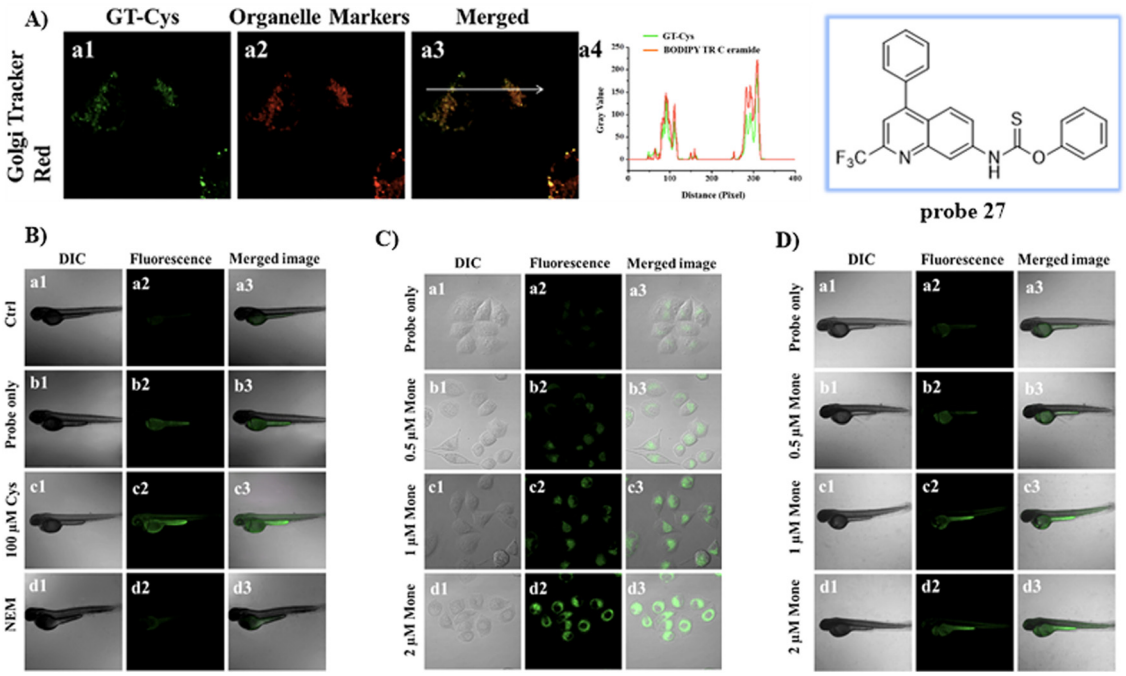

Fig. 25 (A) Co-localization cell fluorescence imaging of **27** and Golgi Tracker Red. (B) Confocal fluorescence images of zebrafish. (C) Confocal microscopic images for detection of Cys production during Golgi stress in HeLa cells. (D) Confocal microscopic images for detection of Cys production during Golgi stress in zebrafish. Reproduced with permission from ref. 93. Copyright 2020, Elsevier.

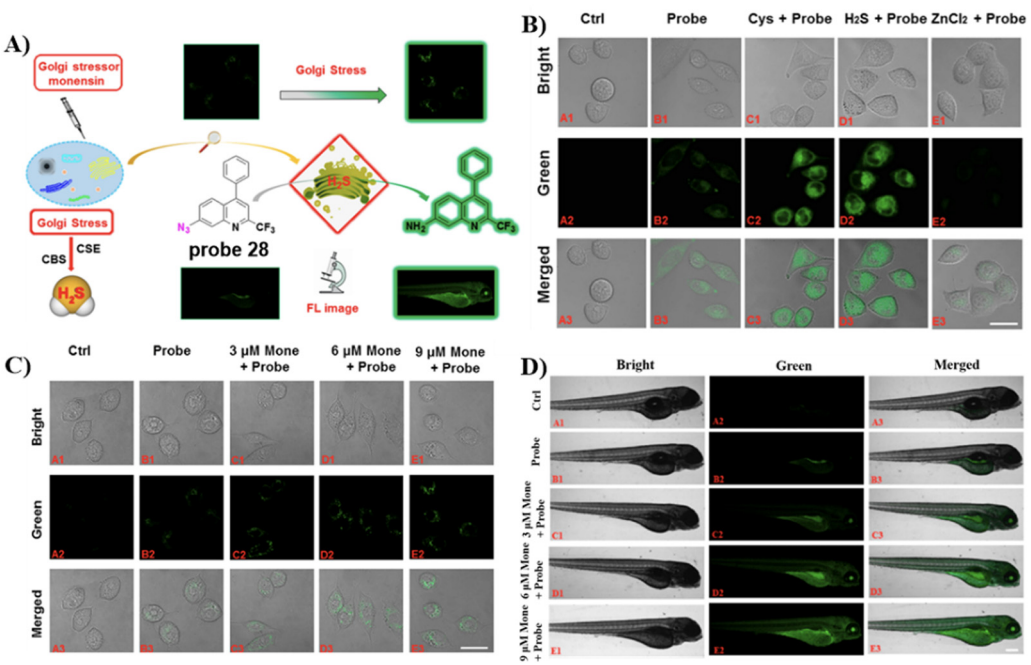

Fig. 26 (A) Response of probe **28** for H_2S. (B) Cell fluorescence imaging by probe **28**. (C) Golgi stress response results in cells. (D) Zebrafish imaging of probe **28**. (E) Golgi stress response results in zebrafish. Reproduced with permission from ref. 94. Copyright 2020, American Chemical Society.

peptide, to generate a FRET system. Which resulted in a Golgi-targeting and dual-emission "Turn-On" probe **29** for the imaging of intracellular furin. As a result of FRET between quinoline and DCM and inhibition of the intramolecular charge transfer (ICT), probe **29** was initially nonfluorescent but was activated upon amide bond cleavage, generating Q-RVRR and DCM-NH_2, which resulted in fluorescence "Turn-On" at 420 and 640 nm (Fig. 27).[95]

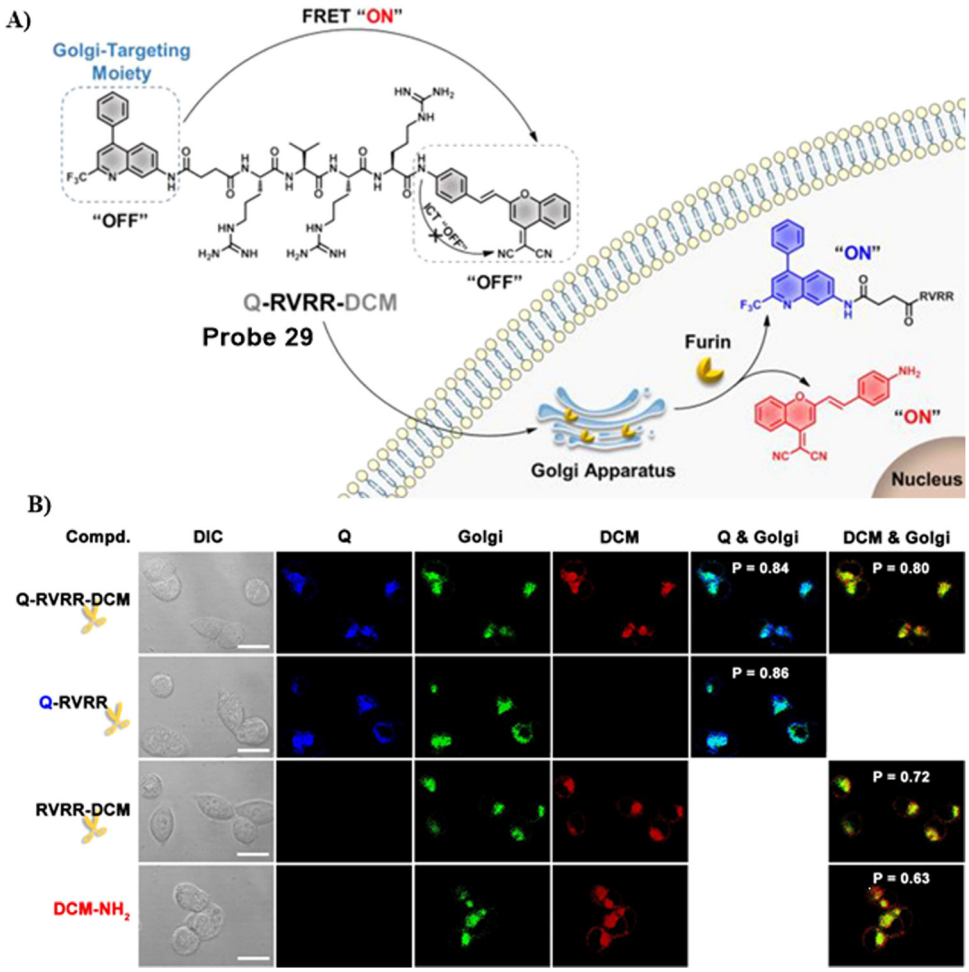

Fig. 27 (A) Response of probe **29** for Furin. (B) Co-localization cell imaging. Reproduced with permission from ref. 95. Copyright 2021, American Chemical Society.

In 2021, the Zhu group developed a ratiometric fluorescent Golgi-targeting probe **30** for GSH constructed using 4-CF_3-7-aminoquinoline as a Golgi-targeting fluorophore containing an anticancer drug and GSH responsive receptor. Probe **30** reacted with GSH, releasing the drug in the Golgi to kill cancerous cells. Ratiometric probe **30** was able to selectively and sensitively trace changes of GSH concentration during Golgi stress in living cells. This GSH-responsive fluorescent probe exhibiting Golgi-targeting and therapeutic effects provides an approach for monitoring changes of GSH concentration in the Golgi apparatus and for precise disease treatments (Fig. 28).[96]

In 2021, the group of Feng developed a Golgi-targeting fluorescent probe **31** using a aminoquinoline as both the Golgi-targeting group and fluorophore for the selective and sensitive imaging of CO based on the Tsuji–Trost reaction. The probe exhibited excellent Golgi-targeting ability and was used to ratiometricaly image exogenous and endogenous CO in zebrafish and cells, Moreover, probe **31** could be used for visually monitoring increases in CO of living cells under oxidative stress (Fig. 29).[97]

By integrating an isothiocyanate (cysteine recognition site) with an aminoquinoline (fluorophore and Glogi-targeting group), the Zhu group developed a specific and sensitive fluorescent cysteine (Cys) probe **32** in 2022, which exhibited low cytotoxicity for the imaging of exogenous and endogenous cysteine in zebrafish and cells. In addition, it was used to confirm that cystathionine γ-lyase enzyme plays a critical role in the generation of Cysteine (Fig. 30).[98]

By combining the Golgi-targeting aminoquinoline fluorophore with α-keto acid $ONOO^-$ reaction site, the Jiang group developed a Golgi-targeting fluorescent probe **33** for monitoring $ONOO^-$ production during Golgi stress in a sepsis-induced acute lung injury (ALI) model.[99] The probe exhibited good selectivity and high sensitivity towards $ONOO^-$ and as such was used for monitoring increases of $ONOO^-$ in the Golgi apparatus of live cells generated by different stimuli. Moreover, significant increases in $ONOO^-$ levels in the Golgi apparatus were observed in mice during sepsis-induced ALI (Fig. 31).

The Jiang group developed another Golgi-targeting fluorescent probe **34** by anchoring a NTR-sensitive *p*-nitrobenzyl moiety to a Golgi-targeting aminoquinoline fluorophore, for the accurate monitoring and assessment of sepsis-induced ALI. The probe exhibited good selectivity and high sensitivity with a

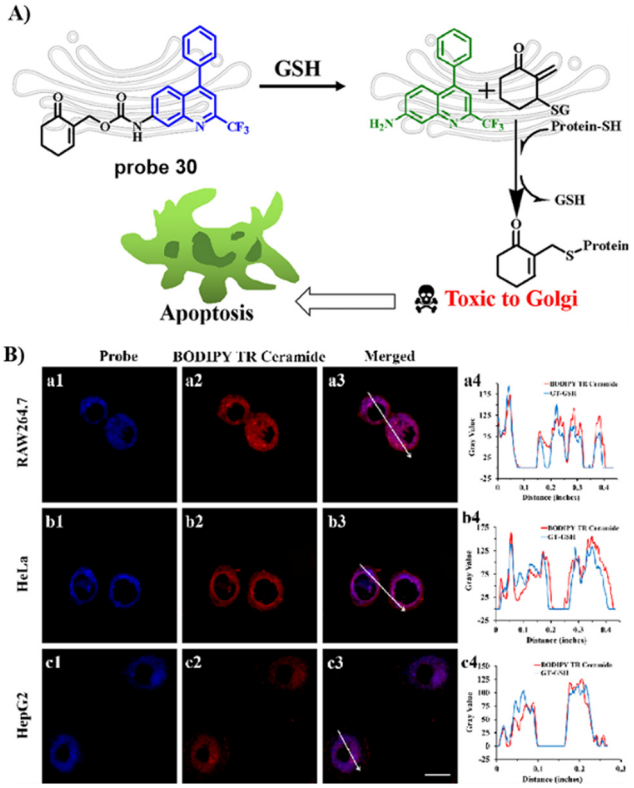

Fig. 28 (A) Response and cancer therapeutic effect of probe **30** towards GSH. (B) Fluorescence imaging of HeLa cells. Reproduced with permission from ref. 96. Copyright 2021, American Chemical Society.

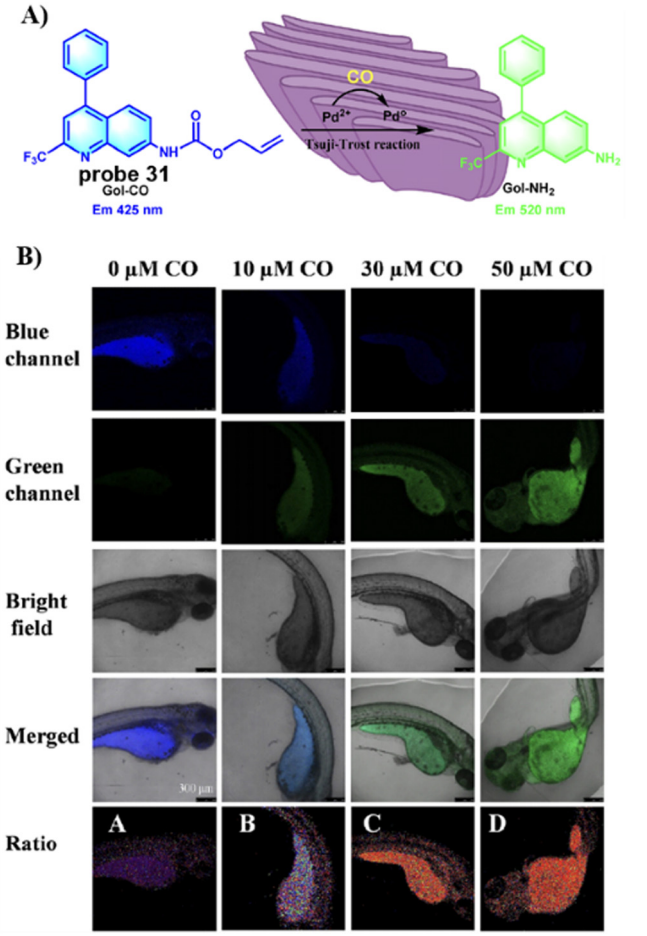

Fig. 29 (A) Response of probe **31** for CO. (B) CO fluorescence imaging in zebrafish with **31**. Reproduced with permission from ref. 97. Copyright 2021, Elsevier.

LOD of 54.8 ng mL^{-1}.[100] As such, the probe could be used for tracking the enhancement NTR in the Golgi of zebrafish and cells under the action various stimuli. Golgi NTR production in sepsis-induced ALI and the prolyl hydroxylase (PHD) inhibitor (dimethyloxalylglycine, DMOG) for combating sepsis-induced ALI could be monitored using GoI-NTR (Fig. 32).

Recently, the Wu group developed a novel Golgi-targeting and H_2O_2-specific ratiometric fluorescent probe **35** where a borate ester was chosen as the H_2O_2 recognition site, and an aminoquinoline derivative was selected as the fluorophore as well as the targeting group for the Golgi apparatus.[101] the probe could be employed to monitor endogenous/exogenous H_2O_2 in zebrafish and cells using one-photon or two photon confocal imaging, and exhibited high selectivity, low toxicity and exceptional photostability. As such probe **35** represents an useful tool for monitoring H_2O_2 levels in biological environments (Fig. 33).

3.4 Probes with L-Cys group

Cys is the main biothiol found in living organisms, involved in many physiological and pathological processes, and plays an important role in maintaining the redox stability of biological systems. Some physiological and pathological processes (such as aging, neurological decline) are associated with changes in oxidation/antioxidant balance and Cys content. It has been reported that both galactosyltransferase and protein kinase D are able to anchor to the Golgi apparatus using Cys residues or Cys-rich domains,[102,103] since the Cys thiol group is able to bind with a thiol groups of the Golgi through the generation of disulphide bonds in the oxidizing environment of the Golgi lumen,[22,104] thus inspiring researchers to use a cysteine targeting strategy to develop optical imaging probes for the early disease diagnosis and Golgi-related disease therapeutics. Scheme 5 and Table 4 highlight Golgi-targeting probes using Cys as the functional motif and illustrates their applications.

Using L-Cys as the Golgi-targeting group, and a caffeic acid group as the $O_2^{\bullet-}$ response site, the Tang group in 2019 developed a fluorescent Golgi-targeting probe **36** for the dynamic and reversible detection of $O_2^{\bullet-}$. Enhanced levels of $O_2^{\bullet-}$ in addition to an increase of caspase-2 activity and apoptosis were identified in the Golgi apparatus of an ischaemia-reperfcfusion (IR) mouse liver, indicating that the tumor necrosis factor (TNF-α) acts as a positive mediator for $O_2^{\bullet-}$ generation. These results illustrate how the Golgi could potentially mediate $O_2^{\bullet-}$ variations in IR mice and illuminated the related molecular mechanisms (Fig. 34).[105]

In 2019, the Tang group developed a NIR fluorescent Golgi-targeting probe **37** for visualizing polarity, in which **37** can aggregate in the Golgi apparatus with the help of cysteine, and

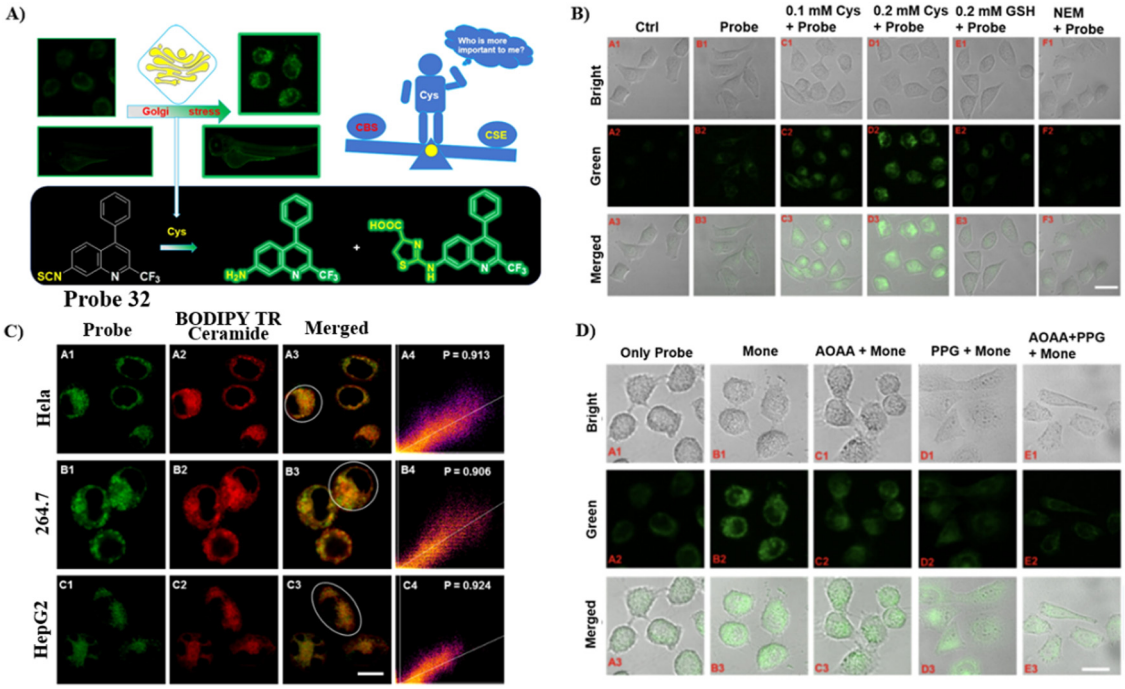

Fig. 30 (A) Response of probe **32** to Cys. (B) Cys imaging in cells using **32**. (C) Co-localization cell imaging. (D) Fluorescence imaging for the inhibition of endogenous Cys with **32**. Cells treated with probe **32** only (A). Cells treated with monensin and probe **32** in turn (B). Cells treated by AOAA, monensin and probe **32** in turn (C). Cells treated by PPG, monensin and probe **32** in turn (D). Cells treated by AOAA, PPG then incubated by monensin, probe **32**. Reproduced with permission from ref. 98. Copyright 2022, Elsevier.

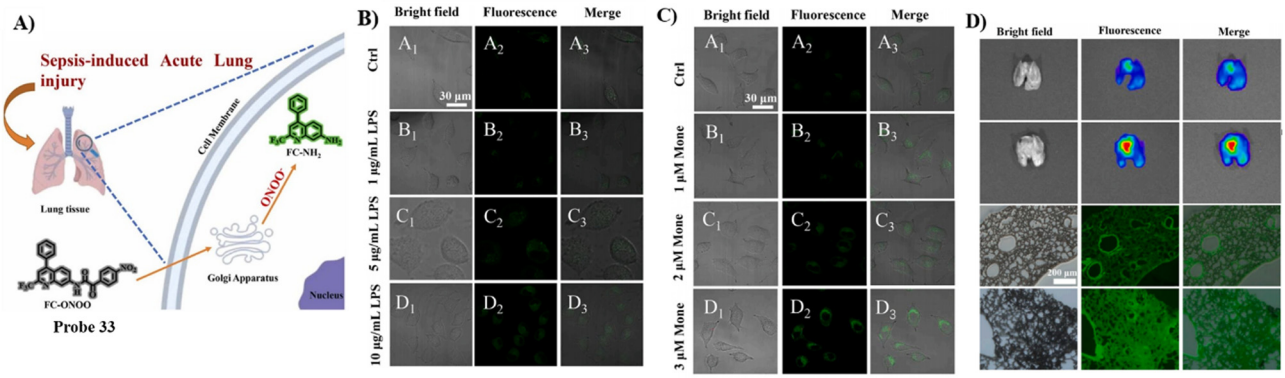

Fig. 31 (A) Probe **33** response for $ONOO^-$. (B) Imaging of exogenous and endogenous $ONOO^-$ in A549 cells. (C) Imaging of $ONOO^-$ under Golgi stress in A549 cells. (D) Fluorescence images of **33** stained lung organs and slices of control group mice and LPS group mice. Reproduced with permission from ref. 99. Copyright 2022, Elsevier.

the benzoyl difluoroboronate and merocyanine units are able to detect changes of polarity. Probe **37** exhibited not only excellent sensitivity and selectivity towards changes in polarity, but also good biocompatibility. Probe **37** was used for monitoring polarity differences between normal and cancerous cell lines and tracking changes of polarity on glutamate-stimulation of PC12 cells, in order to discover the inter-relationship between the polarity of the Golgi and the depression phenotype. Furthermore, the results indicated that an elevation of polarity may be caused by the reduced synthesis of brain-derived neurotrophic factor (BDNF) (Fig. 35).[106]

Using a trityl protected cysteine as the Golgi-targeting group, which can be cleaved to release a latent Golgi-targeting L-Cys group, the Watkinson group developed a Golgi-targeting probe **38** to image mobile Zn^{2+}, which contains an *S*-trityl protected cysteine moiety introduced using 'click' chemistry, for the increased hydrophobicity and membrane permeability of probe **38**. The *S*-trityl protecting group was removed within 24 hours to release free Cysteine, and the probe was then anchored to the Golgi apparatus. The probe exhibited good Golgi-targeting ability, selectivity, and low cellular toxicity, good photophysical properties, and was used to monitor changes of mobile Zn^{2+}

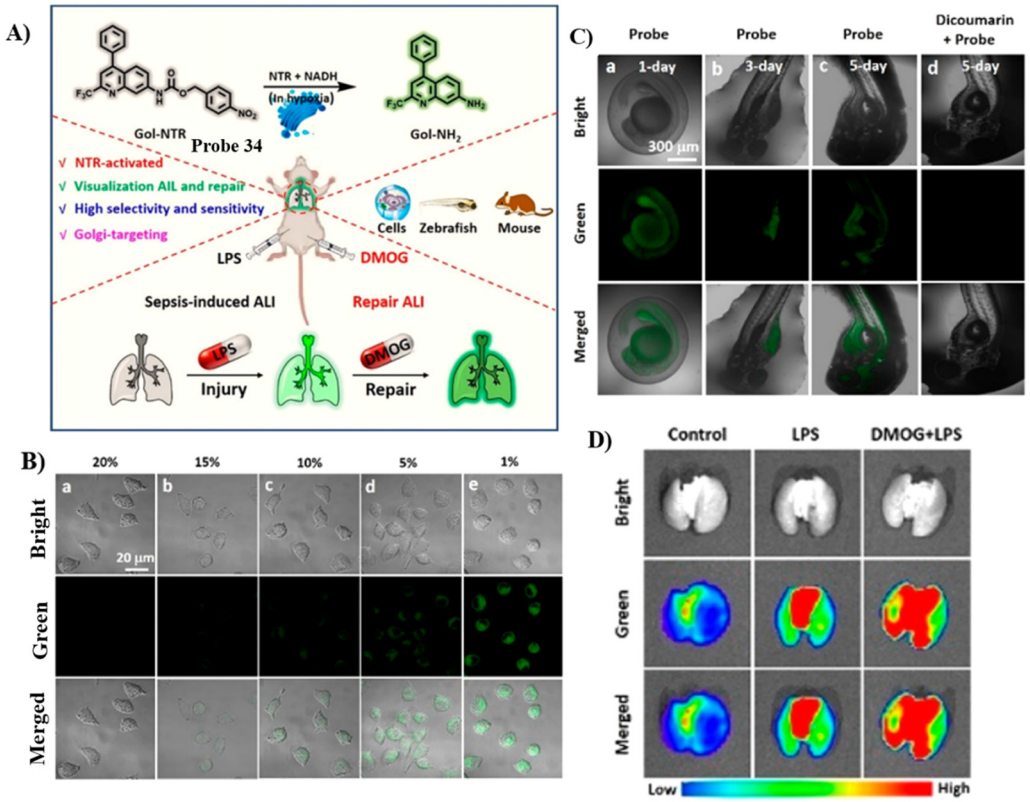

Fig. 32 (A) Probe **34** response for NTR. (B) Fluorescence images of NTR under normoxic (20% O_2) and various hypoxic (15%, 10%, 5%, and 1% O_2) conditions for 8 h, respectively. (C) Fluorescence images of NTR in living zebrafish cultured for different days (1–5 days). (D) Fluorescence imaging of lungs from the control group, LPS group, and DMOG + LPS group. Reproduced with permission from ref. 100. Copyright 2022, American Chemical Society.

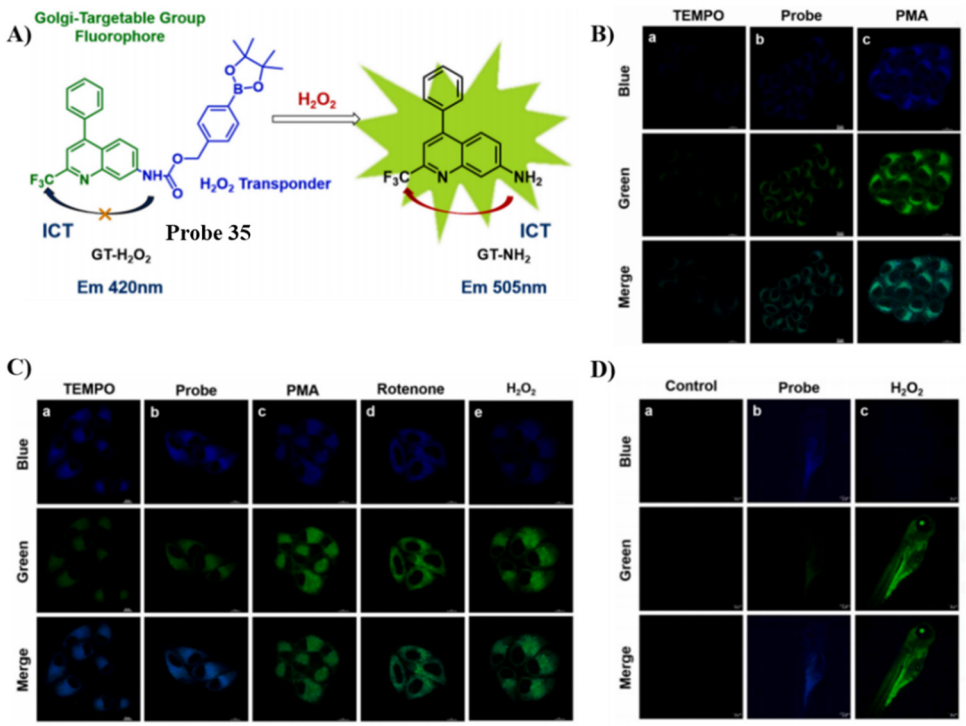

Fig. 33 (A) Probe **35** response mechanism. (B) Fluorescence images of probe **35** in HeLa cells. (C) Two-photon fluorescence images of probe **35** in HeLa cells. (D) Two-photon fluorescence images of probe **35** in zebrafish. Reproduced with permission from ref. 101. Copyright 2023, Elsevier.

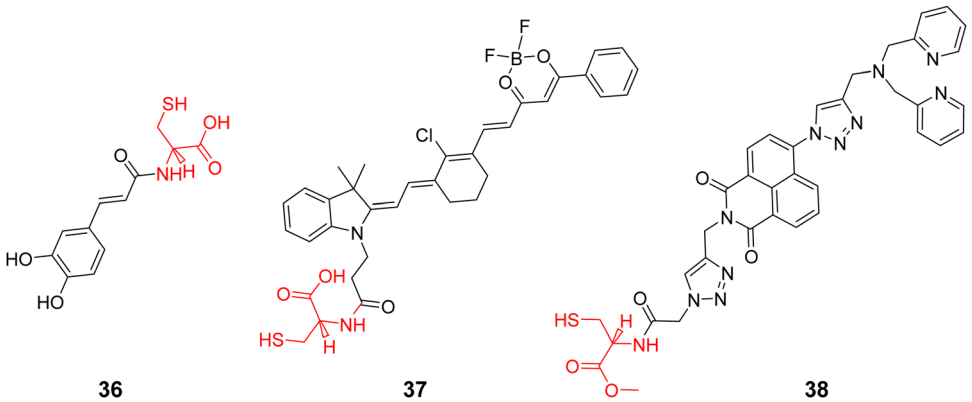

Scheme 5 Golgi-targeting probes with L-Cys as functional motif. Red indicates the Golgi-targeting unit.

Table 4 Golgi-targeting fluorescent probes with L-Cys as functional motif

Probe	Analyte	$\lambda_{ex}/\lambda_{em}$ (nm)	Detection range	LOD	Pearson's correlation coefficient	Application	Ref.
36	$O_2^{\bullet-}$	OP 370 nm/495 nm TP 800 nm/495 nm	—	—	0.93	Imaging in live cells and mice	105
37	Polarity	700 nm/800–825 nm	0–5 μM	18 nM	0.93	Imaging in live cells	106
38	Zn^{2+}	346 nm/414 nm			0.92	Imaging in live cells	107

levels in the the Golgi apparatus during H_2O_2 induced oxidative stress (Fig. 36).[107]

3.5 Probes with targeting peptides

Peptides are privileged biomolecules in nature and play essential roles in living systems. Because of their unique molecular structure, peptides have been widely used in drug discovery, disease diagnosis, fluorescence detection and materials science. Peptides with organelle-specific import or retention sequences, are able to enable probes to target the subcellular apparatus such as nucleus, the trans-Golgi network (TGN) or endoplasmic reticulum (ER), when anchored to the fluorophore of the probes. In addition, furin is a Golgi-resident protein that is overexpressed in cancer cells and is a good target for lighting up the Golgi of cancer cells. Furin can cleave the C-terminal of the amino acid motif Arg-X-Lys/Arg-Arg (X any amino acid), and therefore, fluorescence imaging of the Golgi apparatus can be performed using a furin cleavage strategy.[108–113] Both Scheme 6 and Table 5 highlight Golgi-targeting probes using peptides as functional motifs and their applications.

In 2016, the Lee group developed a Golgi-targeting probe **39** to detect Cu^+ by conjugating the N-terminal of a tripeptide (Leu-Leu-Cys) with a dansyl fluorophore, probe **39** formed a 1 : 1 complex with Cu^+ resulting in fluorescence "turn-on" response for Cu^+. Evaluation of the binding mode indicated the critical role played by the thiol group of the peptide receptor in the strong binding with Cu^+, with additional support from the sulfonamide and amide groups. Meanwhile, probe **39** was able to penetrate living RKO cells and detect Cu^+ in the Golgi apparatus (Fig. 37).[114]

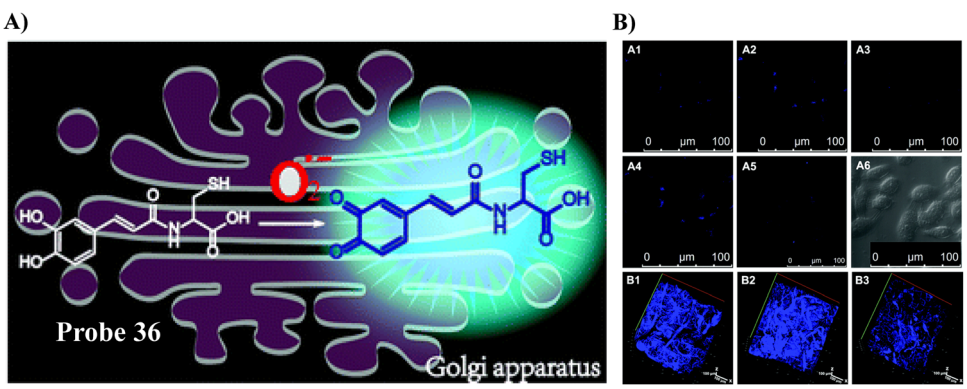

Fig. 34 (A) Response of probe **36** towards $O_2^{\bullet-}$. (B) Validation of **36** for the imaging of living cells and mice. Reproduced with permission from ref. 105. Copyright 2019, The Royal Society of Chemistry.

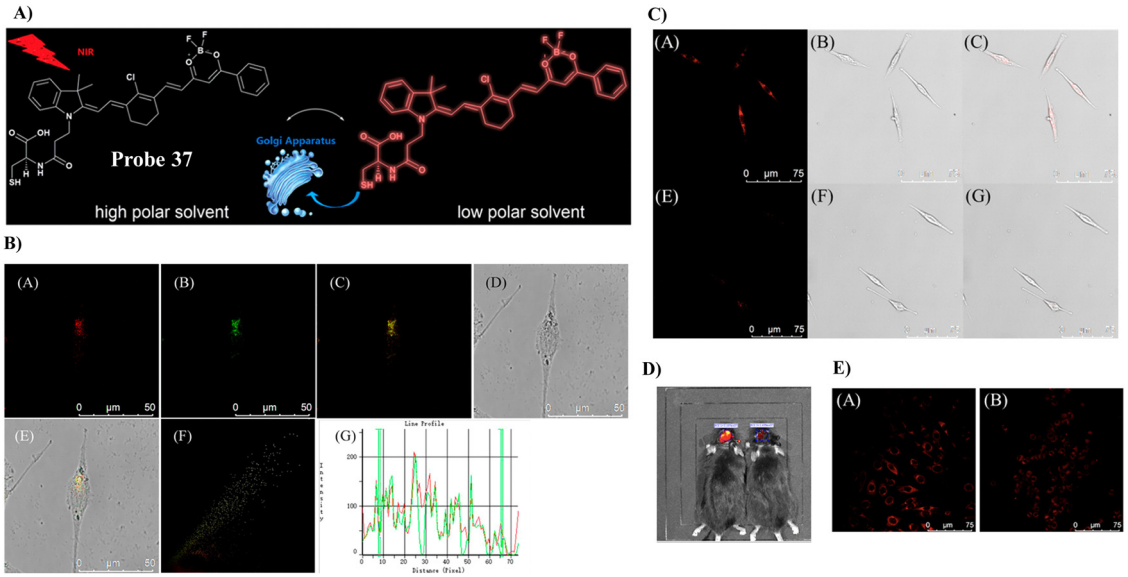

Fig. 35 (A) Response of probe **37** towards polarity. (B) Co-localization cell imaging of **37** and Golgi Tracker Red. (C) Imaging of polarity fluctuation in PC12 cells induced by excess glutamate. (D) Fluorescence image of the brains of mice with depression-like behavior. (E) Fluorescence images of PC12 cells using small interfering RNA (siRNA) to silence BDNF genes. Reproduced with permission from ref. 106. Copyright 2019, American Chemical Society.

In 2018, the Zhang group developed a Golgi-targeting probe **40** for the long-term *in situ* detection of endogenous furin activity. A furin-specific peptide (RVRR) was integrated with an insoluble solid-state fluorophore 6-chloro-2-(2-hydroxyphenyl)quinazolin-4(3*H*)-one through a self-immolative linker. Probe **40** exhibited high sensitivity and selectivity towards furin and released the free fluorophore, which precipitated in proximity to the enzyme active site and emitted bright solid-state fluorescence enabling *in situ* imaging. Probe **40** was able to realize the long-term bioimaging of intracellular furin, and was used to monitor the changes of furin

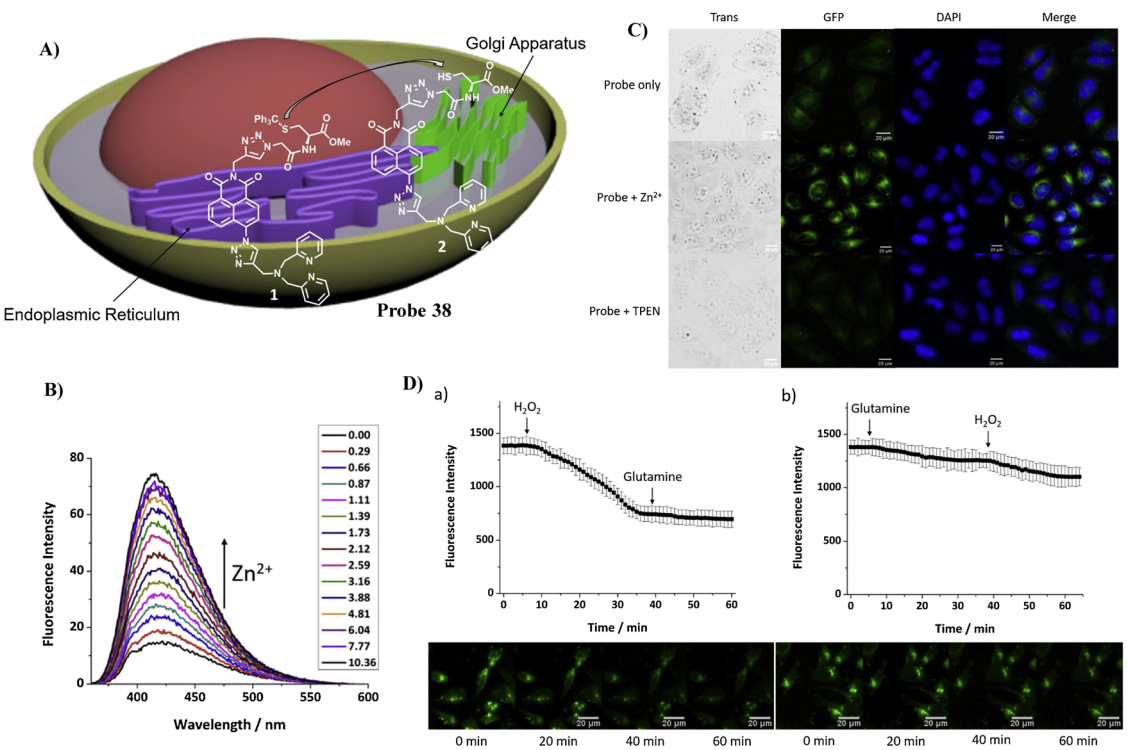

Fig. 36 (A) Response of probe **38** for Zn^{2+}. (B) Fluorescence spectra of **38** at varying concentrations of Zn^{2+}. (C) Fluorescence microscopic images of HeLa cells treated with probe **38**, probe **38** with Zn^{2+}, and probe **38** with TPEN. (D) Zn^{2+} level fluctuations during oxidative stress. Reproduced with permission from ref. 107. Copyright 2021, Elsevier.

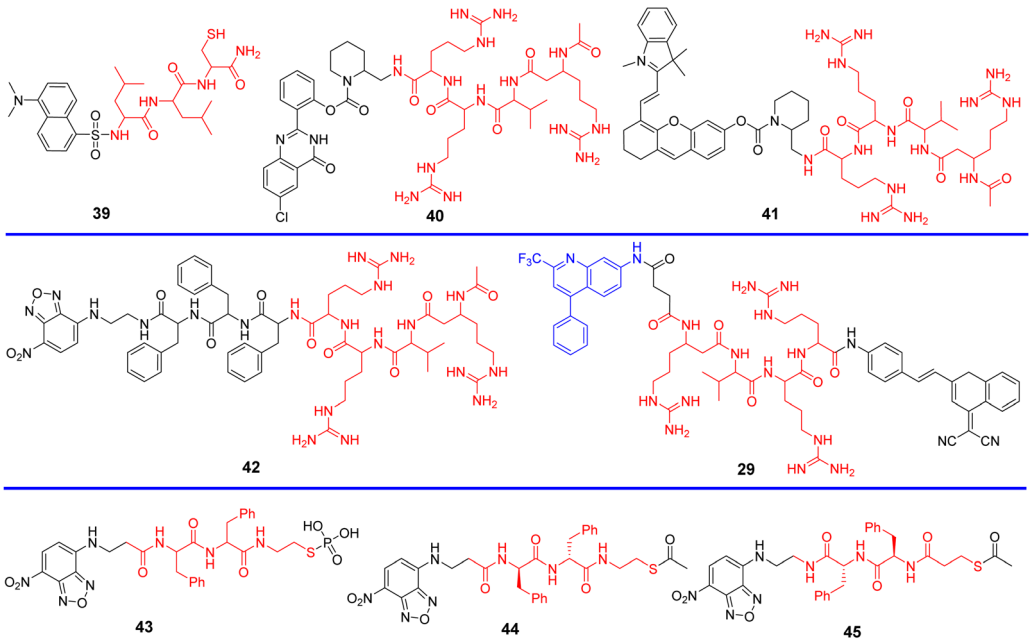

Scheme 6 Golgi-targeting probes with peptides as functional unit. Red indicates Golgi-targeting unit.

under the stabilization of hypoxia-inducible factor (HIF) regulated by cobalt chloride ($CoCl_2$) in addition to facilitating the imaging of furin in MDA-MB-468 cells and tumor tissues (Fig. 38).[115]

In 2019, the Zhang group reported on a Golgi-targeting furin-activatable NIR fluorescent probe **41** by substituting the fluorophore 6-chloro-2-(2-hydroxyphenyl) quinazolin-4(3*H*)-one linked through a self-eliminating linker to a furin specific peptide substrate as Golgi-targeting group, for the specific, sensitive, real-time imaging of furin in several tumor tissues, cells, and tumor-bearing mouse models. Moreover, probe **41** was used to unveil the relationship between furin content and $CoCl_2$ stabilization of HIF-1 (Fig. 39).[116]

In 2019, the Yi group developed a biocompatible amphiphilic peptide probe **42** with a Golgi-targeting RVRRFFF sequence and a nitrobenzoxadiazole (NBD) fluorophore that self-assemble into micelles for the detection of furin, where the as-formed β-sheet nanostructured probe **42** could respond to furin rapidly due to the RVRR moiety, and was able to distinguish high furin-expressing cancerous cells from normal cells. (Fig. 40).[117]

By changing an oxygen for a sulphur atom in the phosphoester bond of phosphopeptides, the as-generated thiophosphopeptide undergoes rapid alkaline phosphatase (ALP)-catalyzed dephosphorylation to form a self-assembled thiopeptide. This assembly can target the GA and selectively kill cancer cells. Using fast enzymatic kinetics and redox reactions in the oxidative environment of the Golgi, the Xu group have developed a Golgi-targeting fluorescent probe **43**, consisting of three units: (i) a 4-nitro-2,1,3-benzoxadiazole (NBD) group, which in a hydrophobic environment emits green fluorescence; (ii) a hydrophobic D-diphenylalanine (ff) that facilitates self-assembly and withstands proteolysis; (iii) a thiophosphate as enzymatic self-assembly trigger group. The probe enters the cells through caveolin-mediated endocytosis and macropinocytosis, and accumulates in the GA assisted by dephosphorylation and generation of disulfide bonds to selectively kill cancer cells (Fig. 41).[118]

Replacing the thiophosphate group with different sulfur-containing groups such as peptide thioesters, the Xu group have developed Golgi-targeting fluorescent probes **44** and **45**.

Table 5 Golgi-targeting fluorescent probes with peptide as functional motif

Probe	Analyte	$\lambda_{ex}/\lambda_{em}$ (nm)	Detection range	LOD	Pearson's correlation coefficient	Application	Ref.
39	Cu^{+}	400 nm/510 nm	0–60 nM	8 nM	0.9	Imaging in live cells	114
40	Furin	365 nm/500 nm	—	—	0.91	Imaging in live cells and tumor tissue slices of mice	115
41	Furin	680 nm/708 nm	—	—	0.930	Imaging in live cells and tumor bearing mice	116
42	Furin	470 nm/549 nm	2.0–10.0 ng μL^{-1}	0.11 ng μL^{-1}	—	Imaging in live cells	117
29	Furin	350, 470 nm/420, 640 nm	0–500 U mL^{-1}	0.265 U mL^{-1} 0.388 U mL^{-1}		Imaging in live cells	95
43	—	—	—	—	—	Localization cell imaging	118
44, 45	—	—	—	—	—	Localization cell imaging	119

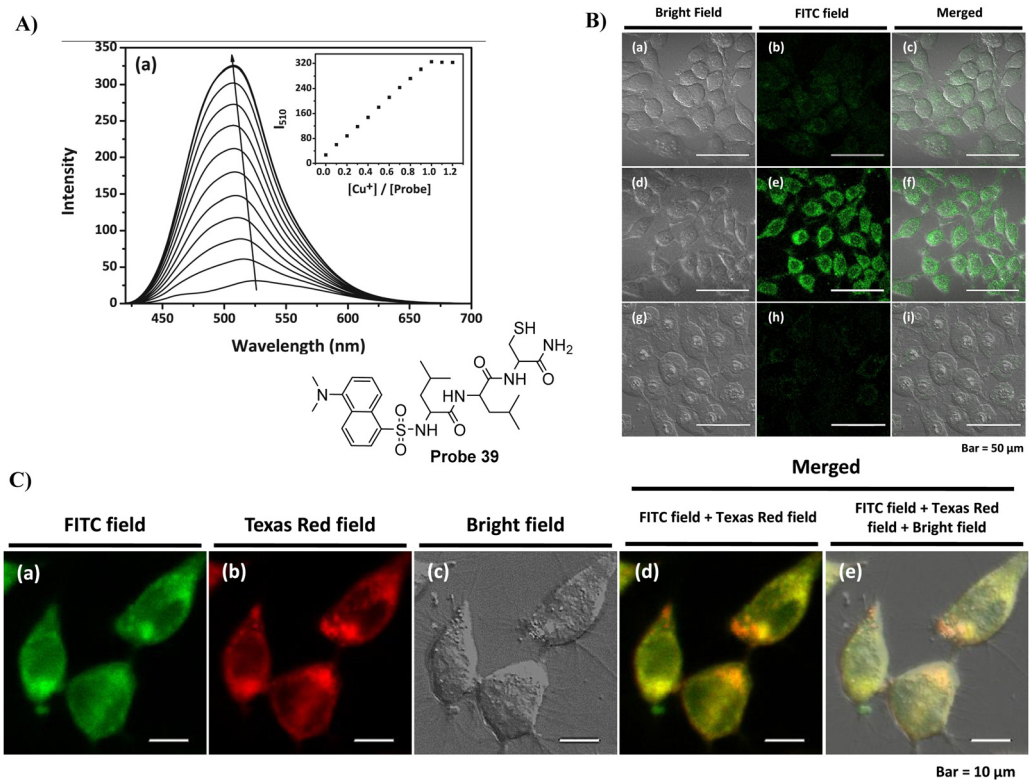

Fig. 37 (A) Fluorescence spectra of **39** at different concentrations of Cu^{+}. (B) Cu^{+} response of probe **39** in cells. (C) Co-localization cell imaging of **39** and BODIPY TR ceramide. Reproduced with permission from ref. 114. Copyright 2016, Elsevier.

The probes contain nitrobenzoxadiazole (NBD) as the fluorophore and an enzyme-responsive aminoethyl thioester locking group attached to the self-assembling D-diphenylalanine (ff), for targeting the GA in a wide range of cells. Peptide thioesters

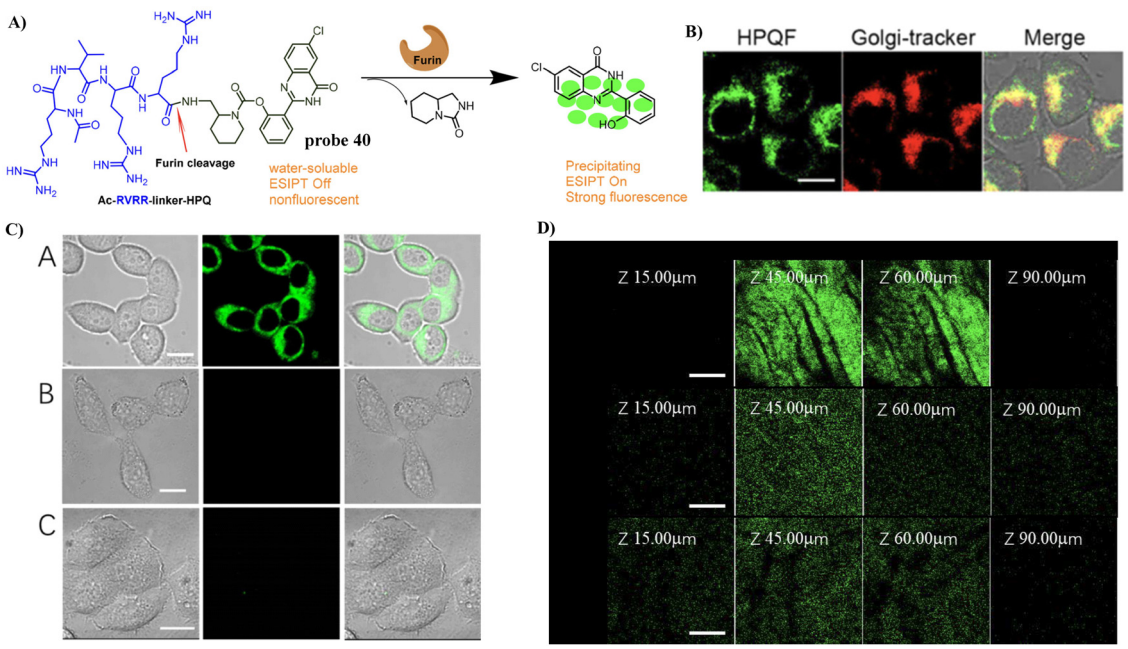

Fig. 38 (A) Response mechanism of **40** towards furin. (B) Co-localization cell fluorescence imaging of **40** and Golgi-tracker Red. (C) Fluoresence imaging of endogenous furin enzyme in Live Cells. (D) Fluorescence imaging of endogenous furin enzyme in cancer tissues. Reproduced with permission from ref. 115. Copyright 2018, American Chemical Society.

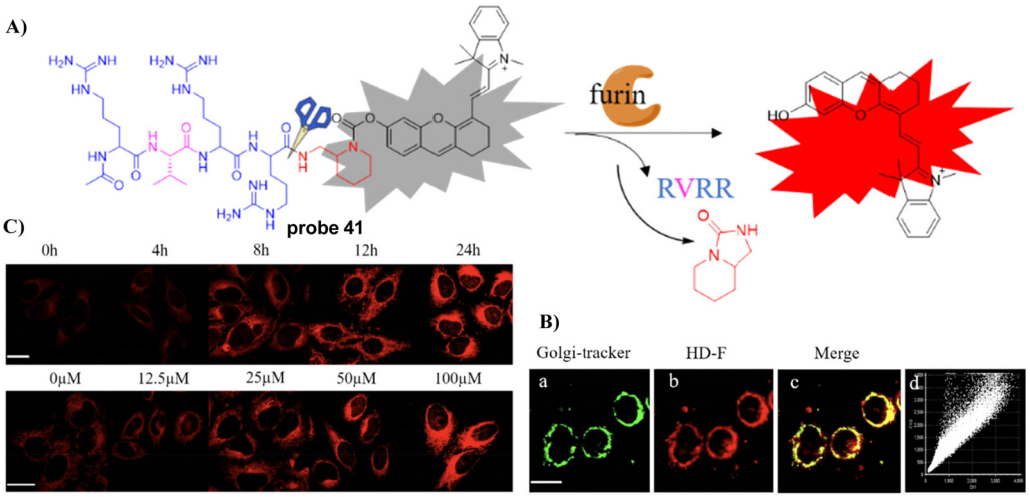

Fig. 39 (A) Response mechanism of **41** towards furin. (B) Co-localization cell imaging of **41** and Golgi-tracker Red. (C) Visualization of the furin fluctuations induced by HIF-1. Reproduced with permission from ref. 116. Copyright 2019, American Chemical Society.

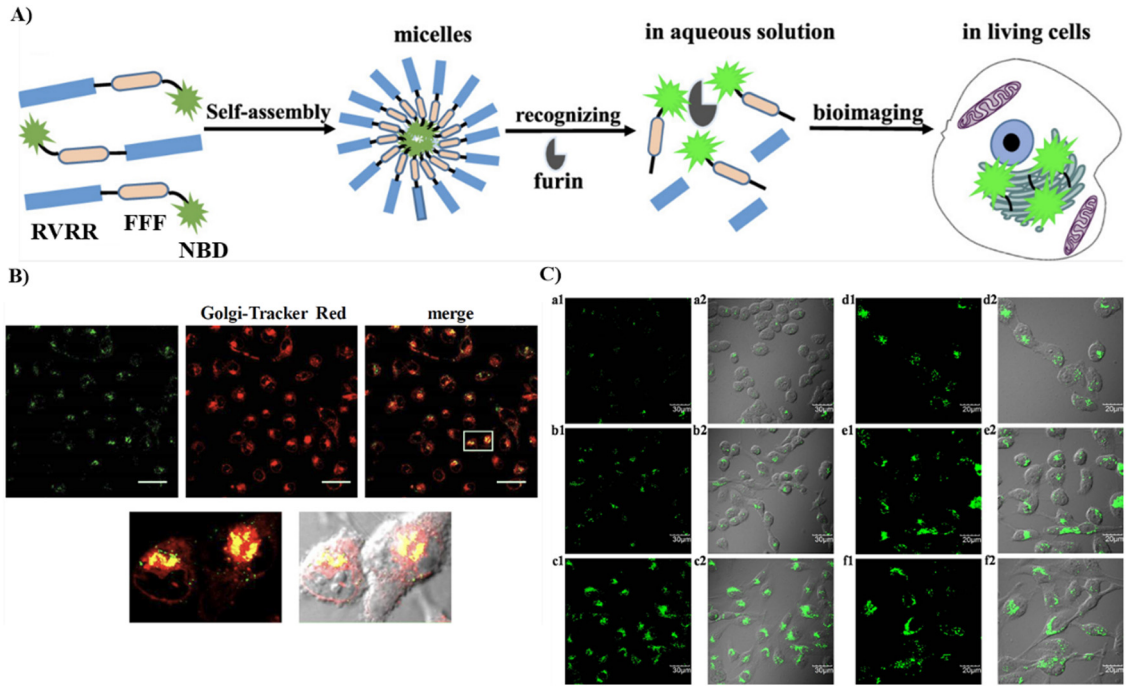

Fig. 40 (A) Schematic of the self-assembly process and furin enzyme response of **42**. (B) Co-localization cell imaging of **42** and Golgi Tracker Red. (C) Fluorescence and long-term imaging by **42** of furin in living cells. Reproduced with permission from ref. 117. Copyright 2019, American Chemical Society.

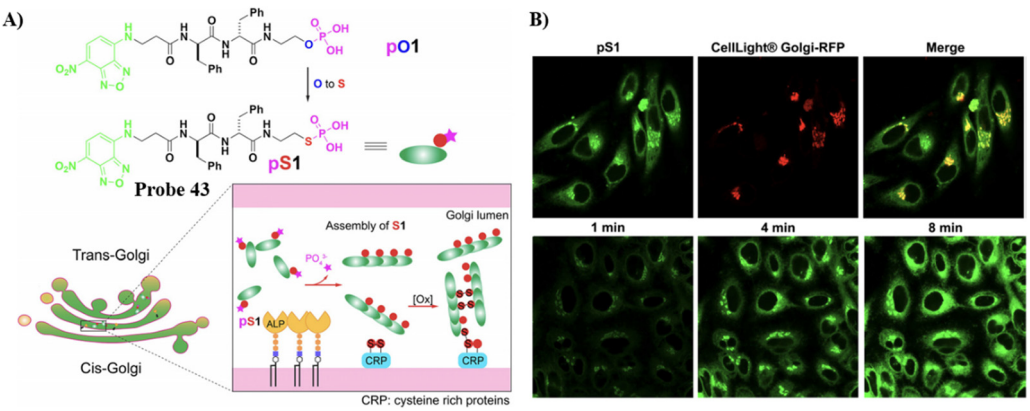

Fig. 41 (A) Thiophosphopeptide **43** targeting the Golgi apparatus. (B) CLSM images of HeLa cells (top) stained with Golgi-tracker Golgi-RFP after treating with **43** for 8 minutes and (bottom) treated with **43** for 1, 4, and 8 min. Reproduced with permission from ref. 118. Copyright 2021, Wiley.

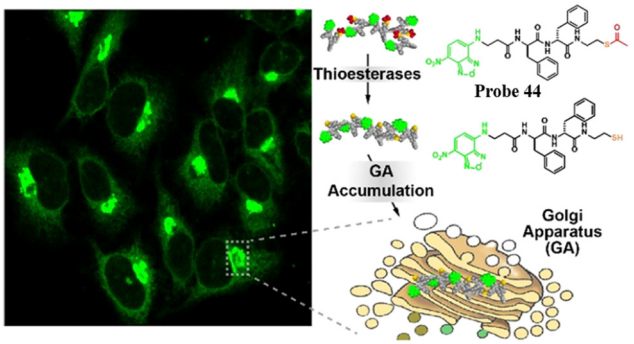

Fig. 42 Thioesterase-responsive fluorescent probe **44** in Golgi apparatus. Reproduced with permission from ref. 119. Copyright 2022, American Chemical Society.

enter cells *via* caveolin-mediated endocytosis or macropinocytosis, the thiopeptides generated then aggregate in the GA after being hydrolyzed by GA-associated thioesterases, resulting in cell death (Fig. 42).[119]

3.6 Probes containing lipids

Ceramide is a precursor of complex sphingolipids which are synthesized in the ER and transported to the GA through the ceramide transporter protein (CERT) in mammalian cells for further processing into complex sphingolipids.[120] As such, small molecular fluorophores containing lipid-based tagging groups such as NBD-ceramide and Bodipy-ceramide have been used for Golgi apparatus labeling.[19,121] Scheme 7 and Table 6 highlight current Golgi-targeting probes using lipids as a functional motif and their applications.

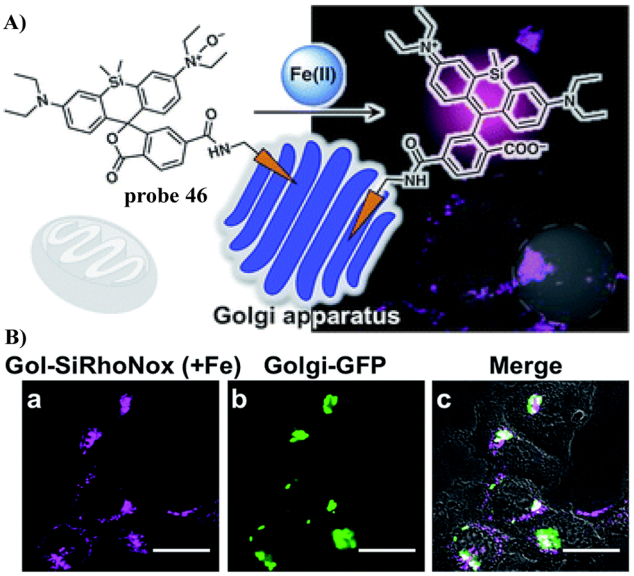

Fig. 43 (A) The response mechanism of **46** towards Fe^{2+}. (B) Co-localization experiment of HepG2 cells with Golgi-specific GFP and **46**. Reproduced with permission from ref. 122. Copyright 2019, The Royal Society of Chemistry.

In 2019, the Hirayama group developed fluorescent probe **46** for the detection of Fe(II) ions in the Golgi by combining their *N*-oxide-based Fe(II)-specific chemical switch, with a Golgi

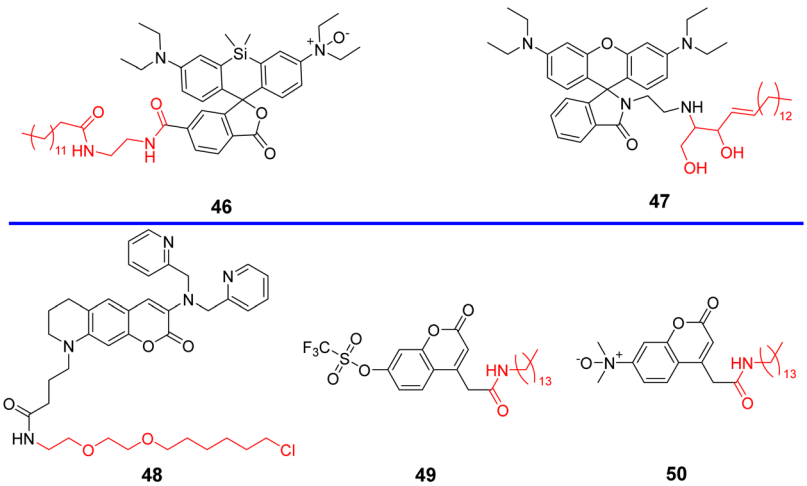

Scheme 7 Golgi-targeting probes with lipids as the functional motif. Red indicates the Golgi-targeting unit.

Table 6 Golgi-targeting fluorescent probes with lipids as functional motif

Probe	Analyte	$\lambda_{ex}/\lambda_{em}$ (nm)	Detection range	LOD	Pearson's correlation coefficient	Application	Ref.
46	Fe^{2+}	630 nm/665 nm	0–10 μM	50 nM	0.64	Imaging in live cells	122
47	pH	570 nm/600 nm	pH 3.80–5.40	pK_a 4.32	0.9	Imaging in live cells and mice	123
48	Zn^{2+}	440 nm/507 nm	—	—	0.85	Imaging in live cells	124
49	$O_2^{\bullet-}$	405 nm/450 nm	0–100 μM	0.39 μM	0.99	Imaging in live cells and zebrafish	125
50	Fe^{2+}	370 nm/460 nm	0–140 μM	52 nM	0.99	Imaging in live cells	126

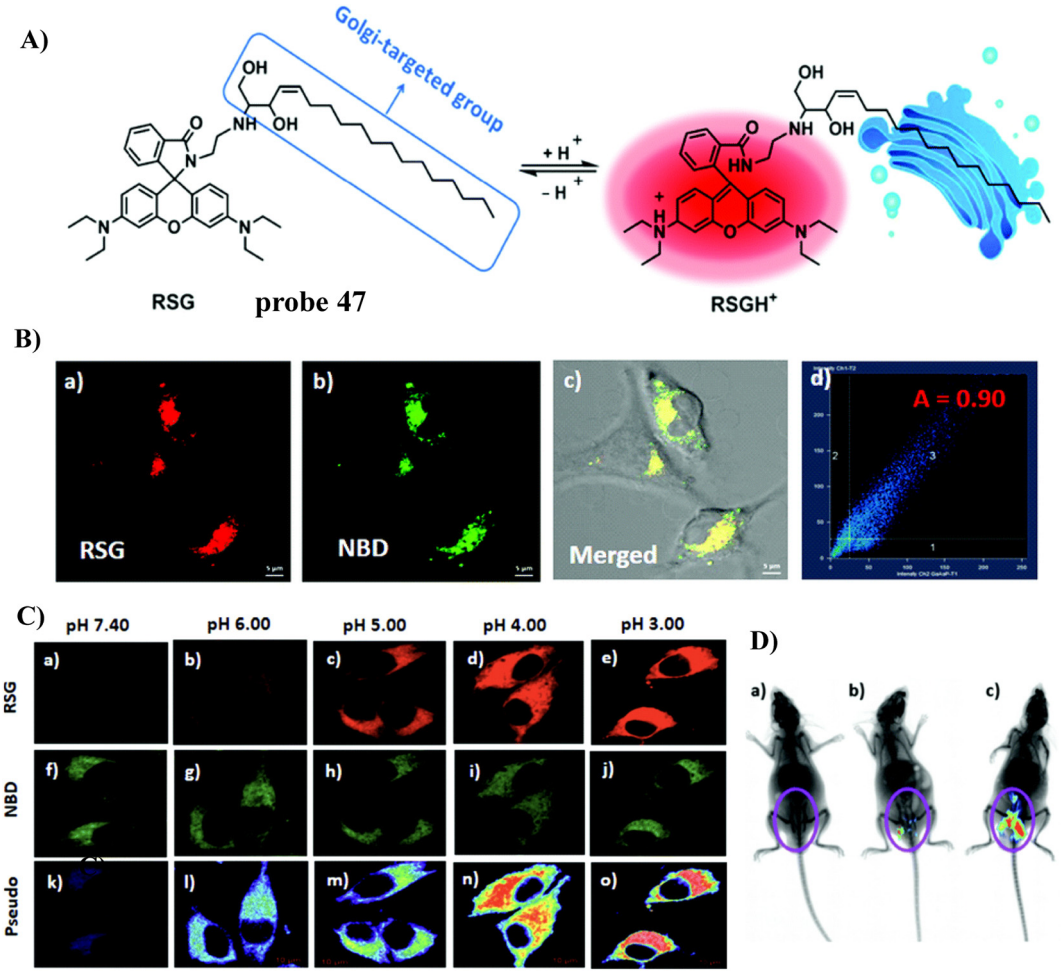

Fig. 44 (A) Response mechanism of **47** towards pH. (B) Co-staining experiment of SMMC-7721 cells with NBD and **47**. (C) pH fluorescence imaging using **47** in living cells. (D) *In vivo* fluorescence images of **47** in mice stimulated using LPS. Reproduced with permission from ref. 123. Copyright 2019, The Royal Society of Chemistry.

targeting unit, and polarity-sensitive fluorogenic unit. Probe **46** confirmed that the intracellular Fe(II) ion distribution is greater in the Golgi apparatus than lysosomes, using a synchronous imaging study with a previously reported lysosome-specific fluorescent probe LysoRhoNox, whereas the elevation of Fe(II) in lysosomes was observed in cells with the induced dysfunction of vacuolar protein sorting-associated protein 35 (VPS35). It is found that the treatment of dysfunctional VPS35 by a molecular chaperone (R55) restored the Golgi-dominant distribution of Fe(II) ions, indicating that the impairment of the divalent metal transporter 1 (DMT1) traffic machinery influences subcellular iron homeostasis and promotes Fe(II) escape at the Golgi and accumulation of Fe(II) at the lysosome (Fig. 43).[122]

In 2019, the Dong group developed a Golgi-targeting fluorescent pH-responsive probe **47** based on the rhodamine B skeleton with sphingosine as the Golgi-targeting group, generating an off–on fluorescence response to the reduced pH in the Golgi resulting in spirocyclic ring opening with high specificity and sensitivity. The probe was used to monitor pH changes of the Golgi caused by LPS-mediated inflammation and drug treatment *in vivo* (Fig. 44).[123]

In 2020, the Mizukami group developed a Golgi-targeting Zn^{2+}-selective probe **48** that exhibits high Zn^{2+} selectivity and low sensitivity to pH. The HaloTag labeling technology ensured that the probe targeted organelles such as the mitochondria, nucleus, Golgi apparatus and endoplasmic reticulum. In response to labile Zn^{2+} the probe exhibited reversible fluorescence response and as such was used for monitoring the concentration of Zn^{2+} in the Golgi apparatus (Fig. 45).[124] Subsequently, a protocol for the use of probe **48** in live cells for quantifying labile Zn^{2+} in the Golgi apparatus was reported.[127]

Probes containing a tetradecyl chain exhibit Golgi targeting ability in cell imaging. Recently, the Chen group developed two Golgi-targeting fluorescent probes **49** and **50** using myristoyl as the Golgi targeting group and coumarin as the fluorophore. Probe **49** was able to detect endogenous and exogenous $O_2^{\bullet-}$ in zebrafish and cells. The probe was then used to monitor the $O_2^{\bullet-}$ levels up-regulated during ischemia-reperfusion (I/R) processes in cardiomyocytes. As such, probe **49** provides a diagnostic tool for myocardial oxidative stress injury and could be used to provide insight for role of GOLPH3 (a potential Golgi stress marker) in myocardial I/R injury (Fig. 46).[125] While, probe **50** is a turn-on Golgi-targeting fluorescent

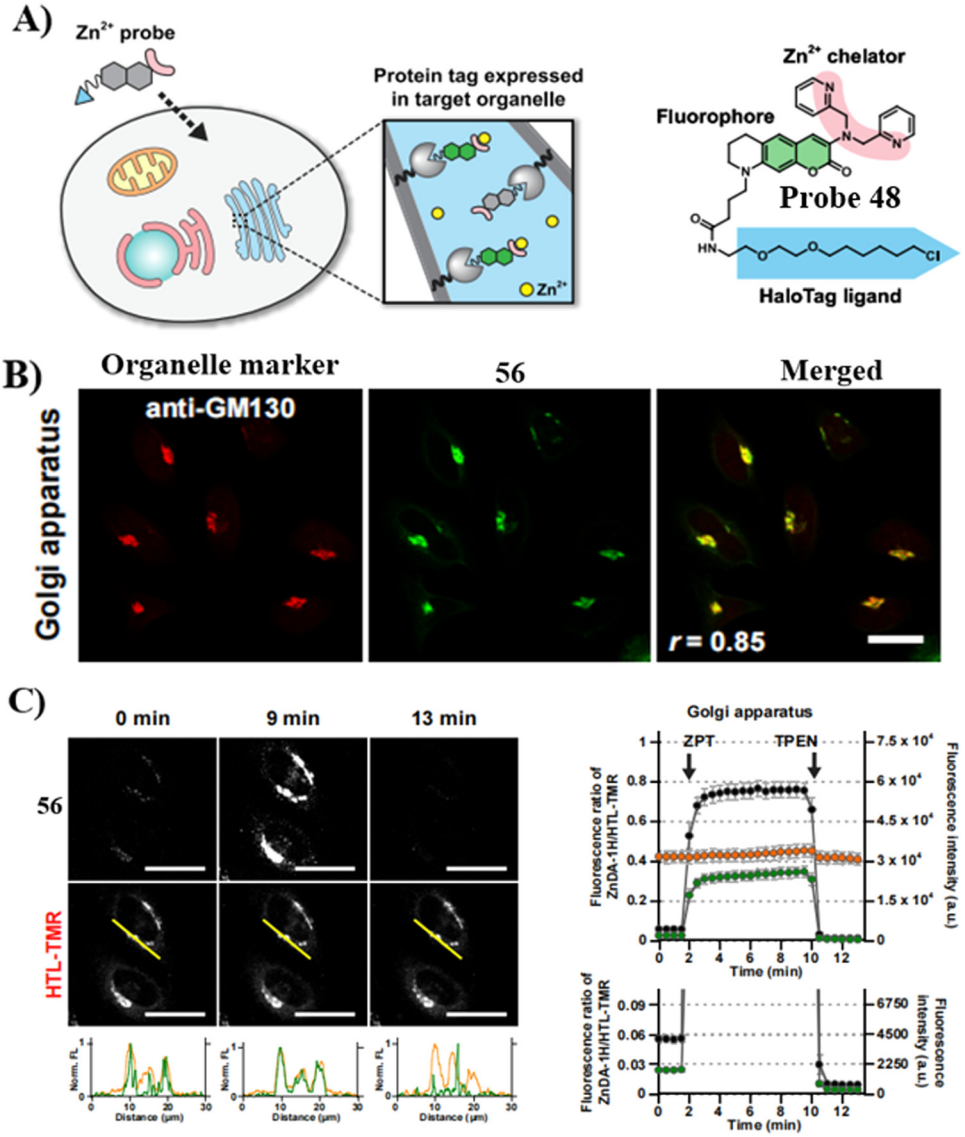

Fig. 45 (A) Illustration of organelle-targeting by small-molecule fluorescent probes using a HaloTag. (B) Fluorescent images of HeLa cells using **48** and anti-GM130 antibody. (C) Detection of intracellular [Zn^{2+}] changes in live HeLa cells in the Golgi apparatus. Reproduced with permission from ref. 124. Copyright 2020, Elsevier.

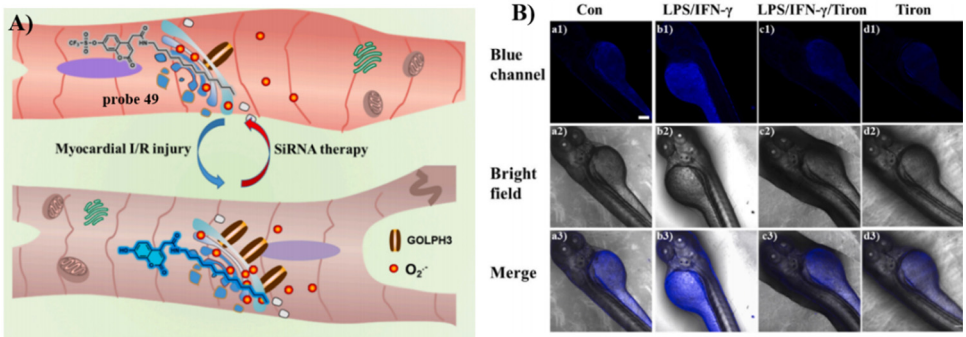

Fig. 46 (A) Probe **49** for detecting $O_2^{\bullet-}$ levels in myocardial ischemia-reperfusion injury and SiRNA therapy and elucidating the function of GOLPH3. (B) Fluorescence imaging (blue scale) of probe **49** responding to $O_2^{\bullet-}$ in zebrafish. Reproduced with permission from ref. 125. Copyright 2023, Elsevier.

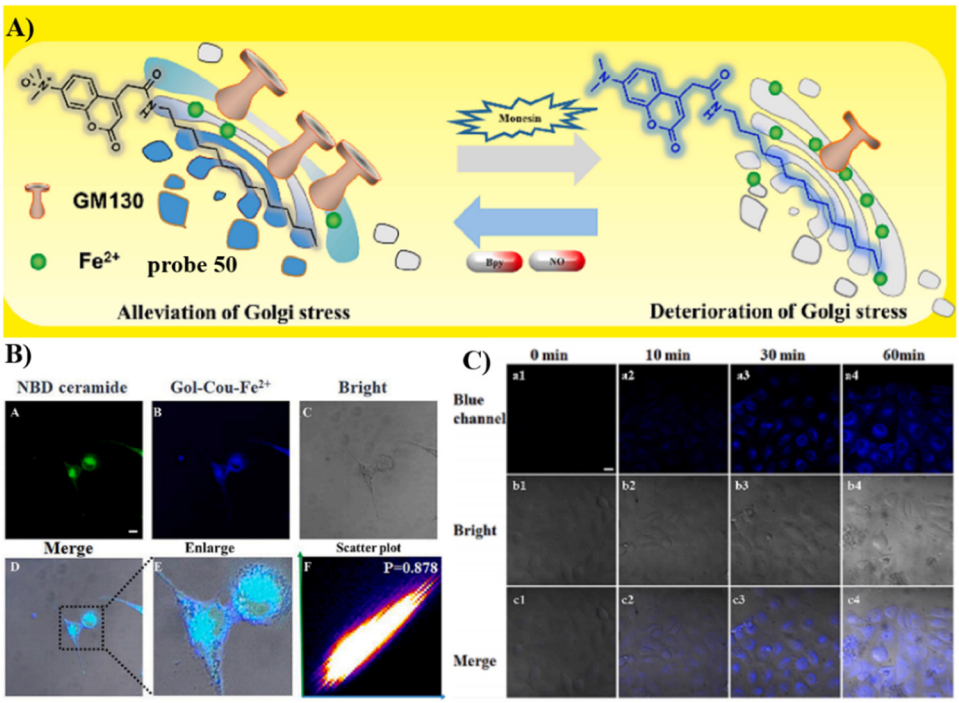

Fig. 47 (A) Response mechanism of probe **50**. (B) Confocal fluorescence co-stained experiment in HUVEC co-incubated with **50** (10 μM) pre-treated with Fe^{2+} (50 μM) and NBD-ceramide (5 μM). (C) Confocal fluorescence image of HUVEC cell at various times under hypoxic conditions. Reproduced with permission from ref. 126. Copyright 2023, Elsevier.

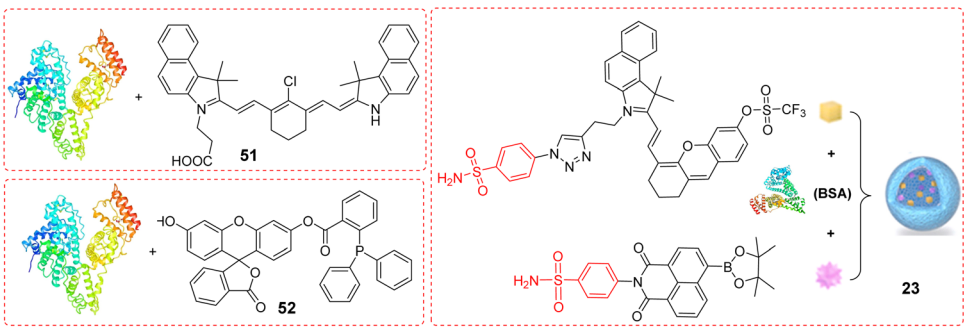

Scheme 8 Golgi-targeting probes using BSA as a functional motif.

Table 7 Golgi-targeting fluorescent probes with BSA as functional motif

Probe	Analyte	$\lambda_{ex}/\lambda_{em}$ (nm)	Detection range	LOD	Pearson's correlation coefficient	Application	Ref.
51	pH	540 nm/808 nm	pH 5.39–7.97	pK_a 6.92	—	Killing of cancer cells, photothermal therapy in mice	130
52	HNO	480 nm/520 nm	0–30 μM	130 nM	0.84	Imaging in live cells and DILI mice	131
23	$O_2^{\bullet-}$, H_2O_2	633 nm/740 nm	0–35 μM	62 nM	0.827, 0.839	Imaging in live cells and mice	77

probe for the sensitive and selective detection of Fe^{2+}. Probe **50** could be used to detect exogenous and endogenous Fe^{2+} in HUVEC and HepG2 cells (Fig. 47).[126]

3.7 Probes encapsulated by BSA

Bovine serum albumin (BSA) is a complex serum globular protein with a single chain of 582 amino acids cross-linked with 17 cystine residues, that plays an important role in the transportation of exogenous and endogenous ligands (such as drugs) to specific targets.[128] Probes encapsulated with BSA can form large nanoparticulate structures through hydrophobic interactions and the system can preferentially aggregate in the Golgi apparatus.[35,77,129] In our opinion, the Golgi-targeting ability of BSA can be attributed to the abundant cysteine residues in BSA, which

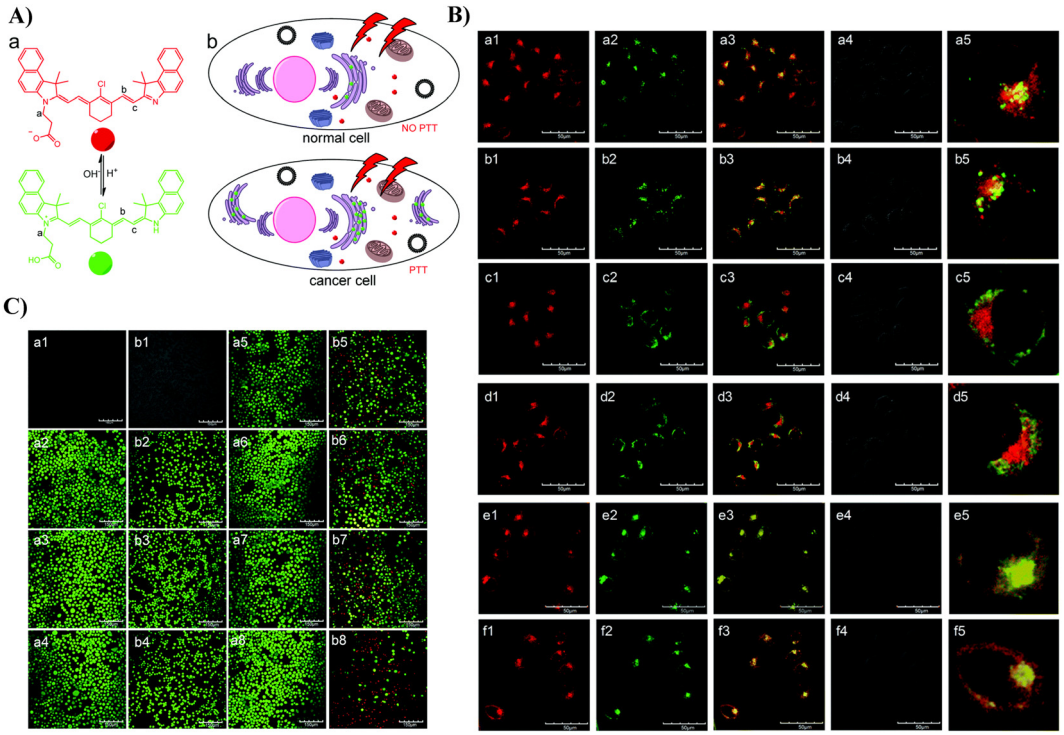

Fig. 48 (A) Illustration of **pH-PTT** as an intelligent drug for specific PTT activation in the Golgi apparatus. (B) CLSM images of HepG2 (a), (c) and (e) and HL-7702 (b), (d) and (f) cells co-stained with **51**/Lyso tracker (a) and (b), Mito tracker (c) and (d) and **51**/Golgi green. (C) CLSM images of Calcein AM/PI stained (a) HL-7702 and (b) HepG2 cells with or without **51** treated after exposure to an 808 nm laser (1.45 W cm^{-2}) for different times. Reproduced with permission from ref. 130. Copyright 2017, The Royal Society of Chemistry.

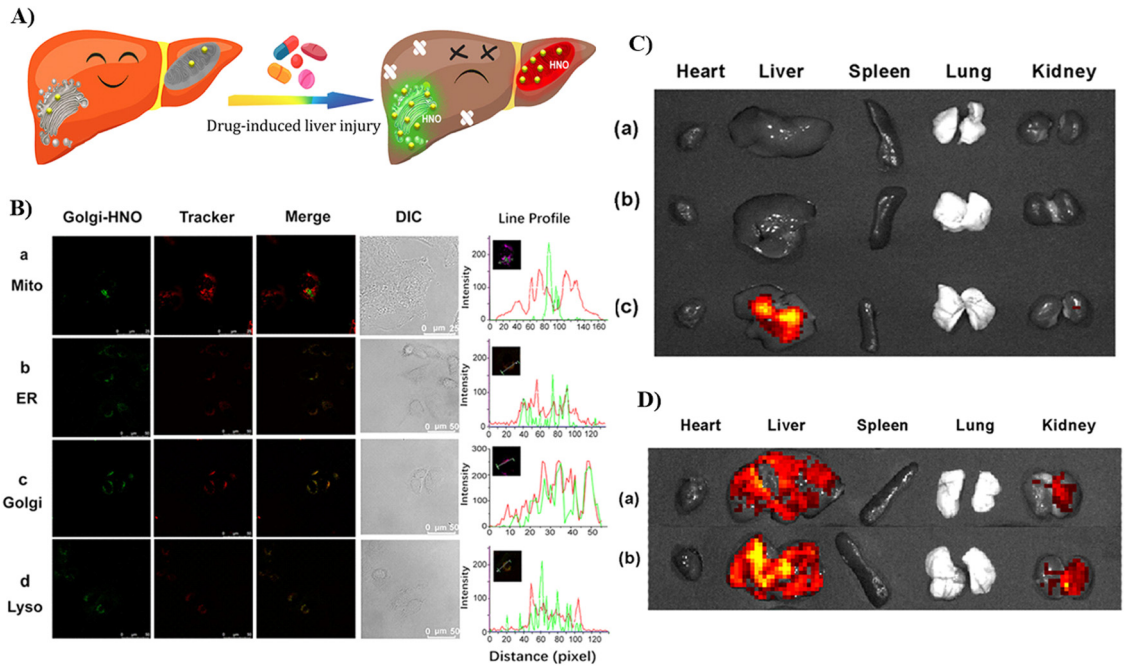

Fig. 49 (A) Green-colored fluorescence imaging of Golgi-HNO **52** in Mice with DILI. (B) Co-localization imaging of **52** with different commercial localization dyes. (C) Fluorescence imaging of APAP-induced mice organs, where the mice were injected with probe **52**. Control group mice (a); 75 mg mL^{-1} low-dose (LD) APAP-induced mice (b); 150 mg mL^{-1} high-dose (HD) APAP-induced mice (c). (D) Fluorescence imaging of organs from bleomycin-induced mice, where the mice were injected with probe **52**. Control group mice (a) and bleomycin-induced mice (b). Reproduced with permission from ref. 131. Copyright 2021, American Chemical Society.

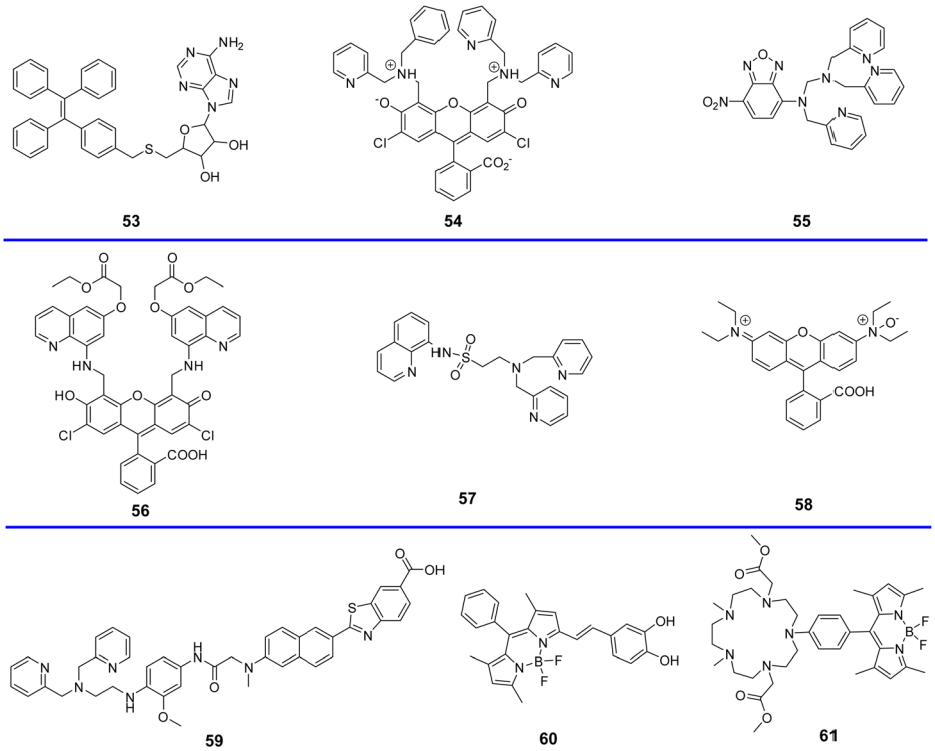

Scheme 9 Golgi-targeting probes using other groups.

Table 8 Golgi-targeting probes with other groups

Probe	Analyte	$\lambda_{ex}/\lambda_{em}$ (nm)	Detection range	LOD	Pearson's correlation coefficient	Application	Ref.
53	—	375 nm/450 nm	—	—	0.86	Imaging in live cells	132
54	Zn^{2+}	507 nm/— nm	—	—	—	Imaging in live cells	133
55	Zn^{2+}	469 nm/550 nm	—	—	—	Imaging in live cells and zebrafish	134
56	Zn^{2+}	492 nm/515 nm	—	—	—	Imaging in live cells	135
57	Zn^{2+}	364 nm/497 nm	—	4.2×10^{-14} M	—	Localization cell imaging	136
58	Fe^{2+}	540 nm/575 nm	—	0.2 μM	—	Localization cell imaging	137
59	Zn^{2+}	388 nm/518 nm	—	—	0.92	3D distributions in live cells and tissues	138
60	HOCl	550 nm/586 nm	—	—	0.98	SIM and 3D-SIM imaging in living cells	139
61	Mn^{2+}	—	—	—	—	Confocal microscopy and nanosynchrotron X-ray fluorescence imaging	140

can form disulphide bonds through binding with thiol groups of the Golgi. Scheme 8 and Table 7 highlight Golgi-targeting probes using BSA as a functional motif and their applications.

In 2017, the Yi group developed a pH-responsive photothermal ablation agent (pH-PTT) for the Golgi apparatus using asymmetric cyanine dyes for photothermal therapy (PTT), which was highly pH sensitive from 6.2–7.5. pH-PTT efficiently generates thermal energy due to 808 nm light irradiation and formation of extended conjugated structure at low pH conditions. Nanoparticles (**51**) assembled using BSA with pH-PTT preferentially accumulate in the Golgi apparatus of cancerous cells. Thus, the system could be exclusively activated by the acidic microenvironment of the Golgi apparatus of cancer cells resulting in efficient PTT (Fig. 48).[130]

In 2021, the Tang group developed a fluorescent probe Golgi-HNO (**52**), using 2-(diphenylphosphino)-benzoate as the recognition group and fluorescein as the fluorophore, for the imaging and detection of nitroxyl (HNO) in the Golgi apparatus. Probe **52** was encapsulated using Golgi targeting BSA. Biological results indicated that an increase in HNO levels was closely associated with drug-induced liver injury, and catalase was associated HNO synthesis, indicating that HNO is suitable biomarker for DILI diagnosis, and is suitable for providing guidance on the design and development of therapeutic drugs. (Fig. 49).[131]

3.8 Probes with other targeting groups

In addition to the Golgi imaging strategies described above, there are several other types of fluorescent probes used for Golgi imaging. Unlike the usual Golgi-targeting groups mentioned above, the precise mode of targeting is unknown. Therefore, such fluorescent probes do not fully elucidate what part of the probe is Golgi-targeting or the localization mechanism. As such we provide appropriate suggestions on how the probes specifically target the

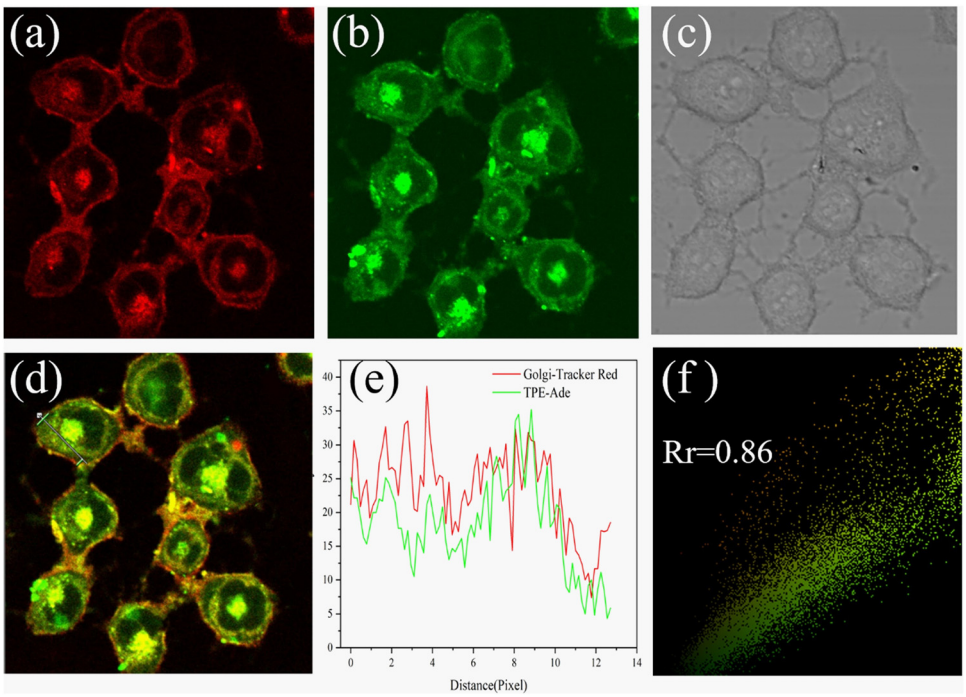

Fig. 50 Co-localization fluorescence images of **53** with commercial Golgi-tracker Red in HL-7402 cells. Reproduced with permission from ref. 132. Copyright 2021, Elsevier.

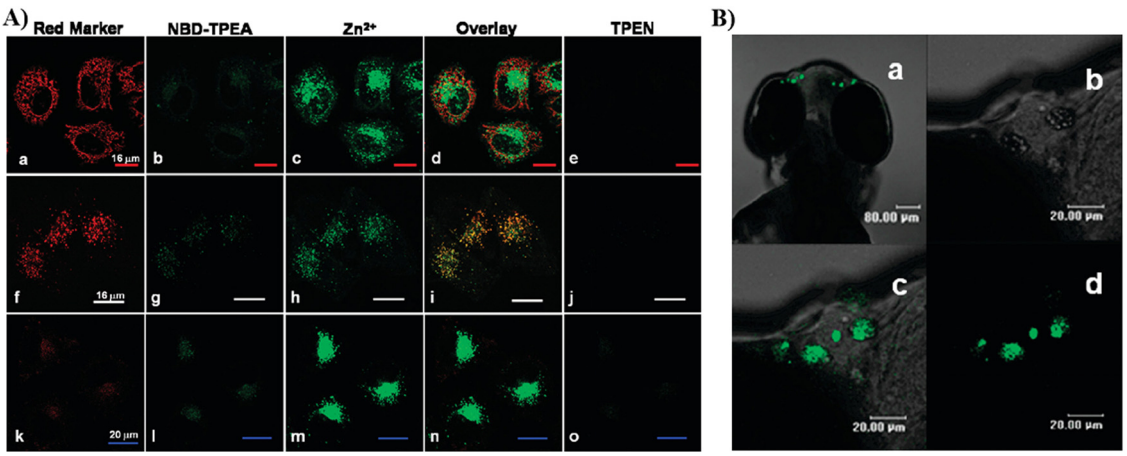

Fig. 51 (A) Co-localization imaging of **55** and MitoTracker Red CMXRos (top row), LysoTracker Red DND-99 (middle row), BODIPY TR ceramide (bottom row) in HeLa cells. (B) Confocal fluorescence images of the head of a 4-day-old zebrafish larva fed Zn^{2+} solution (5 μM) at 28.5 °C for 12 h. Reproduced with permission from ref. 134. Copyright 2009, American Chemical Society.

Golgi apparatus following our current understanding of the GA, in order to better understand how to design Golgi-targeting fluorescent probes. (Scheme 9 and Table 8).

In 2021, using adenosine (Ade) as a Golgi-targeting group and tetraphenylethylene (TPE) with AIE characteristics as fluorophore, the Zhao group developed fluorescent probe **53**, that exhibited excellent Golgi apparatus co-localization efficacy and photostability (Fig. 50).[132]

By using a pyridyl moiety to match with the weakly acidic microenvironment in the Golgi, some reported fluorescent probes have been developed over the past several decades to target the Golgi. In 2000, the Tsien group developed a fluorescent Zn^{2+} probe (**54**) based on fluorescein derivatives with a Zn^{2+} chelating group bis(2-pyridylmethyl)amine (DPA), to preferentially stain Golgi-associated vesicles and the Golgi.[133] In 2009, the Guo group created a Zn^{2+} visible light excitable fluorescent probe (**55**) using a standard ICT fluorophore, 4-amino-7-nitro-2,1,3-benzoxadiazole (ANBD), which was integrated with a *N,N,N′*-tri(pyridin-2-ylmethyl)ethane-1,2-diamine (TPEA) group and a bis(pyridin-2-ylmethyl)amine (BPA)

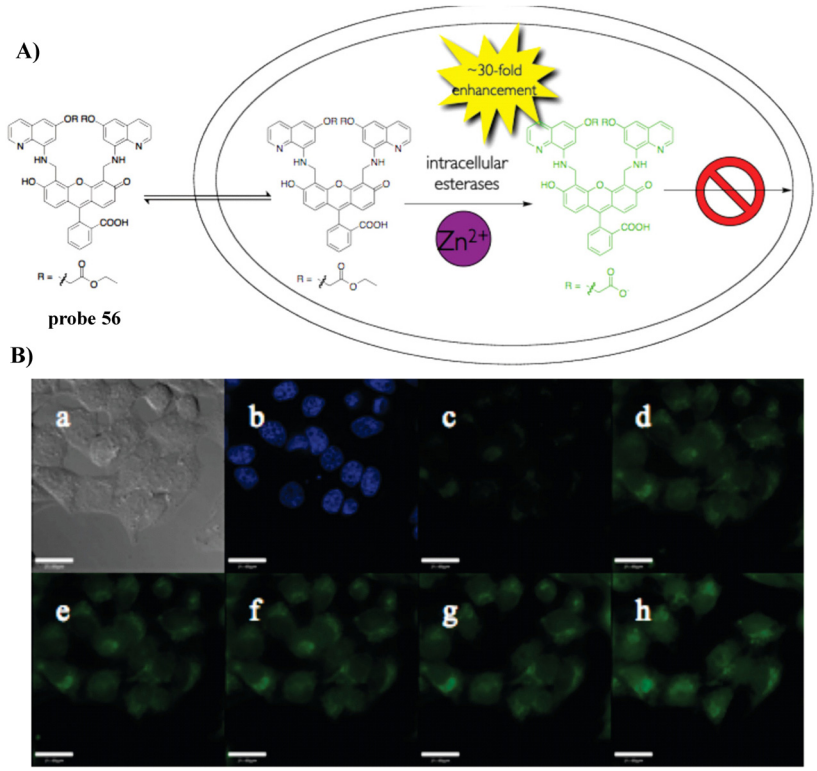

Fig. 52 (A) The structure and possible reaction mechanism of **56** for identifying Zn^{2+}. (B) Cell imaging results confirming the retention of **56** in HeLa cells coincubated with **56** and Hoechst 33258 for 18 h. Reproduced with permission from ref. 135. Copyright 2010, American Chemical Society.

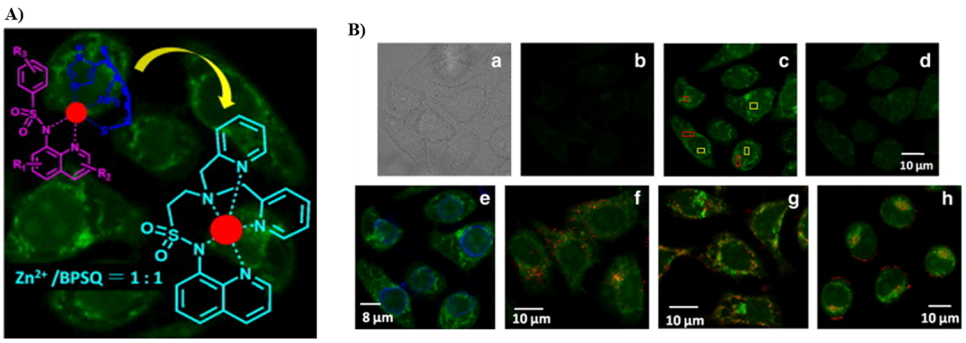

Fig. 53 (A) Structure and possible mechanism of **57** for monitoring Zn^{2+}. (B) Confocal microscopic images of HeLa cells stained by **57** with Zn^{2+} (a)–(d). Co-stained images of cells incubated with Zn^{2+} followed by colocalization with **57** and organelle dye. (e) Hochest 33342, (f) LysoTracker Red DND-99, (g) MitoTracker Red CMXRos, (h) Golgi marker BODIPY TR ceramide. Reproduced with permission from ref. 136. Copyright 2011, Elsevier.

group.[134] Probe **55** exhibits a large Stokes shift, visible ICT absorption band, and good biocompatibility. Preferential accumulation in the lysosomes and Golgi was observed, enabling Zn^{2+} imaging of zebrafish and cells (Fig. 51).

In 2010, the Lippard group developed a fluorescent cell-permeable probe **56** based on similar fluorescein derivatives with dramatic fluorescence enhancements upon addition of Zn^{2+}. Probe **56** localizes in the Golgi apparatus of living cells, due to the generation of a negative charge after intracellular hydrolysis of the ester groups (Fig. 52).[135]

Also utilizing the pyridyl group to closely match the Golgi environment, in 2011, taking advantage of the synergistic coordination of Zn^{2+} by bis(pyridin-2-ylmethyl)amine (BPA) and 8-sulfonamidoquinoline (SQ) motifs, and by integrating BPA with SQ, the Guo group developed fluorescent probe (**57**), which exhibits Golgi-targeting and physiological pH-independent Zn^{2+} response, that was used for live cell imaging (Fig. 53).[136]

In 2013, the Nagasawa group reported on a fluorescent reaction-based turn-on probe (**RhoNox-1**, **58**) using a

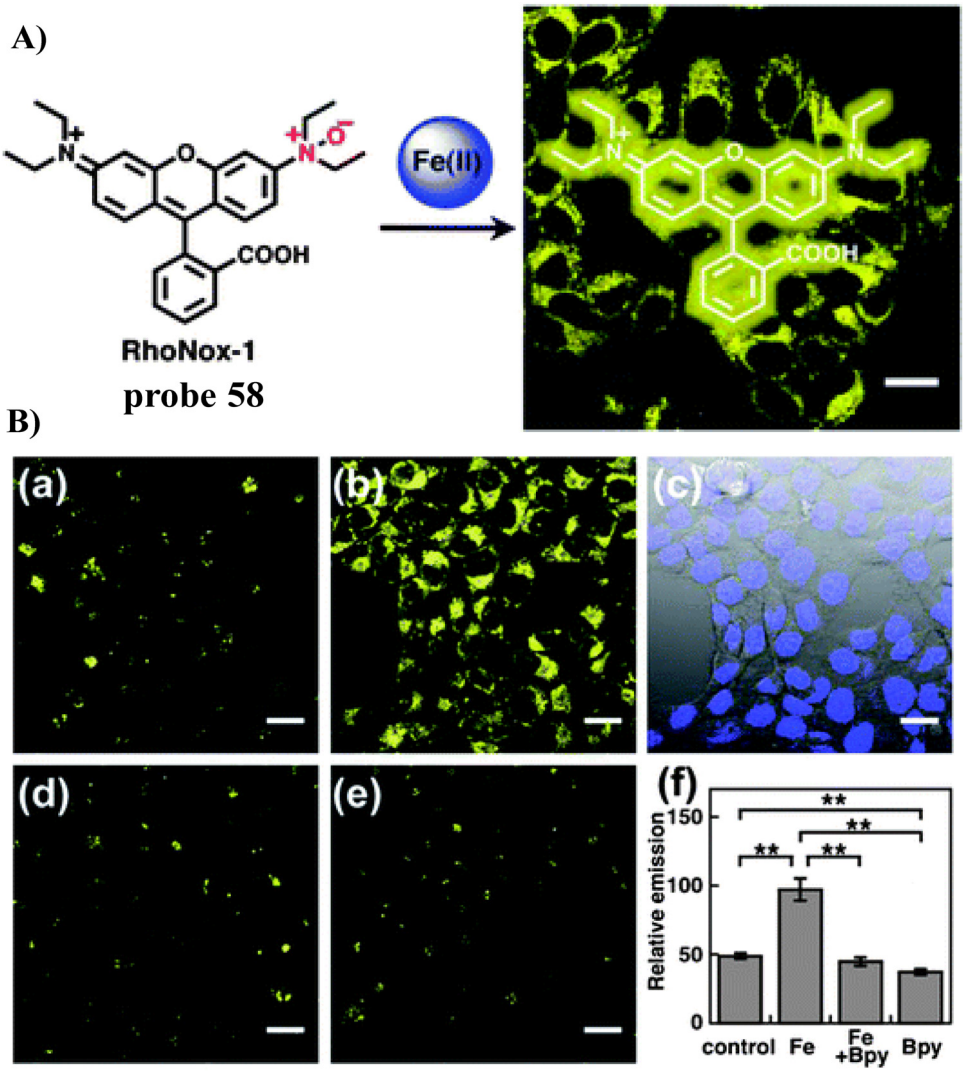

Fig. 54 (A) Probe **58** reaction mechanism for Fe^{2+}. (B) Confocal fluorescence microscopic images of Fe^{2+} detection in HepG2 cells using **58**. (C) Co-stained fluorescence images of **58** treated HepG2 cells with BODIPY-FL-ceramide. Reproduced with permission from ref. 137. Copyright 2013, The Royal Society of Chemistry.

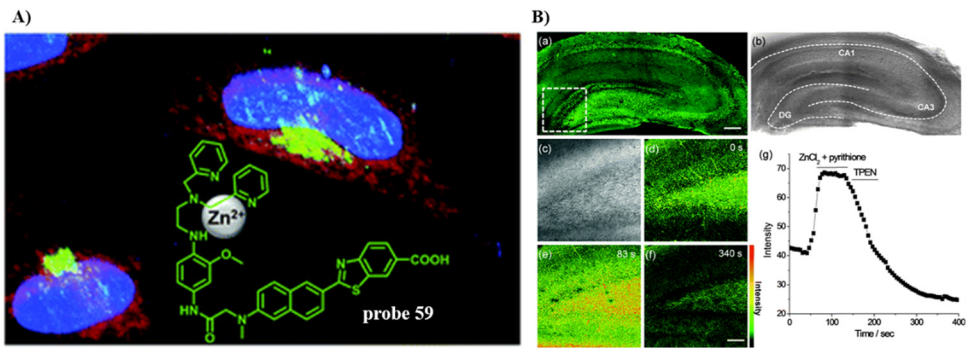

Fig. 55 (A) Mechanism of **59** for identifying Zn^{2+}. (B) TPM images of a rat hippocampal slice stained with 20 μM SZnC for 1 h. (a) 150 TPM images along the *z*-direction at the depth of approximately 100–200 μM, accumulated at 10× magnification. (b) Bright-field image. (c)–(f) 20× magnification in the dentate gyrus (DG) regions white box in (a) at a depth of 120 μM. (c) Bright-field image, (d)–(f) TPM images before (d) and after (e) addition of 200 mM Zn^{2+}/pyrithione to the imaging solution. (f) After addition of 1 mM TPEN to (e). (g) Relative TPEF intensity of (d)–(f) as a function of time. Reproduced with permission from ref. 138. Copyright 2015, The Royal Society of Chemistry.

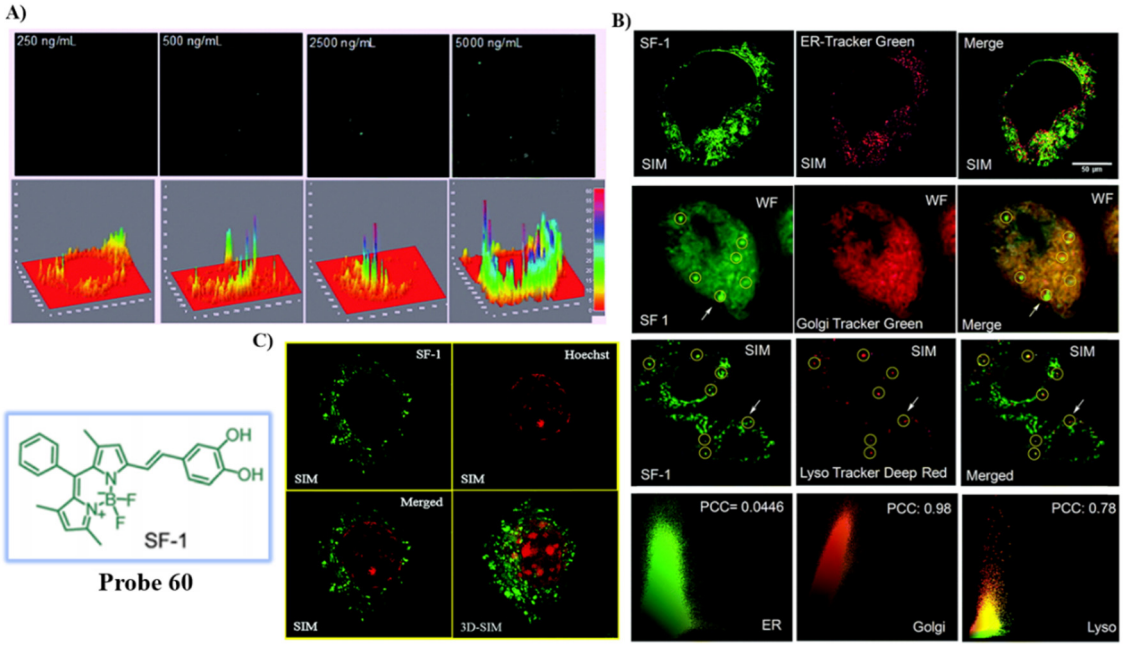

Fig. 56 (A) Response of probe **60** for endogenous HOCl: SIM images and emission intensity profiles of **60** in the presence of different concentration of LPS incubated for 12 h in fixed RAW 264.7 cells. (B) Co-stained cell imaging of **60** and ER-Green, Golgi Tracker Green and Lyso Tracker Deep Red. (C) Dual colour SIM and 3D-SIM of **60** in the presence of LPS and Hoechst 33442. Reproduced with permission from ref. 139. Copyright 2018, The Royal Society of Chemistry.

rhodamine as the fluorophore and *N*-oxide for the selective detection of Fe^{2+}. The initial fluorescence was quenched due to non-radiative deactivation by twisted internal charge transfer (TICT) of the excited state of the tertiary amine *N*-oxide substituted rhodamine and photo-induced electron transfer (PeT). Probe **58** exhibited significant fluorescence enhancements in Fe^{2+}-loaded cells due to *N*-oxide deoxygenation mediated by Fe^{2+}, and was successfully used for monitoring basal and endogenous labile Fe^{2+} in live cells (Fig. 54).[137]

In 2015, the Kim group developed a fluorescent Golgi-targeting turn-on probe (**SZnC**, **59**) for the detection of Zn^{2+}, that was insensitive to pH changes, exhibited easy cell loading, low cytotoxicity, good Golgi-localization and high photostability. Using two-photon microscopic imaging the probe facilitated the real-time monitoring of Golgi Zn^{2+} changes in addition to the 3D distribution in tissues and live cells (Fig. 55).[138] More importantly, it is worth noting that both the lipophilicity and the weakly basic pyridyl moiety of probe **59** are probably responsible for the specific Golgi apparatus localization.

In 2018, the Das group reported a fluorescent BODIPY-based HOCl turn-on probe (**SF-1**, **60**), that was used to image HOCl that was generated endogenously in RAW 264.7 macrophages using structured-illumination microscopy (SIM). Due to a low charge/intermediate amphiphilicity, the probe localized in the Golgi and lysosomes which was confirmed by widefield and super resolution structured illumination microscopy which enabled the monitoring of HOCl generated in these organelles. Moreover, 3D-SIM images of individual cells were also constructed (Fig. 56).[139]

In 2019, the Datta group reported a sensitive ''turn-on'' fluorescent manganese sensor (**61**) to monitor the storage locations of manganese ions in the Golgi apparatus under exposure to micromolar manganese using X-ray fluorescence imaging and confocal microscopy. The experimental results, suggest the important role of the Golgi apparatus for manganese trafficking and storage at sub-cytotoxic levels (Fig. 57).[140]

4. Conclusion and outlook

The Golgi apparatus is widely distributed in eukaryotic cells and is dynamically regulated during cell cycles, and as such plays an important role in a variety of metabolic pathways and cell signaling mechanisms, including collecting, processing, sorting, transporting and secreting some important proteins/enzymes from the endoplasmic reticulum to intra- and extra-cellular destinations. Organelle-targeting fluorescent probes have made significant advances recently, due to their numerous advantages in monitoring biological systems. Amongst these probes, fluorescent Golgi-targeting probes have provided an opportunity to monitor the physiological and pathological changes and to further diagnose and treat relevant diseases associated with the Golgi apparatus. Here, we have extensively covered Golgi-targeting fluorescent probes and highlighted their application. Specifically, appropriate design strategies and Golgi-targeting mechanisms have been discussed to provide guidance for developing improved systems. Subsequently, examples of probes suitable for sensing different targets and with diverse characteristics have been elucidated, including probes containing cyclooxygenase-2 (COX-2) inhibitors, probes containing a

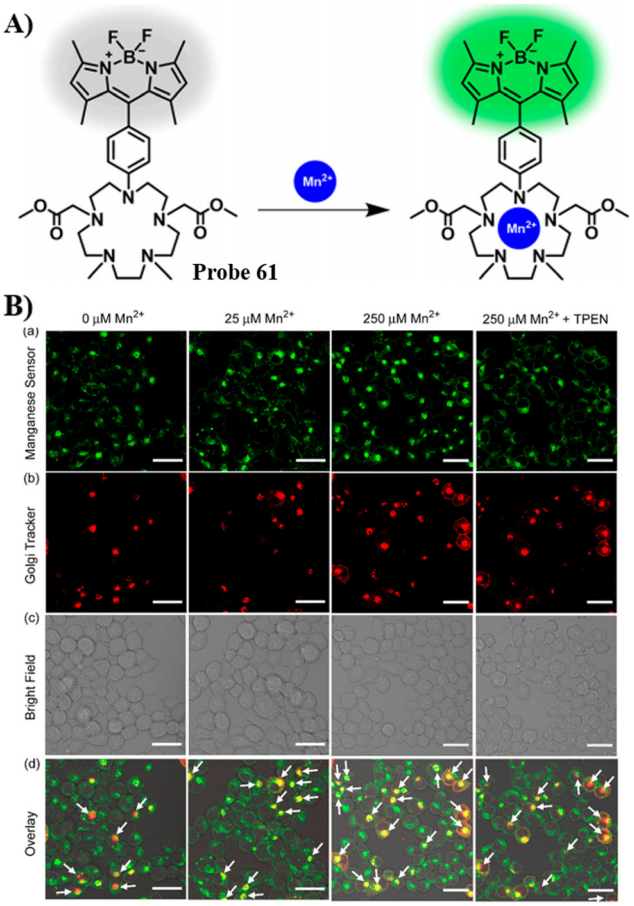

Fig. 57 (A) Mechanism of **61** for identifying Mn^{2+}. (B) Left to right: Confocal fluorescence images of live HEK293T cells with different concentrations of $MnCl_2$, followed by a cell-permeable divalent metal-ion chelator, TPEN. Cells were tranduced with CellLight Golgi-RFP and incubated with **61**. Probe **61** emission in the green channel (λ_{ex} = 488 nm) (a). Golgi-RFP emission in the red channel (λ_{ex} = 543 nm) (b). Bright-field images (c). Bright-field images of cells overlaid with confocal images (d). Reproduced with permission from ref. 140. Copyright 2019, American Chemical Society.

phenylsulfonamide group, probes with a 2-trifluoromethyl-7-aminoquinoline group, probes with a L-Cys group, probes with targeting peptides, probes containing lipids, probes encapsulated by BSA, and probes with other targeting groups.

While many selective systems have been developed significant improvements are required, since current Golgi-targeting strategies need to overcome some remaining challenges including a better understanding of the biological mechanisms, provide a single highly Golgi selective response, as well as providing extended targeting duration, *etc.*, while advances have been made in the development of Golgi-targeting probes. Going forward, we propose that the following areas should be particularly targeted: (1) explore Golgi targeting functional groups with improved optical properties such as multi-photon excitation and high quantum yield, that exhibit enhanced precision of localization in the Golgi apparatus. (2) Elucidate the exact targeting mechanism of current targeting motifs to enhance the function of Golgi-targeting fluorescent probes. (3) Develop multiplexing probes with different signal modes to enable simultaneous dynamic monitoring of multiple physiological changes in the same cell. This will help determine the intricate dynamics and physiological parameters of the complex cellular environment. (4) Develop novel multifunctional fluorescent probes with both Golgi targeted imaging and disease therapy by integrating Golgi-targeted imaging with therapeutic systems. The combination of targeted imaging and disease treatment systems will help enhance our understanding of the Golgi apparatus in the pathological state, whilst simultaneously achieving the desired therapeutic effect. (5) Develop Golgi-targeting probes for other important biomarkers such as protein glycosylation and phosphorylation, which will help understand the relationship between these biomarkers and disease development. (6) Improve the performance of the probes, by enhancing biocompatibility, incorporating reversibility, reducing toxicity, and improving optical performance. We believe that the design and development of high-precision and multi-functional fluorescent probes will be an important research direction in the field of Golgi targeting fluorescent probes in the future, and this review will provide guidance for researchers working on probe design and construction.

Conflicts of interest

There are no conflicts to declare.

Acknowledgements

We acknowledge the Joint Program for Fostering Talents of National Natural Science Foundation of China and Henan Province (U1304202), State Scholarship Fund (CSC 201908410366), Natural Science Foundation of Henan Province (232300420402), Henan Province Science and Technology Project (222300420523) (212102210646) and The Scientific Research Innovation Team of Xuchang University (2022CXTD001) for financial support. T. D. J. wishes to thank the University of Bath and the Open Research Fund of the School of Chemistry and Chemical Engineering, Henan Normal University (2020ZD01) for support.

References

1 C. P. Satori, M. M. Henderson, E. A. Krautkramer, V. Kostal, M. D. Distefano and E. A. Arriaga, *Chem. Rev.*, 2013, **113**, 2733–2811.
2 R. Heald and O. Cohen-Fix, *Curr. Opin. Cell Biol.*, 2014, **26**, 79–86.
3 J. Li, E. Ahat and Y. Wang, *Results Probl. Cell Differ.*, 2019, **67**, 441–485.
4 J. H. Lin, P. Walter and T. S. B. Yen, *Annu. Rev. Pathol.: Mech. Dis.*, 2008, **3**, 399–425.
5 F. Zappa, M. Failli and M. A. De Matteis, *Curr. Opin. Cell Biol.*, 2018, **50**, 102–116.
6 A. Eisenberg-Lerner, R. Benyair, N. Hizkiahou, N. Nudel, R. Maor, M. P. Kramer, M. D. Shmueli, I. Zigdon, M. C. Lev, A. Ulman, J. Y. Sagiv, M. Dayan, B. Dassa, M. Rosenwald,

I. Shachar, J. Li, Y. Wang, N. Dezorella, S. Khan, Z. Porat, E. Shimoni, O. Avinoam and Y. Merbl, *Nat. Commun.*, 2020, **11**, 409.
7 J. Gao, A. Gao, H. Zhou and L. Chen, *Cell Biol. Int.*, 2022, **46**, 1309–1319.
8 Y. Zhang, Y. Wang, E. Read, M. Fu, Y. Pei, L. Wu, R. Wang and G. Yang, *Antioxid. Redox Signaling*, 2019, **32**, 583–601.
9 J. Li and Y. Wang, *Cells*, 2022, **11**, 289.
10 S. Kellokumpu, *Front. Cell Dev. Biol.*, 2019, **7**, 93.
11 C. Preisinger, B. Short, V. De Corte, E. Bruyneel, A. Haas, R. Kopajtich, J. Gettemans and F. A. Barr, *J. Cell Biol.*, 2004, **164**, 1009–1020.
12 J. I. Sbodio, B. D. Paul, C. E. Machamer and S. H. Snyder, *Cell Rep.*, 2013, **4**, 890–897.
13 L. Lu, Q. Zhou, Z. Chen and L. Chen, *J. Cell. Physiol.*, 2018, **233**, 2911–2919.
14 J. I. Sbodio, S. H. Snyder and B. D. Paul, *Proc. Natl. Acad. Sci. U. S. A.*, 2018, **115**, 780–785.
15 C. Kienzle and J. von Blume, *Trends Cell Biol.*, 2014, **24**, 584–593.
16 H. Singh, D. Sareen, J. M. George, V. Bhardwaj, S. Rha, S. J. Lee, S. Sharma, A. Sharma and J. S. Kim, *Coord. Chem. Rev.*, 2022, **452**, 214283.
17 M. Tian, J. Zhan and W. Lin, *Coord. Chem. Rev.*, 2022, **451**, 214266.
18 Y. Wei, Y. Liu, Y. He and Y. Wang, *J. Mater. Chem. B*, 2021, **9**, 908–920.
19 J. Lin, K. Yang and E. J. New, *Org. Biomol. Chem.*, 2021, **19**, 9339–9357.
20 S. K. Pramanik and Amitva Das, *Chem. Commun.*, 2021, **57**, 12058–12073.
21 J. Yin, L. Huang, L. Wu, J. Li, T. D. James and W. Lin, *Chem. Soc. Rev.*, 2021, **50**, 12098–12150.
22 H. Yu, Y. Guo, W. Zhu, K. Havener and X. Zheng, *Coord. Chem. Rev.*, 2021, **444**, 214019.
23 D. Singh, D. Rajput and S. Kanvah, *Chem. Commun.*, 2022, **58**, 2413–2429.
24 C. Ma, F. Xia and S. O. Kelley, *Bioconjugate Chem.*, 2020, **31**, 2650–2667.
25 K. Yu, J. Pan, E. Husamelden, H. Zhang, Q. He, Y. Wei and M. Tian, *Chem. – Asian J.*, 2020, **15**, 3942–3960.
26 L. Fang and Michael Watkinson, *Chem. Sci.*, 2020, **11**, 11366–11379.
27 S. Samanta, Y. He, A. Sharma, J. Kim, W. Pan, Z. Yang, J. Li, W. Yan, L. Liu, J. Qu and J. S. Kim, *Chem*, 2019, **5**, 1697–1726.
28 Y. Wen, F. Huo and C. Yin, *Chin. Chem. Lett.*, 2019, **30**, 1834–1842.
29 X. Zhang, Q. Sun, Z. Huang, L. Huang and Y. Xiao, *J. Mater. Chem. B*, 2019, **7**, 2749–2758.
30 P. Gao, W. Pan, N. Li and B. Tang, *Chem. Sci.*, 2019, **10**, 6035–6071.
31 J. Zhu, Z. Xu, Y. Yang and L. Xu, *Chem. Commun.*, 2019, **55**, 6629–6671.
32 H. Zhu, J. Fan, J. Du and X. Peng, *Acc. Chem. Res.*, 2016, **49**, 2115–2126.
33 W. Xu, Z. Zeng, J. Jiang, Y. Chang and L. Yuan, *Angew. Chem., Int. Ed.*, 2016, **55**, 13658–13699.
34 G. H. Luo, T. Z. Xu, X. Li, W. Jiang, Y. H. Duo and B. Z. Tang, *Coord. Chem. Rev.*, 2022, **462**, 214508.
35 C. Liu, H. Zhu, Y. Zhang, M. Su, M. Liu, X. Zhang, X. Wang, X. Rong, K. Wang, X. Li and B. Zhu, *Coord. Chem. Rev.*, 2022, **462**, 214504.
36 M. G. Farquhar and G. E. Palade, *Trends Cell Biol.*, 1998, **8**, 2–10.
37 N. Lipsky and R. Pagano, *Science*, 1985, **228**, 745–747.
38 N. B. Cole, C. L. Smith, N. Sciaky, M. Terasaki, M. Edidin and J. Lippincott-Schwartz, *Science*, 1996, **273**, 794–797.
39 A. Dragulescu-Andrasi, G. Liang and J. Rao, *Bioconjugate Chem.*, 2009, **20**, 1660–1666.
40 H. Wang, X. T. Zhang, T. C. Xiu, H. T. Wang, P. Li and B. Tang, *Coord. Chem. Rev.*, 2024, **502**, 215618.
41 C. Denkert, K. J. Winzer, B. M. Muller, W. Weichert, S. Pest, M. Kobel, G. Kristiansen, A. Reles, A. Siegert, H. Guski and S. Hauptmann, *Cancer*, 2003, **97**, 2978–2987.
42 M. J. Uddin, B. C. Crews, K. Ghebreselasie and L. J. Marnett, *Bioconjugate Chem.*, 2013, **24**, 712–723.
43 L. Fourriere, S. Divoux, M. Roceri, F. Perez and G. Boncompain, *J. Cell Sci.*, 2016, **129**, 3238–3250.
44 J. Kim, H. R. Cho, H. Jeon, D. Kim, C. Song, N. Lee, S. H. Choi and T. Hyeon, *J. Am. Chem. Soc.*, 2017, **139**, 10992–10995.
45 J. L. Masferrer, K. M. Leahy, A. T. Koki, B. S. Zweifel, S. L. Settle, B. M. Woerner, D. A. Edwards, A. G. Flickinger, R. J. Moore and K. Seibert, *Cancer Res.*, 2000, **60**, 1306–1311.
46 E. Richardsen, R. D. Uglehus, J. Due, C. Busch and L. T. Busund, *Cancer Epidemiol.*, 2010, **34**, 316–322.
47 M. J. Uddin, B. C. Crews, A. L. Blobaum, P. J. Kingsley, D. L. Gorden, J. O. McIntyre, L. M. Matrisian, K. Subbaramaiah, A. J. Dannenberg, D. W. Piston and L. J. Marnett, *Cancer Res.*, 2010, **70**, 3618–3627.
48 M. T. Rizzo, *Clin. Chim. Acta*, 2011, **412**, 671–687.
49 C. Denkert, M. Kobel, S. Berger, A. Siegert, A. Leclere, U. Trefzer and S. Hauptmann, *Cancer Res.*, 2001, **61**, 303–308.
50 H. M. Kandil, G. Tanner, W. Smalley, S. Halter, A. Radhika and R. N. Dubois, *Dig. Dis. Sci.*, 2001, **46**, 785–789.
51 C. E. Eberhart, R. J. Coffey, A. Radhika, F. M. Giardiello, S. Ferrenbach and R. N. DuBois, *Gastroenterology*, 1994, **107**, 1183–1188.
52 A. Bhardwaj, J. Kaur, F. Wuest and E. E. Knaus, *ChemMedChem*, 2014, **9**, 109–116.
53 A. Bhardwaj, J. Kaur, S. K. Sharma, Z. Huang, F. Wuest and E. E. Knaus, *Bioorg. Med. Chem. Lett.*, 2013, **23**, 163–168.
54 W. F. Hood, J. K. Gierse, P. C. Isakson, J. R. Kiefer, R. G. Kurumbail, K. Seibert and J. B. Monahan, *Mol. Pharmacol.*, 2003, **63**, 870–877.
55 H. Zhang, J. Fan, J. Wang, S. Zhang, B. Dou and X. Peng, *J. Am. Chem. Soc.*, 2013, **135**, 11663–11669.
56 B. Wang, J. Fan, X. Wang, H. Zhu, J. Wang, H. Mu and X. Peng, *Chem. Commun.*, 2015, **51**, 792–795.

57 B. Gurram, S. Zhang, M. Li, H. Li, Y. Xie, H. Cui, J. Du, J. Fan, J. Wang and X. Peng, *Anal. Chem.*, 2018, **90**, 5187–5193.
58 B. Gurram, M. Li, J. Fan, J. Wang and X. Peng, *Front. Chem. Sci. Eng.*, 2020, **14**(1), 41–52.
59 Y. Luo, S. Zhang, H. Wang, Q. Luo, Z. Xie, B. Xu and W. Tian, *CCS Chem.*, 2022, **4**, 456–463.
60 K. Huang, H. Zhang, M. Yan, J. Xue and J. Chen, *Dyes Pigm.*, 2022, **198**, 109997.
61 C. Liu, L. Zhou, Y. Zheng, H. Man, Z. Ye, X. Zhang, L. Xie and Y. Xiao, *Chem. Commun.*, 2022, **58**, 10052–10055.
62 R. G. Kurumbail, A. M. Stevens, J. K. Gierse, J. J. McDonald, R. A. Stegeman, J. Y. Pak, D. Gildehaus, J. M. Miyashiro, T. D. Penning, K. Seibert, P. C. Isakson and W. C. Stallings, *Nature*, 1996, **384**, 644–648.
63 H. Wang, Z. He, Y. Yang, J. Zhang, W. Zhang, W. Zhang, P. Li and B. Tang, *Chem. Sci.*, 2019, **10**, 10876–10880.
64 H. Zhu, C. Liu, C. Liang, B. Tian, H. Zhang, X. Zhang, W. Sheng, Y. Yu, S. Huang and B. Zhu, *Chem. Commun.*, 2020, **56**, 4086–4089.
65 H. Wang, Y. Yang, F. Huang, Z. He, P. Li, W. Zhang, W. Zhang and B. Tang, *Anal. Chem.*, 2020, **92**, 3103–3110.
66 H. Wang, M. Dong, H. Wang, F. Huang, P. Li, W. Zhang, W. Zhang and B. Tang, *Chem. Commun.*, 2021, **57**, 5838–5841.
67 P. Xiao, K. Ma, M. Kang, L. Huang, Q. Wu, N. Song, J. Ge, D. Li, J. Dong, L. Wang, D. Wang and B. Z. Tang, *Chem. Sci.*, 2021, **12**, 13949–13957.
68 M. M. Fortibui, W. Lim, S. Lee, S. Park and J. Kim, *Molecules*, 2021, **26**, 4980.
69 S. Li, K. Yang, J. Zeng, Y. Ding, D. Cheng and L. He, *ACS Omega*, 2022, **7**, 9929–9935.
70 S. Feng, Z. Zheng, S. Gong and G. Feng, *Sens. Actuators, B*, 2022, **361**, 131751.
71 J. Li, J. Tang, X. Yang, P. Xie, J. Liu, D. Zhang and Y. Ye, *Sens. Actuators, B*, 2022, **358**, 131513.
72 X. Zhang, L. Chen, Y. Y. Wei, J. L. Du, S. P. Yu, X. G. Liu, W. Liu, Y.-J. Liu, Y.-Z. Yang and Q. Li, *Dyes Pigm.*, 2022, **201**, 110213.
73 Z. Feng, J. Wu, M. Jiang, J. Sha, W. Liu, H. Ren, W. Zhang, C.-S. Lee and P. Wang, *Sens. Actuators, B*, 2022, **366**, 131963.
74 Q. Zhang, Y. Tang, S. Song, J. Peng and W. Y. Lin, *New J. Chem.*, 2022, **46**, 14333–14337.
75 S. Han, H. Wang, H. Li, K. Li, J. Wang and X. Song, *Anal. Chem.*, 2023, **95**, 8002–8010.
76 Z. He, D. Liu, Y. Liu, X. Li, W. Shi and H. Ma, *Anal. Chem.*, 2022, **94**, 10256–10262.
77 H. Wang, C. Liu, X. Zhang, T. Xiu, P. Li, W. Zhang, W. Zhang, X. Wang, Z. Liu and B. Tang, *Biosens. Bioelectron.*, 2022, **213**, 114480.
78 G. Fei, S. Ma, C. Wang, T. Chen, Y. Li, Y. Liu, B. Tang, T. D. James and G. Chen, *Coord. Chem. Rev.*, 2021, **447**, 214134.
79 S. M. Usama, F. Inagaki, H. Kobayashi and M. J. Schnermann, *J. Am. Chem. Soc.*, 2021, **143**, 5674–5679.
80 R. M. Exner, F. Cortezon-Tamarit and S. I. Pascu, *Angew. Chem., Int. Ed.*, 2021, **60**, 6230–6241.
81 Z. Xu, H. Wang, X. Hou, W. Xu, T. Xiang and C. Wu, *Sens. Actuators, B*, 2014, **201**, 469–474.
82 L. Feng, W. Chen, X. Ma, S. H. Liu and J. Yin, *Org. Biomol. Chem.*, 2020, **18**, 9385–9397.
83 N. Zhou, F. Huo, Y. Yue and C. Yin, *J. Am. Chem. Soc.*, 2020, **142**, 17751–17755.
84 H. Mu, K. Miki, H. Harada, K. Tanaka, K. Nogita and K. Ohe, *ACS Sens.*, 2021, **6**, 123–129.
85 C. Zhang, Z. Qiu, L. Zhang, Q. Pang, Z. Yang, J.-K. Qin, H. Liang and S. Zhao, *Chem. Sci.*, 2021, **12**, 4883–4888.
86 L. Chen, J. Chen, Y. Fang, F. Zeng and S. Wu, *Chem. Commun.*, 2021, **57**, 7842–7845.
87 H. Fang, Y. Chen, Y. Wang, S. Geng, S. Yao, D. Song, W. He and Z. Guo, *Sci. China: Chem.*, 2020, **63**, 699–706.
88 J. Xiang, C. Liu, L. Zhou, X. Yang, Y. Li, Y. Jiang, T. Mahmood, P. Zhang, P. Gong and L. Cai, *Anal. Chem.*, 2020, **92**, 4721–4725.
89 Y. Zhou, P. Li, X. Wang, C. Wu, N. Fan, X. Liu, L. Wu, W. Zhang, W. Zhang, Z. Liu and B. Tang, *Chem. Sci.*, 2020, **11**, 12149–12156.
90 J. R. Casey, S. Grinstein and J. Orlowski, *Nat. Rev. Mol. Cell Biol.*, 2010, **11**, 50–61.
91 J. Chen, H. Liu, L. Yang, J. Jiang, G. Bi, G. Zhang, G. Li and X. Chen, *ACS Med. Chem. Lett.*, 2019, **10**, 954–959.
92 X. Zhang, C. Liu, Y. Chen, X. Cai, W. Sheng, H. Zhu, P. Jia, Z. Li, S. Huang and B. Zhu, *Chem. Commun.*, 2020, **56**, 1807–1810.
93 X. Zhang, C. Liu, X. Cai, B. Tian, H. Zhu, Y. Chen, W. Sheng, P. Jia, Z. Li, Y. Yu, S. Huang and B. Zhu, *Sens. Actuators, B*, 2020, **310**, 127820.
94 H. Zhu, C. Liang, X. Cai, H. Zhang, C. Liu, P. Jia, Z. Li, Y. Yu, X. Zhang, W. Sheng and B. Zhu, *Anal. Chem.*, 2020, **92**, 1883–1889.
95 X. Hu, Z. Hai, C. Wu, W. Zhan and G. Liang, *Anal. Chem.*, 2021, **93**, 1636–1642.
96 X. Rong, C. Liu, M. Li, H. Zhu, Y. Zhang, M. Su, X. Wang, X. Li, K. Wang, M. Yu, W. Sheng and B. Zhu, *Anal. Chem.*, 2021, **93**, 16105–16112.
97 Z. Zheng, S. Feng, S. Gong and G. Feng, *Sens. Actuators, B*, 2021, **347**, 130631.
98 H. Zhu, C. Liu, X. Rong, Y. Zhang, M. Su, X. Wang, M. Liu, X. Zhang, W. Sheng and B. Zhu, *Bioorg. Chem.*, 2022, **122**, 105741.
99 Z. Yan, Z. Tang, X. Wang, Z. Zheng, Z. Tian, X. Geng, Y. Li and H. Jiang, *Sens. Actuators, B*, 2022, **369**, 132352.
100 Z. Tang, Z. Yan, L. Gong, L. Zhang, X. Yin, J. Sun, K. Wu, W. Yang, G. Fan, Y. Li and H. Jiang, *Anal. Chem.*, 2022, **94**, 14778–14784.
101 Z. Feng, J. Wu, W. Liu, H. Ren, X. Zheng, W. Zhang, C.-S. Lee and P. Wang, *Sens. Actuators, B*, 2023, **384**, 133668.
102 D. Aoki, N. Lee, N. Yamaguchi, C. Dubois and M. N. Fukuda, *Proc. Natl. Acad. Sci. U. S. A.*, 1992, **89**, 4319–4323.
103 Y. Maeda, G. V. Beznoussenko, J. Van Lint, A. A. Mironov and V. Malhotra, *EMBO J.*, 2001, **20**, 5982–5990.
104 K. Maeda, P. Hägglund, C. Finnie, B. Svensson and A. Henriksen, *Structure*, 2006, **14**, 1701–1710.

105 W. Zhang, J. Zhang, P. Li, J. Liu, D. Su and B. Tang, *Chem. Sci.*, 2019, **10**, 879–883.
106 P. Li, X. Guo, X. Bai, X. Wang, Q. Ding, W. Zhang, W. Zhang and B. Tang, *Anal. Chem.*, 2019, **91**, 3382–3388.
107 L. Fang, R. Crespo-Otero, C. R. Jones and M. Watkinson, *Sens. Actuators, B*, 2021, **338**, 129850.
108 N. Yamaguchi and M. N. Fukuda, *J. Biol. Chem.*, 1995, **270**, 12170–12176.
109 M. Kneen, J. Farinas, Y. Li and A. S. Verkman, *Biophys. J.*, 1998, **74**, 1591–1599.
110 S. H. Wong and W. Hong, *J. Biol. Chem.*, 1993, **268**, 22853–22862.
111 K. Bos, C. Wraight and K. K. Stanley, *EMBO J.*, 1993, **12**, 2219–2228.
112 J. S. Humphrey, P. J. Peters, L. C. Yuan and J. S. Bonifacino, *J. Cell Biol.*, 1993, **120**, 1123–1135.
113 E. H. W. Pap, T. B. Dansen, R. van Summeren and K. W. A. Wirtz, *Exp. Cell Res.*, 2001, **265**, 288–293.
114 K. H. Jung, E. T. Oh, H. J. Park and K. H. Lee, *Biosens. Bioelectron.*, 2016, **85**, 437–444.
115 K. Li, X. X. Hu, H. W. Liu, S. Xu, S. Y. Huan, J. B. Li, T. G. Deng and X.-B. Zhang, *Anal. Chem.*, 2018, **90**, 11680–11687.
116 L. Zhu, H. W. Liu, Y. Yang, X. X. Hu, K. Li, S. Xu, J. B. Li, G. Ke and X. B. Zhang, *Anal. Chem.*, 2019, **91**, 9682–9689.
117 X. Li, C. Cao, P. Wei, M. Xu, Z. Liu, L. Liu, Y. Zhong, R. Li, Y. Zhou and T. Yi, *ACS Appl. Mater. Interfaces*, 2019, **11**, 12327–12334.
118 W. Tan, Q. Zhang, J. Wang, M. Yi, H. He and B. Xu, *Angew. Chem., Int. Ed.*, 2021, **60**, 12796–12801.
119 W. Tan, Q. Zhang, M. C. Quiñones-Frías, A. Y. Hsu, Y. Zhang, A. Rodal, P. Hong, H. R. Luo and B. Xu, *J. Am. Chem. Soc.*, 2022, **144**, 6709–6713.
120 S. Limar, C. Körner, F. Martínez-Montañés, V. G. Stancheva, V. N. Wolf, S. Walter, E. A. Miller, C. S. Ejsing, V. V. Galassi and F. Fröhlich, *J. Cell Biol.*, 2023, **222**, e202109162.
121 R. P. Rao, C. Yuan, J. C. Allegood, S. S. Rawat, M. B. Edwards, X. Wang, A. H. Merrill, U. Acharya and J. K. Acharya, *Proc. Natl. Acad. Sci. U. S. A.*, 2007, **104**, 11364–11369.
122 T. Hirayama, M. Inden, H. Tsuboi, M. Niwa, Y. Uchida, Y. Naka, I. Hozumib and H. Nagasawa, *Chem. Sci.*, 2019, **10**, 1514–1521.
123 L. Fan, X. Wang, J. Ge, F. Li, C. Zhang, B. Lin, S. Shuang and C. Dong, *Chem. Commun.*, 2019, **55**, 6685–6688.
124 T. Kowada, T. Watanabe, Y. Amagai, R. Liu, M. Yamada, H. Takahashi, T. Matsui, K. Inaba and S. Mizukami, *Cell Chem. Biol.*, 2020, **27**, 1521–1531.
125 A. Li, Y. Liu, Labapuchi, Z. Chen, S. Li, R. Zhong, D. Cheng, L. Chen and L. He, *Anal. Chim. Acta*, 2023, **1255**, 341100.
126 A. Li, Y. Liu, Labapuchi, Z. Chen, S. Li, R. Zhong, D. Cheng, L. Chen and L. He, *Spectrochim. Acta, Part A*, 2023, **294**, 122560.
127 T. Kowada, T. Watanabe, R. Liu and S. Mizukami, *STAR Protoc.*, 2021, **2**, 100395.
128 X. Zeng, X. Zhang, B. Zhu, H. Jia, Y. Li and J. Xue, *Analyst*, 2011, **136**, 4008–4012.
129 R. W. Horobin and F. R. Doubell, *Biotech. Histochem.*, 2013, **88**, 461–476.
130 F. Xue, Y. Wen, P. Wei, Y. Gao, Z. Zhou, S. Xiao and T. Yi, *Chem. Commun.*, 2017, **53**, 6424–6427.
131 H. Wang, C. Liu, Z. He, P. Li, W. Zhang, W. Zhang and B. Tang, *Anal. Chem.*, 2021, **93**, 6551–6558.
132 X. Xing, Y. Jia, J. Zhang, Z. Wu, M. Qin, P. Li, X. Feng, Y. Sun and G. Zhao, *Sens. Actuators, B*, 2021, **329**, 129245.
133 G. K. Walkup, S. C. Burdette, S. J. Lippard and R. Y. Tsien, *J. Am. Chem. Soc.*, 2000, **122**, 5644–5645.
134 F. Qian, C. Zhang, Y. Zhang, W. He, X. Gao, P. Hu and Z. Guo, *J. Am. Chem. Soc.*, 2009, **131**, 1460–1468.
135 L. E. McQuade and S. J. Lippard, *Inorg. Chem.*, 2010, **49**, 9535–9545.
136 C. Zhang, Y. Zhang, Y. Chen, Z. Xie, Z. Liu, X. Dong, W. He, C. Shen and Z. Guo, *Inorg. Chem. Commun.*, 2011, **14**, 304–307.
137 T. Hirayama, K. Okuda and H. Nagasawa, *Chem. Sci.*, 2013, **4**, 1250–1256.
138 H. Singh, H. W. Lee, C. H. Heo, J. W. Byun, A. R. Sarkar and H. M. Kim, *Chem. Commun.*, 2015, **51**, 12099–12102.
139 F. Ali, S. Aute, S. Sreedharan, H. A. Anila, H. K. Saeed, C. G. Smythe, J. A. Thomas and A. Das, *Chem. Commun.*, 2018, **54**, 1849–1852.
140 S. Das, A. Carmona, K. Khatua, F. Porcaro, A. Somogyi, R. Ortega and A. Datta, *Inorg. Chem.*, 2019, **58**, 13724–13732.